Dissertation

TRIMERIC COILED-COILS AS VIRAL FUSION PROTEIN MIMICS

Submitted by

Philip Travisano III

Department of Chemistry

In partial fulfillment of the requirements for the

Degree of Doctor of Philosophy

Colorado State University

Fort Collins, Colorado

Fall 2008

Colorado State University

November 12, 2008

WE HEREBY RECOMMEND THAT THE DISSERTATION PREPARED UNDER OUR SUPERVISION BY PHILIP TRAVISANO III ENTITLED TRIMERIC COILED-COILS AS VIRAL FUSION PROTEIN MIMICS BE ACCEPTED AS FULFILLING IN PART REQUIREMENTS FOR THE DEGREE OF DOCTOR OF PHILOSOPHY.

Committee on Graduate Work

Prof. Louis S. Hegedus

Prof. Charles S. Henry

Prof. Tomislav Rovis

Prof. Olve B. Peersen

Advisor: Prof. Alan J. Kennan

Department Head: Prof. Anthony K. Rappé

ABSTRACT OF DISSERTATION

TRIMERIC COILED-COILS AS VIRAL FUSION PROTEIN MIMICS

α-Helical coiled-coils, a protein structural motif formed by supercoiling of two or more component polypeptide strands, are ubiquitous mediators of biological structure and function. Their characteristic primary heptad repeat, denoted *abcdefg*, makes these complexes attractive scaffolds for studying self-assembly and molecular recognition. Assembly of these structures is driven by the hydrophobic effect in which the hydrophobic sidechains associated with positions *a* and *d* are specifically packed together. Recently we have described methods for controlling the assembly of 1:1:1 heterotrimeric coiled-coils using only interior hydrophobic core residues. These core residues assemble according to steric matching, one large sidechain packs against two small sidechains. In the following text we have explored new sidechain parings.

This steric matching strategy affords maximal sequence flexibility in the patterning of exterior surface residues, which we have exploited to create mimics of therapeutically significant protein-protein interfaces. The Human Immunodeficiency Virus (HIV) envelope protein gp41 facilitates infection by promoting fusion of cellular and viral membranes. At the heart of its function is formation of a trimer-of-hairpins structure in which a C-terminal ligand peptide binds to an N-terminal coiled-coil surface. This interaction is reminiscent of those in numerous other viral systems, including visna, the sheep analog of HIV. The design of protein mimics for viral systems by installation of key contact residues onto heterotrimer coiled-coils will be further discussed.

The following text will highlight the structural verification of these mimics through various spectroscopic techniques. Also the validation of these mimics will be

tested by exposure to known viral inhibitors. The work included in this text builds on previous research conducted in our laboratory, but it provides new avenues for future projects to explore the detailed interactions within the viral fusion mimics. This will hopefully lead to a better understanding of the viruses being studied as well as the underlying molecular interactions taking place.

Philip Travisano III
Department of Chemistry
Colorado State University
Fort Collins, CO 80523
Fall 2008

ACKNOWLEDGEMENTS

I first have to thank Alan for his generous support. He constantly encouraged me to improve every aspect of my scientific acumen. His guidance over the years has certainly made me a better scientist. I truly appreciate the many hours of discussion on various research topics as well as the stress relieving conversions about sports and television.

I would also like to thank the members of the Kennan group. Without them I would have never come up with interesting games such as "beat down" and "crutch." I also appreciate all the valuable insight they provided on numerous topics.

When it comes to developing new experiments and challenging me to take on new problems I want to sincerely thank Olve. He enlightened me about various spectroscopic techniques, but more importantly his eagerness to share his knowledge and passion for science is truly inspiring.

I cannot forget my parents and family, who have been there to support me throughout my life. This work would not have been possible without their generous support.

Finally, I sincerely thank my wife, Teri. Her support during this endeavor was unyielding. And for that I will be forever thankful.

Table of Contents

Chapter 1

Background

The molecular recognition principles underlying protein-protein interactions have become the focus of recent attention. In particular, trimeric α-helical coiled-coils have inspired numerous investigations.[1] Coiled-coils mediate protein complexation in a wide variety of systems from DNA binding to viral membrane fusion mechanisms.[2] Their ubiquity and simplicity renders them particularly suited for studies in the design of tunable self-assembling systems.

1-1: The Natural System, α-Helical Coiled-Coils

Coiled-coils are comprised of two or more α-helical strands that supercoil onto one another. Interhelical sidechain interactions stabilize the overall structure (Figure 1).

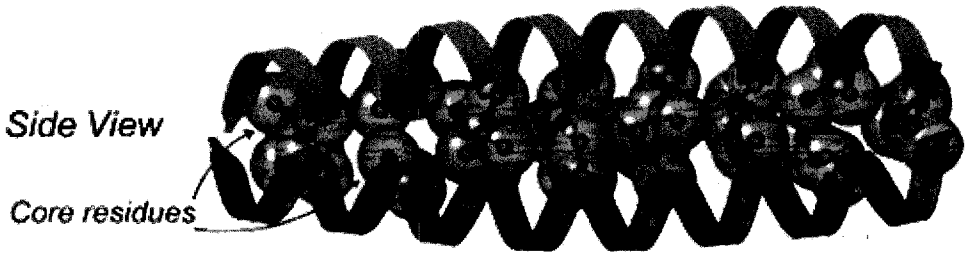

Figure 1. The side view of a dimeric coiled-coil. Core residues are shown as a space filling model. Peptide backbones are shown as ribbons. The supercoiling can be seen with the blue ribbon going from the front of the page on the left to the back of the page on the right, and the red ribbon goes from the back of the page on the left to the front on the right.

The primary sequence consists of a heptad repeat (abcdefg). The *a* and *d* positions have non-polar residues, such as valine (val), leucine (Leu), or isoleucine (Ile) and make up the hydrophobic core. Core close-packing is critical to complex stability, and *a, d* sidechains also control the oligomerization state.[3] The *e* and *g* positions flank the *a, d* sidechains and usually contain polar residues, forming a hydrophilic interhelical interface. The remaining positions are solvent exposed and more variable, containing good helix promoters and hydrophilic sidechains (Figure 2).

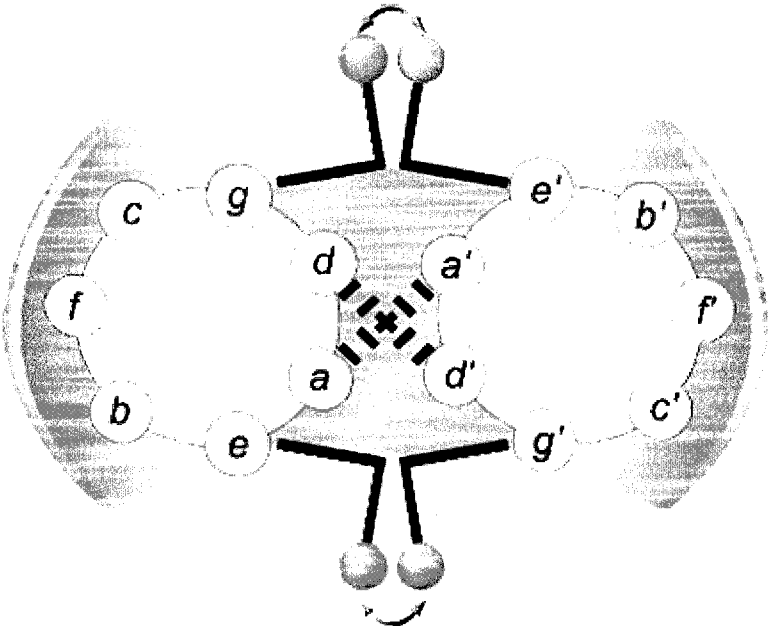

Figure 2. Schematic diagram of coiled-coil heptad positions. Hydrophobic residues at *a* and *d* positions control assembly. Core flanking *e* and *g* positions make up the hydrophilic interface. Remaining positions *b, c,* and *f* are solvent exposed.

Both the hydrophobic core and the hydrophilic interface have an effect on coiled-coil formation and oligomerization state but the hydrophobic core has more control over the oligomerization state, while hydrophilic matchups often govern assembly specificity.[3]

The importance of hydrophobic packing on oligomerization state has been well documented. Kim and co-workers studied the effects of buried polar core sidechains on the oligomerization state of the leucine zipper GCN4-p1.[4] This peptide was derived from the primary sequence of GCN4, which is a well studied yeast transcription factor.[5] It was understood that specific regions of GCN4 were responsible for transcriptional activation, DNA binding, and dimerization.[6] The last 33 residues are responsible for dimerization and it is those residues that were incorporated the GCN4-p1 sequence. In GCN4-p1 all core *d* positions contain leucine and all but two *a* positions contain valine (Figure 3). The

unique central *a* positions contain asparagine which specifies for parallel dimer formation. These polar residues promote specificity by aligning with each other in the hydrophobic core.

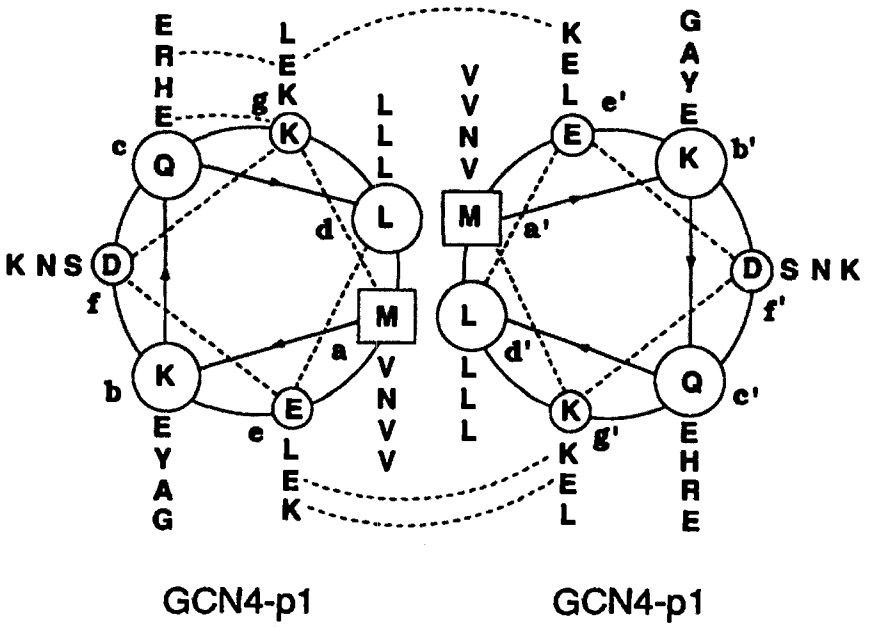

Figure 3. Helical wheel representation of the GCN4-p1 dimer. The central asparagines (N) residues pack up against each other in the hydrophobic core and specify for strand orientation and oligomerization state. The electrostatic interactions are represented as dashed lines.

The role of the core asparagines was later tested by Kim and Lumb in the ACID-p1/BASE-p1 system (Figure 4).[3] This system was modeled after GCN4 but the *e* and *g* positions were changed to either glutamic acid (Glu) or lysine (Lys) respectively and all the core positions except for one *a* position were leucines. With asparagines in the unique core *a* positions ACID-p1/BASE-p1 formed a stable heterodimer, but mutating the asparagines to leucines (ACID-pLL/BASE-pLL) favors the formation of heterotetramers. Thus the asparagines were confirmed as the source of dimer specificity.

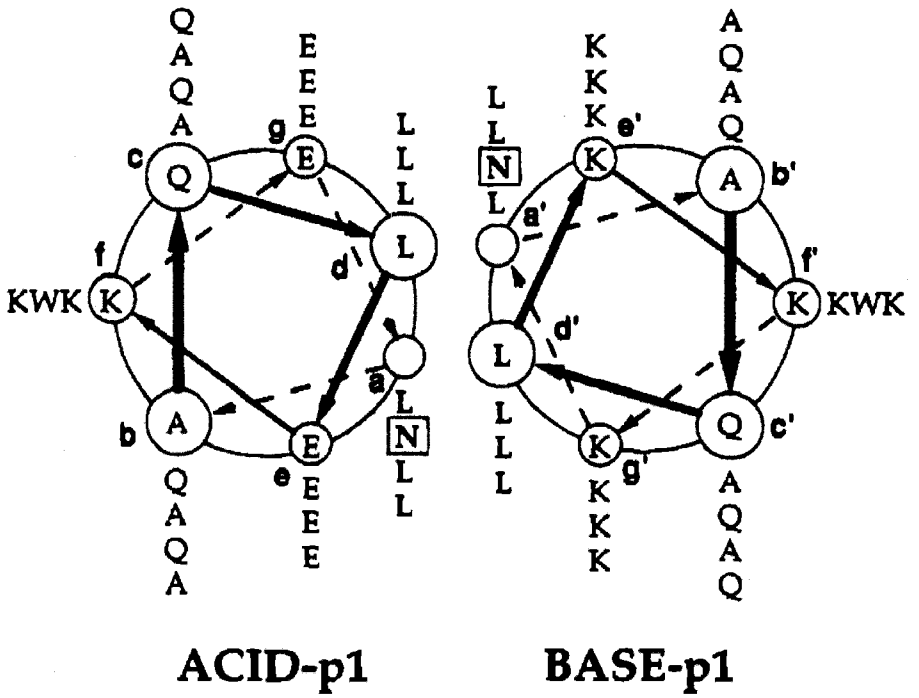

Figure 4. Helical wheel diagram for the ACID-p1 and BASE-p1 peptides. The **a** and **d** positions were substituted with leucine, except for the asparigine in the *a* position 14. In the ACID-pLL and BASE-pLL peptides, the central Asn was substituted with Leu.

Further investigations of the hydrophobic core led to the design of new core interactions. The Alber group introduced an interesting system based on GCN4-p1, in which the central core asparagine was replaced with alanine.[7] The small methyl sidechains produced a destablilizing steric void when packed against each other in the core, which could be stabilized with the addition of small molecules. Without additives the system forms both dimers and trimers, but with the addition of benzene or cyclohexane the equilibrium shifts to trimers. These trimeric scaffolds support the presence of benzene or cyclohexane packed around three alanine residues in the hydrophobic pocket according to X-ray crystallography (Figure 5).

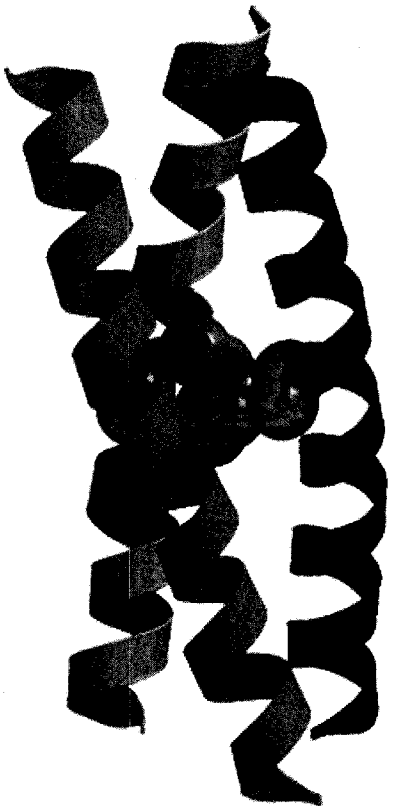

Figure 5. Crystal structure of Alber system with benzene bound in the hydrophobic pocket. In the space filling models are the benzene and the three alanine sidechains that are packing up against it. It is with the incorporation of benzene or cyclohexane that the peptide system specifies for trimers.

1-2: Development of the Tic-Tac-Toe System

Most of the previous methods controlled both specificity and oligomerization state by relying upon matching a hydrophilic residue in the hydrophobic pocket and by electrostatically matching all the *e* and *g* positions on the various peptides. Unfortunately, with all of these substitutions needed to control these parameters, it left very little space on the designed complex to study other interactions. With the knowledge of how important the hydrophobic residues were in controlling specificity and

oligomerization state our laboratory set out to develop a new method to control these parameters.

Our laboratory utilized steric matching as a driving force for garnering specificity and controlling oligomerization state. In this new trimeric model system all substitutions would be conducted in one *a* layer. This layer would contain one large sidechain and two small sidechains (Figure 6). With this model, the preferred complex would contain one large sidechain packing up against two small sidechains. A homotrimeric complex comprised of all peptides with small sidechains would be destabilized by the steric void formed between the sidechains. On the other hand, the packing of more than one large sidechain into the *a* layer would produce a steric clash. This conformation would be disfavored as well.

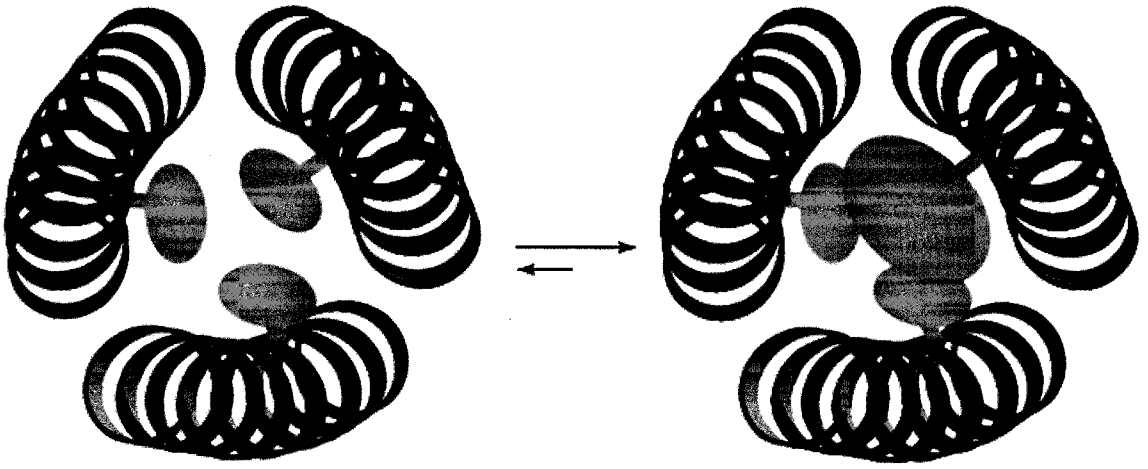

Figure 6. New trimeric system in which steric matching dictates oligomerazation state. The homotrimer with all small sidechains was destabilized by the steric void created in the hydrophobic pocket. The preferred complex had a 2:1 ratio of small to larger sidechains. The large sidechain packed against the two small sidechains created a favorable steric match.

With an eye toward exploiting these steric match-ups, previous work in our laboratory conducted by Nate Schnarr, incorporated cyclohexyalanine (Chx) as the large

sidechain residue for one of the peptides in a heterotrimer, while alanine was incorporated into the two others. Specificity for heterotrimer formation was obtained by core residue steric matching in which the favored complexes permitted formation of 2:1 alanine-cyclohexylalanine layers.[8] However an issue with heterotrimer specificity arose with the one-layer substitution system. The two peptides that contained the alanine were indistinguishable from each other with this steric matching system. A new system had to be developed that differentiated between the two peptides.

The second generation systems involved a Tic-Tac-Toe strategy for 1:1:1 heterotrimer formation by modification of three consecutive *a* positions of the primary sequence heptad repeat (Figure 7).[9] In this system each peptide was unique in that it contained a large sidechain in one of three possible *a* layers and a small sidechain in the other two. Similarly to the first generation system, the large sidechains were cyclohexylalanine residues and the small sidechains were alanine residues. In this system the designed complex proved to be more stable than the individual components because of the unique tic-tac-toe strategy. It would be this tic-tac-toe system that would be further studied and later become the basis for other projects in the laboratory.

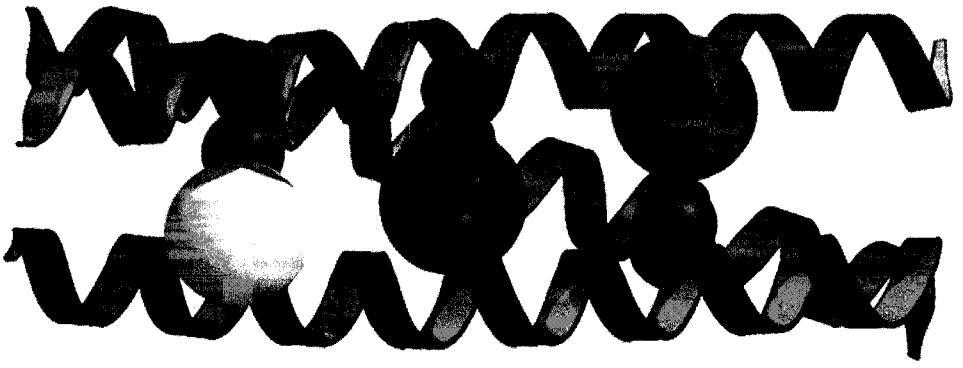

Figure 7. Large core *a* sidechains pack against small core sidechains in the same *a* layer creating a well packed, stable core.

1-3: The Role of Coiled-Coils in Viral Infection

HIV and many other viruses depend on coiled-coil surface recognition for infectivity. The fusion mechanism of HIV-1 highlights the important role that peptides play in viral entry (Figure 8).[10]

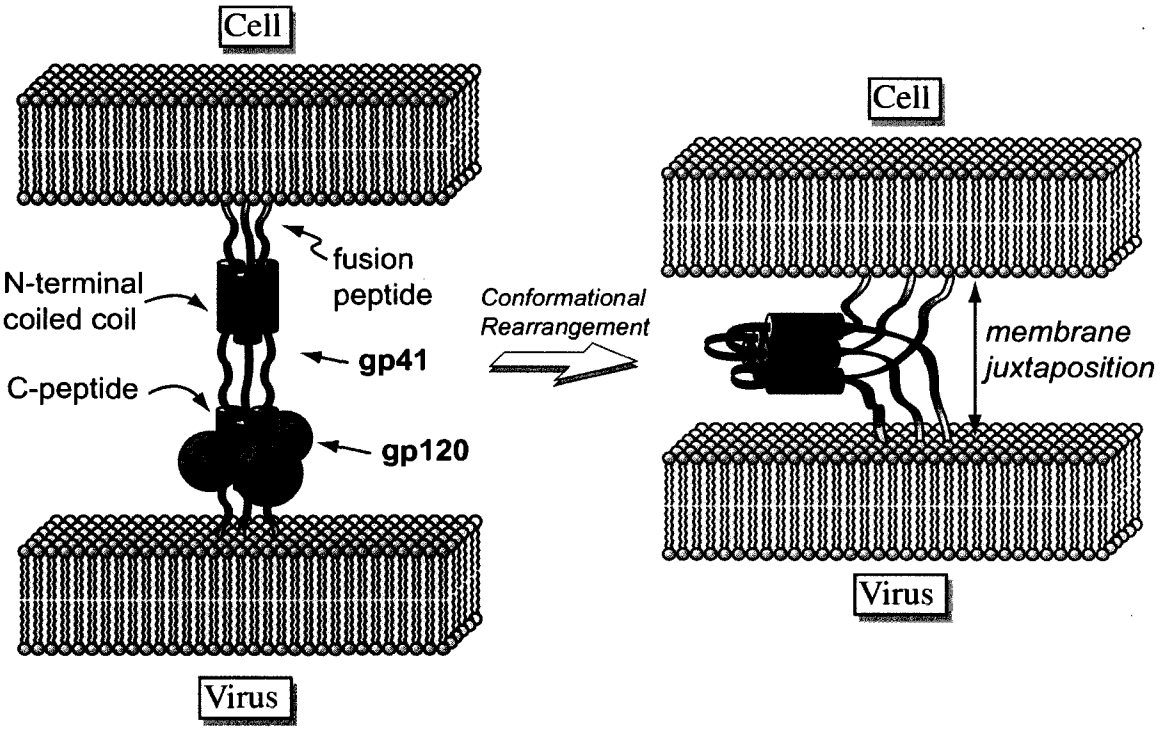

Figure 8. Model of HIV membrane fusion. In order for the two cell membranes to fuse they must be brought closer together in space. This was achieved through the conformational rearrangement of gp41. In this process the C-peptides bind onto the surface of the N-terminal coiled-coil, forming a trimer-of-hairpins. Hence bringing the membranes closer together and allowing membrane fusion.

The HIV-1 envelope protein gp41 comes from the precursor gp160. gp160 is proteolytically cleaved into two subunits, gp120 and gp41 by a cellular convertase. gp120 binds to CD4 and a co-receptor. The binding of gp120 disrupts a gp120/gp41 interaction which leads to a conformational change that forms a pre-hairpin intermediate. The fusion peptide, responsible for linking gp41 to the target cell membrane, is buried prior to the conformational change; subsequently the fusion peptide inserts into the

membrane from the N-terminus of gp41. Finally, a rearrangement occurs to form the trimer-of-hairpins structure in which a gp41 C-terminal helical sequence binds in an antiparallel fashion to the exterior surface of the N-terminal coiled coil. Binding requires the insertion of three C-peptide hydrophobic sidechains (Trp628, Trp631, Ile635) into the pocket formed by the surface residues of the N-terminal coiled coils (Figure 9)[10]. The surface interaction is mediated by the *b* and *e* heptad positions of one helix and the *c* and *g* positions of the other helix.

Figure 9. Crystal structure of gp41. The key binding residues (Trp-Trp-Ile) from the C-peptides are displayed in aqua. They are shown bound in the hydrophobic binding pocket on the N-terminal coiled-coil, shown in yellow.

Because the trimer-of-hairpins structure was required for membrane fusion, it has become an attractive drug target. Although inhibition studies have been successful at elucidating critical interactions between hydrophobic grooves, they have been limited by the aggregation tendencies of the isolated N-terminal trimers. Instead of attempting to model all three trimeric binding grooves, it would be much simpler to only experiment with a single interface, thereby reducing the amount of aggregation that could occur.

The main goal of the viral project was to develop an efficient binding interface mimic. Human Immunodeficiency Virus (HIV), Simian Immunodeficiency Virus (SIV), and visna, the sheep analog, are all lentiviruses that utilize the trimer-of-hairpins motif (Figure 10).

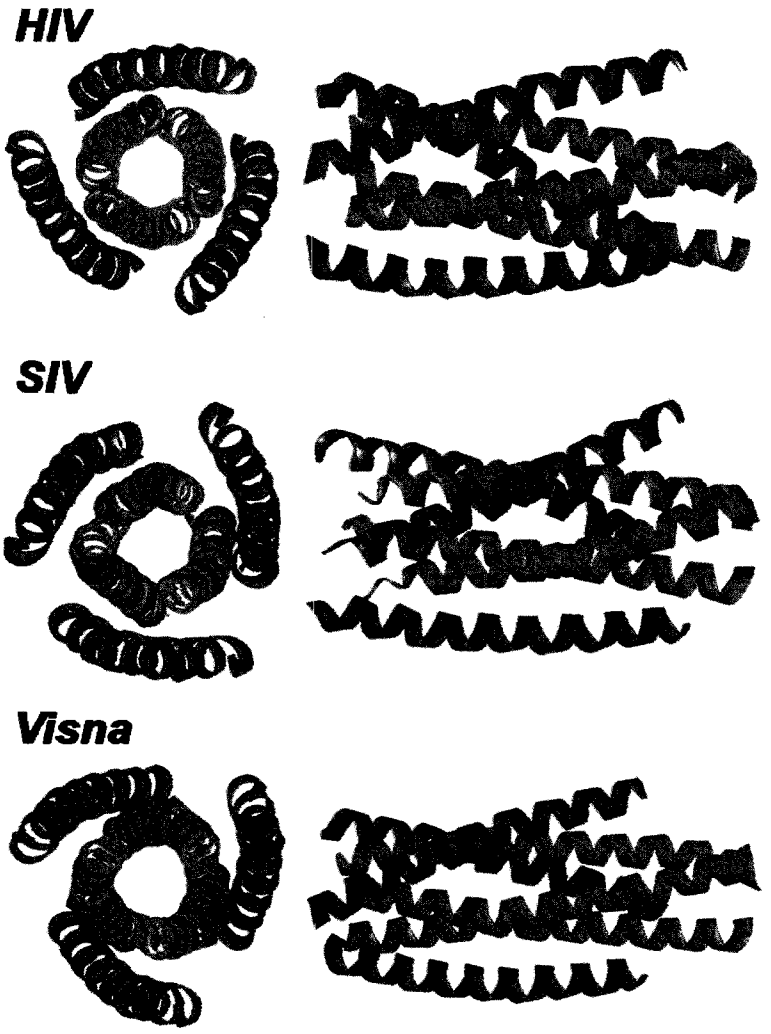

Figure 10. HIV, SIV, and Visna all utilize the same trimer-of-hairpins motif during viral infection. The N-terminal coiled-coil is shown in aqua with the C-peptides bound around it in orange.

The first virus studied in our laboratory was HIV.[11] The heterotrimeric gp41 mimic's primary sequence was based on crystallographic studies by Kim and coworkers.[12] These studies detailed which residues were critical for C-peptide binding. These critical residues were grafted onto one *e/g* interface, which was designed to facilitate ligand peptide, gp41C, binding. It is important to note the heterotrimer contains favorable 2:1 alanine/cyclohexylalanine pairing at three consecutive *a* layers and matched Glu/Lys electrostatic contacts at two *e/g* interfaces (Figure 11).

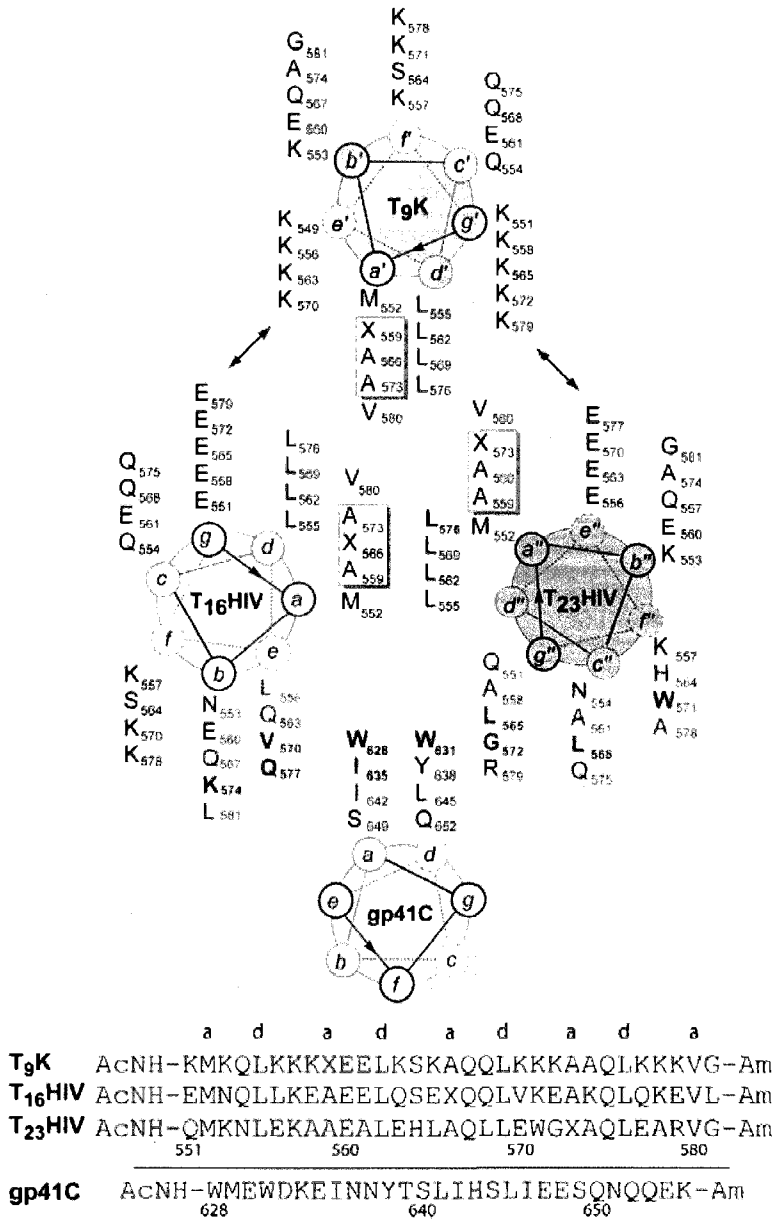

Figure 11. Helical wheel representation and primary sequences of the HIV fusion protein mimic. Critical binding residues are highlighted in red while residues that surround the binding pocket are in green. The conserved Trp, Trp, Ile motif is shown in blue.

Circular dichroism (CD) analysis of the trimer with gp41C showed helicity in significant excess compared to the weighted average of the trimer and ligand peptide alone. This suggests gp41C was binding to the trimer. One would expect the weighted

average signal for two entities that were not interacting during the CD experiments. Control experiments were conducted, by mutating half of the binding pocket. These experiments revealed that the entire trimer was necessary to facilitate ligand binding. Nickel-affinity experiments were used to demonstrate that the trimer bound an equimolar amount of the ligand peptide. Finally, sedimentation equilibrium studies of the trimer and ligand complexes concluded that they bind in a 1:1:1:1 manner, while control trimer with the mutated binding pocket, did not bind the ligand. Overall, these data suggest that grafting the HIV gp41 binding surface onto a well defined coiled-coil heterotrimer generates an efficient mimic capable of recognizing the native ligand.

To this point a self-assembling trimer had been developed and utilized to mimic HIV fusion protein gp41. To determine if this approach to fusion protein mimics was general, I continued these studies with the visna virus. In addition to developing a visna fusion protein mimic, I also implemented a number of new experimental techniques that enabled us to study these systems in a new manner. But I also explored other amino acids, namely phenylalanine, to expand the scope of the original Tic-Tac-Toe system.

1-4: References Cited

(1) (a) Guo, Z.; Zhou, D.; Schultz, P.G. *Science.* **2000**. 2042-2045. (b) Kashiwada, A.; Hiroaki, H.; Kohda, D.; Nango, M.; Tanaka, T. *J. Am. Chem. Soc.* **2000**, *122*, 212-215. (c) Kiyokawa, T.; Kanaori, K.; Tajima, K.; Tanaka, T.; *Biopolymers* **2000**. *55*, 407-414. (d) Nautiyal, S.; Alber, T. *Protein Science*, **1999**, *8*, 84-90. (e) Nautiyal, S.; Woolfson, D.; King, D.; Alber, T. *Biochemistry*, **1995**, *34*, 11645-11651. (f) Lombardi, A.; Bryson, J.; DeGrado, W. *Biopolymers*, **1997**, *40*, 495-504. (g) DeGrado, W.F., et al. *Annu. Rev. Biochem.*, **1999** *68*, 779-819.

(2) (a) Root, M.J.; Kay, M.; Kim, P.S. *Science*, **2001**, *295*, 884-888. (b) Agre, P.; Johnson, P.F.; McKnight, S.L. *Science*, **1989**, *246*, 922-926.

(3) (a) Lumb, K.J.; Kim, P.S. *Biochemistry*, **1995**, *34*, 8642-8648. (b) Harbury, P.B.; Zhang, T.; Kim, P.S.; Alber, T., *Science*, **1993**, *262*, 1401-1407.

(4) O'Shea, E.K.; Klemm, J.D.; Kim, P.S.; Alber, T. *Science*, **1991**, *254*, 539-544.

(5) Jones, E.W.; Fink, G.R. *The Molecular biology of the Yeast Saccharomyces: Metabolism and Gene Expression*, Cold Spring Harbor Laboratory, Cold Spring Harbor, NY, p181-299.

(6) Struhl, K. *Trends Biochem. Sci.*, **1989**, *14*, 137.

(7) Gonzalez, L.; Plecs, J.J.; Alber, T. *Natural Structural Biology*. **1996**, *3*, 510-514.

(8) Schnarr, N.A.; Kennan, A.J. *JACS*, **2001**, *123*, 11081-11082.

(9) (a) Schnarr, N.A.; Kennan, A.J. *JACS*, **2002**, *124*, 9779-9783. (b) Schnarr, N.A.; Kennan, A.J. *JACS*, **2003**, *125*, 667-671. (c) Schnarr, N.A.; Kennan, A.J. *JACS*, **2003**, *125*, 6364-6365. (d) Schnarr, N.A.; Kennan, A.J. *JACS*, **2003**, *125*, 13046-13051.

(10) (a) Markosyan R.M.; Ma, X.; Lu, M.; Cohen, F.S.; Melikyan, G.B. *Virology*, **2002**, *302*, 174-184. (b) Eckert, D.M.; Kim, P.S *Ann. Rev. Biochem.* **2001**, *70*, 777-810.

(11) Schnarr, N.A.; Kennan, A.J. *JACS*, **2004**, *126*, 10260-10261.

(12) Chan, D.C.; Fass, D.; Berger, J.M.; Kim, P.S. *Cell*, **1997**, *89*, 263-273.

Chapter 2

Tuning the Stability of Coiled-Coil Heterotrimers

Extensive studies of natural and model coiled-coils have established firm sequence-structure relationships, including the critical influence of hydrophobic core side chains on stability and aggregation number.[1] Here I describe research I completed on the formation of 1:1:1 coiled-coil heterotrimers whose stability varies over a considerable range, governed by selection of specific hydrophobic core residue patterns. Each independent complex exhibits biophysical signatures expected of well-formed coiled-coil trimers.

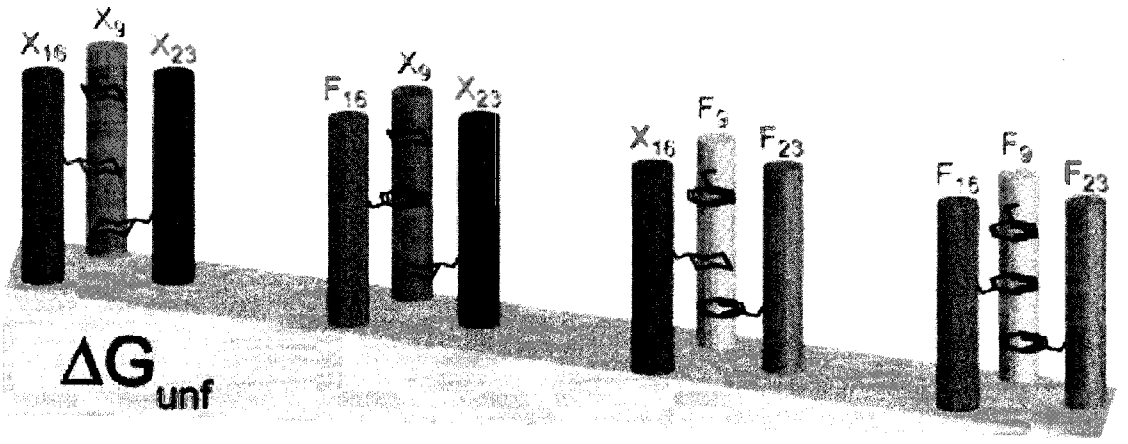

Figure 1. Coiled-coil trimers of differing stability have been designed by judicious choice of hydrophobic core sidechain identity.

2-1: Selection of Steric Matching Partners[2]

We previously described the use of core residue steric matching to control specificity of heterotrimers formation.[3] Favored complexes permit formation of 2:1 alanine-cyclohexylalanine layers at three consecutive *a* positions of the primary sequence heptad repeat (*abcdefg*). To extend the application of this strategy, we have investigated phenylalanine (Phe) as a possible replacement for cyclohexylalanine (Cha) in this arrangement. Besides conferring the potential advantages of purely natural sequences

(e.g., easier *in vivo* expression), such an alternative should allow design of variable-stability trimers by evaluation of mixed-core systems.

The peptides utilized contain alanine at two of the three central core positions (9, 16, 23) and cyclohexylalanine (X_n) or phenylalanine (F_n) at the other (Figure 2). Peptides differ by location of the large side chain (either Cha or Phe), so that a 1:1:1 trimer of X_9:X_{16}:X_{23} or F_9:F_{16}:F_{23} has three sterically matched core layers (two Ala and one Cha/Phe at each layer).

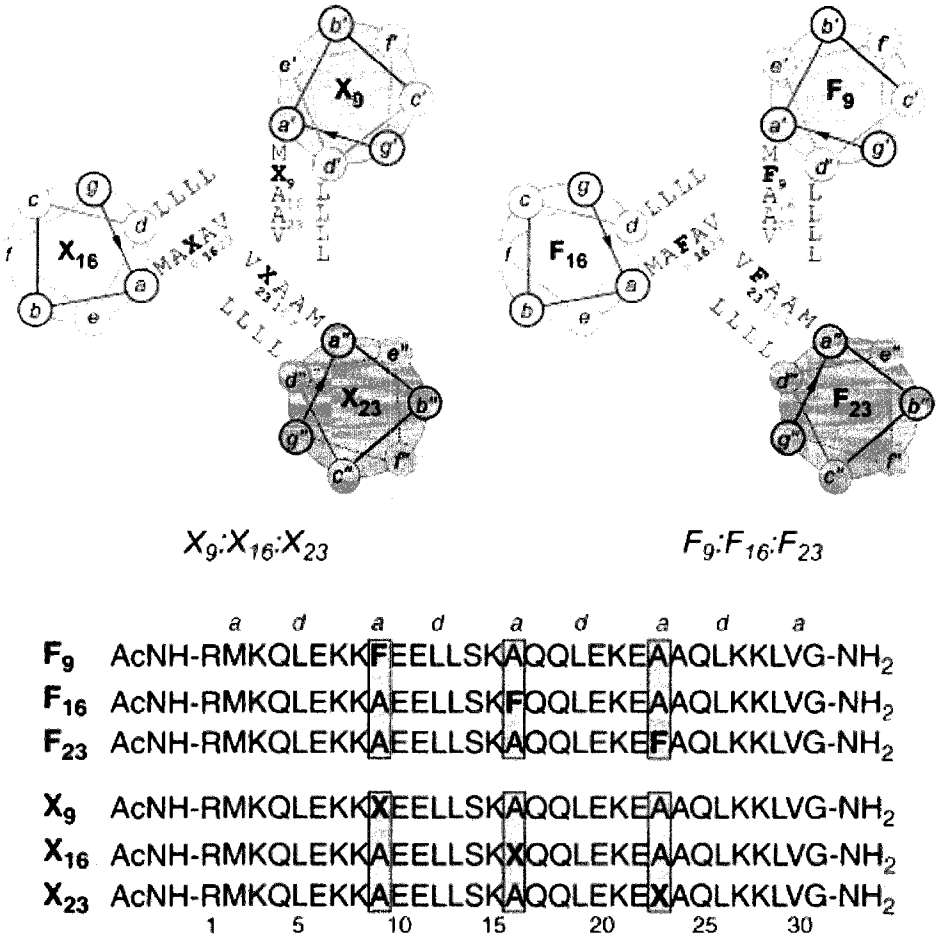

Figure 2. Peptide sequences and helical wheel projections. F_n and X_n peptides have phenylalanine or cyclohexylalanine, respectively, at the indicated positions and alanine at the other two central core *a* layers (modified layers are marked by shaded boxes). Projections of F_9:F_{16}:F_{23} and X_9:X_{16}:X_{23} heterotrimers are also given. Nonhydrophobic core residues are omitted for clarity.

2-2: Structural Analysis of the Phenylalanine Matched Core System

Circular dichroism (CD) analysis of a 1:1:1 F_9:F_{16}:F_{23} mixture revealed the high helicity and cooperative thermal denaturation profile expected of coiled-coils (Figure 3). In contrast, pure solutions of F_9, F_{16}, and F_{23} display dramatically reduced helical structure.

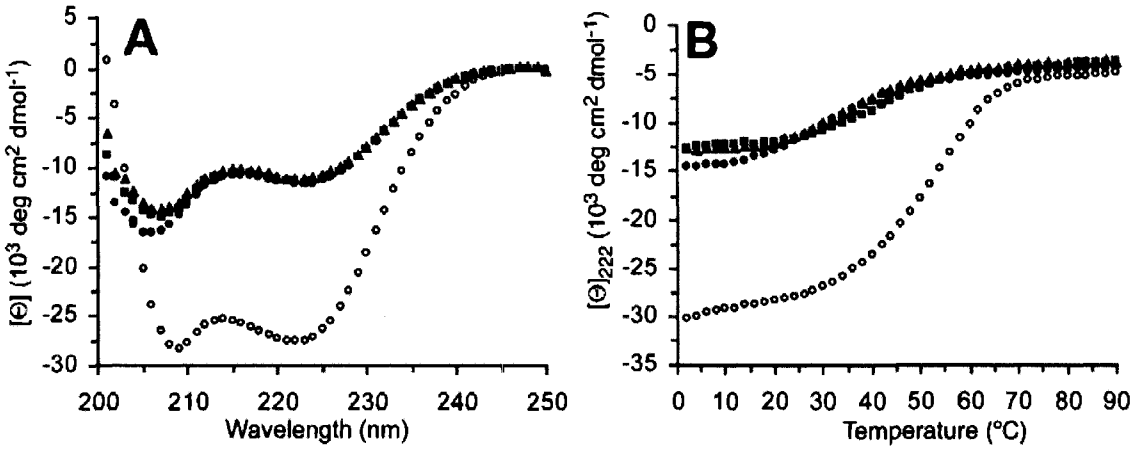

Figure 3. CD analysis of Phe-substituted peptides. Wavelength (A) and thermal unfolding (B) data for F_9 (squares), F_{16} (triangles), F_{23} (circles), and a 1:1:1 F_9:F_{16}:F_{23} mixture (open circles).

Verification of designed trimer stoichiometry was executed using a nickel-nitrilotriacetic acid (Ni-NTA) affinity tagging experiment. The F_{16} peptide was derivatized with a Gly-Gly-$(His)_6$ tag, producing a new sequence (T_{16his}) that binds Ni-NTA agarose beads. Exposure of an initial 1:1:1 F_9:F_{16his}:F_{23} solution to the beads, followed by rinsing to remove nonspecific binders and elution with imidazole buffer afforded an elution fraction containing 1 equivalent of each peptide (Figure 4). This result supported the proposed 1:1:1 stoichiometry between the three peptides.

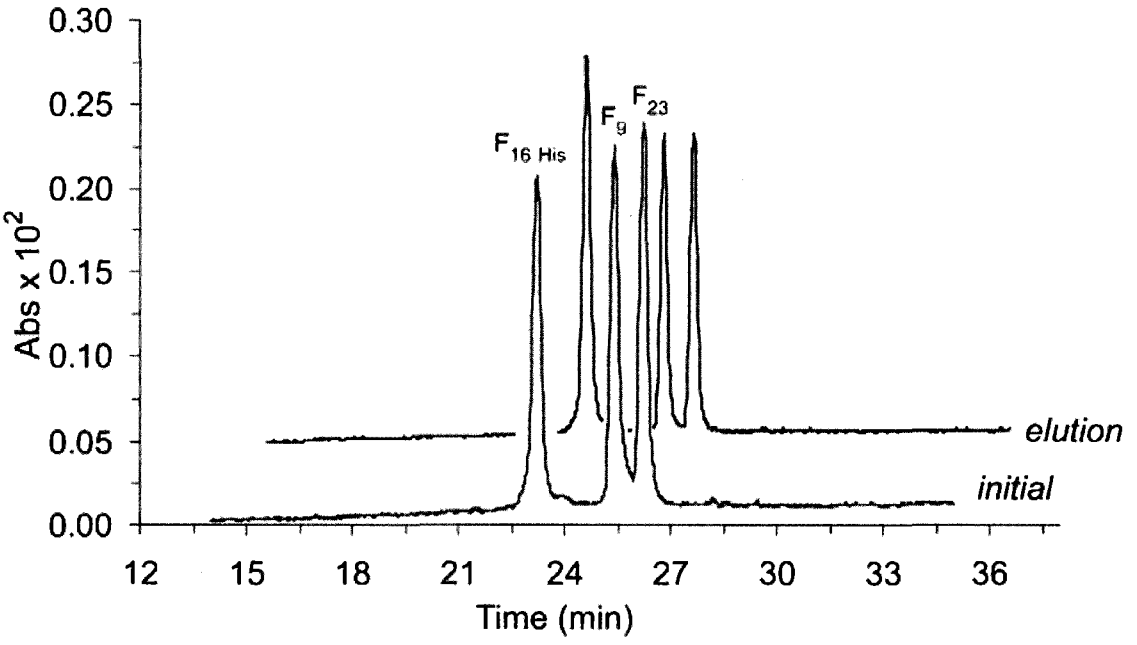

Figure 4. Ni-NTA analysis of F_9:F_{16}:F_{23} complex stoichiometry. HPLC traces of initial 1:1:1 solution along with elution fraction demonstrating retention of one equivalent of each untagged peptide.

2-3: Development of Mixed Core Systems

Having established the feasibility of phenylalanine/alanine steric matching, we turned to the investigation of mixed core systems, in which both phenylalanine and cyclohexylalanine are present, in varying ratios. Equimolar mixtures of F_9:F_{16}:F_{23}, F_9:X_{16}:F_{23}, X_9:F_{16}:X_{23}, and X_9:X_{16}:X_{23} should form heterotrimers with only Phe, Phe/Cha/Phe, Cha/Phe/Cha, and only Cha side chains, respectively, at the three core *a* layers (Figure 5). We hypothesized that such combinations would provide a facile method for tuning heterotrimers stability without sacrificing specificity.

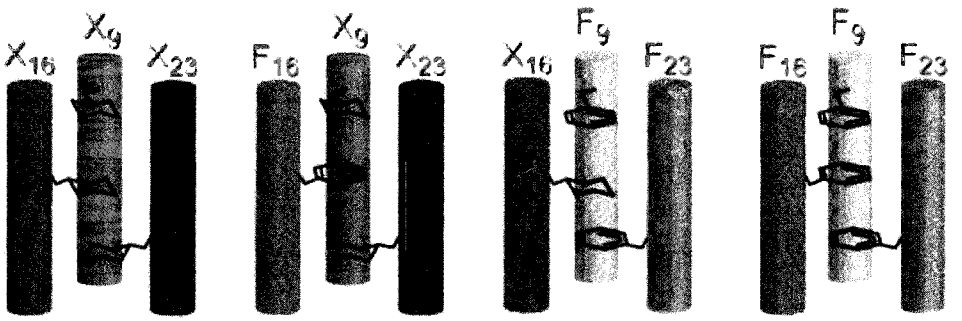

Figure 5. Schematics of mixed core systems. Large side chains at each of the three modified core layers are depicted. Each layer also contains two small alanine side chains (not shown). Other core layers (including intervening *d* layers) and all noncore positions have been omitted for clarity.

Through CD experiments it was demonstrated that all four mixed core trimers exhibited similar helicity, but their thermal stabilities varied inversely with the number of Phe residues (Figure 6). Although all four display cooperative unfolding profiles consistent with stable structures, the observed melting temperatures are spread fairly evenly over about a 20 °C range (Table 1).

sample	T_m (°C)	ΔG_{unf} (kcal/mol)	$M_{r\ obsd}$	$M_{r\ calcd}$
F_9:F_{16}:F_{23}	61	16.27 ± 0.25	10 900	11 535
F_9:X_{16}:F_{23}	67	17.74 ± 0.36	11 400	11 541
X_9:F_{16}:X_{23}	73	18.05 ± 0.28	11 600	11 547
X_9:X_{16}:X_{23}	83	19.60 ± 0.21	10 200	11 556

Table 1. Sedimentation Equilibrium and Thermodynamic Data

Further characterization was conducted by chemical denaturation (Figure 7). Each complex displayed a cooperative unfolding transition, with significant variation between the samples (Table 1). Unfolding free energies differed by over 3 kcal/mol between the most and least stable assemblies, and the correlation with Phe content held true. The all

Phe complex, F_9:F_{16}:F_{23}, was the least stable at 16.27 kcal/mol, while the all Cha complex, X_9:X_{16}:X_{23}, was the most stable at 19.60 kcal/mol.

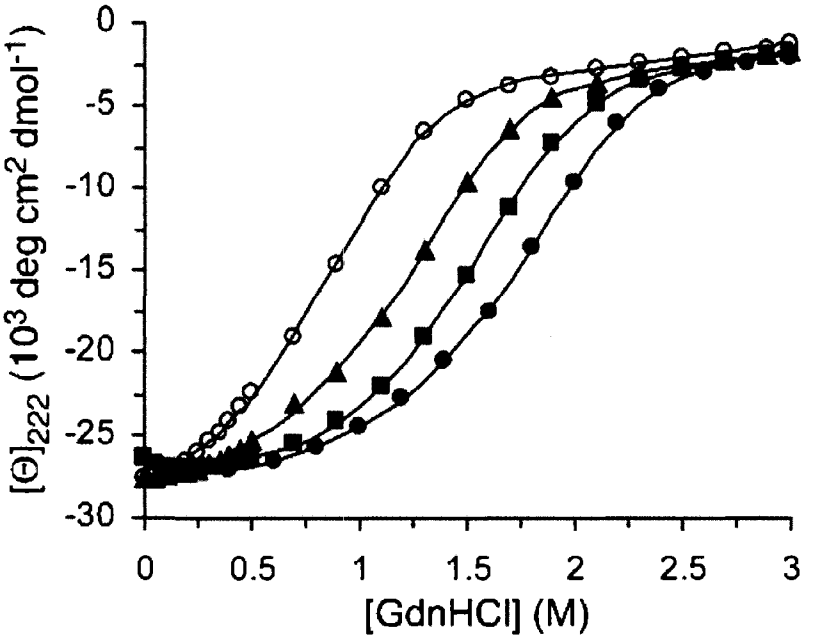

Figure 7. GdnHCl denaturation profiles for 1:1:1 X_9:F_{16}:X_{23} (squares), F_9:X_{16}:F_{23} (triangles), X_9:X_{16}:X_{23} (circles, and F_9:F_{16}:F_{23} (open circles). Lines are fits to the data; for unfolding free energies, see Table 1.

Considerable stability variance can indeed be programmed simply by selection of the core makeup. The stability variance appeared to be context independent. Wavelength and thermal melt data are very similar for all possible single Cha trimers (X_9:F_{16}:F_{23}, F_9:X_{16}:F_{23}, F_9:F_{16}:X_{23}) (Figure 8).

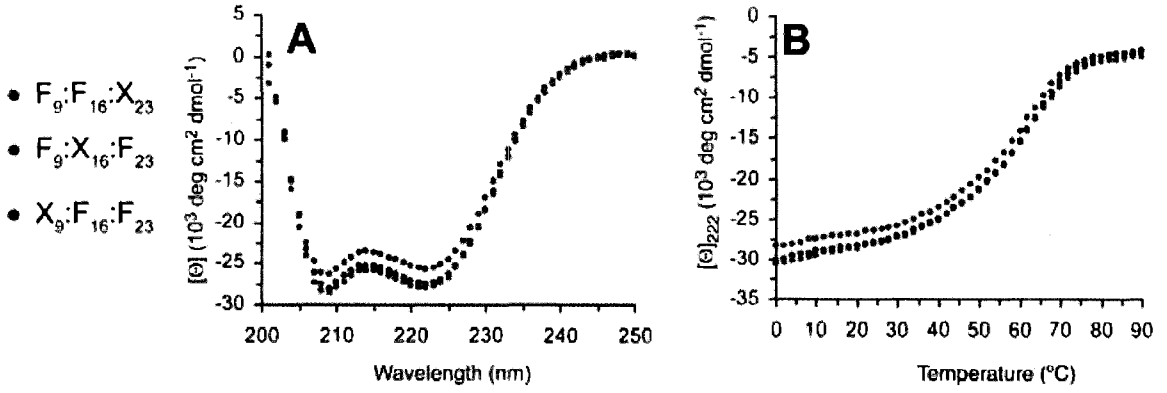

Figure 8. Wavelength scan (**A**) and thermal denaturation (**B**) CD data for equimolar solutions of X_9:F_{16}:F_{23} (blue), F_9:X_{16}:F_{23} (red), and F_9:F_{16}:X_{23} (green).

Final confirmation of trimeric assemblies was obtained by analytical ultracentrifugation. Each of the three Phe containing complexes (F_9:F_{16}:F_{23}, F_9:X_{16}:F_{23}, X_9:F_{16}:X_{23}) give observed reduced mass values consistent with those calculated for the appropriate trimer molecular weights (Table 1). This was consistent with results for the all Cha trimer (X_9:X_{16}:X_{23}).

Overall, these data confirm that phenylalanine side chains can assume the role of large hydrophobic groups in a 2:1 small:large matching scheme. Although increasing Phe content gradually diminishes complex stability, even the F_9:F_{16}:F_{23} assembly remains a perfectly viable trimeric coiled-coil. Thus, in addition to providing an alternative to cyclohexylalanine for controlling trimer assembly, introduction of phenylalanine side chains established a mechanism for smooth variation in complex stability without sacrificing specificity. Such systems could be useful in various applications such as peptidic drug delivery systems where thermal triggering of trimer disassembly at tunable

temperatures is desired. Another application would be to use the F_9:X_{16}:F_{23} trimeric complex as a linchpin to bring two expressed proteins together in solution (Figure 9).

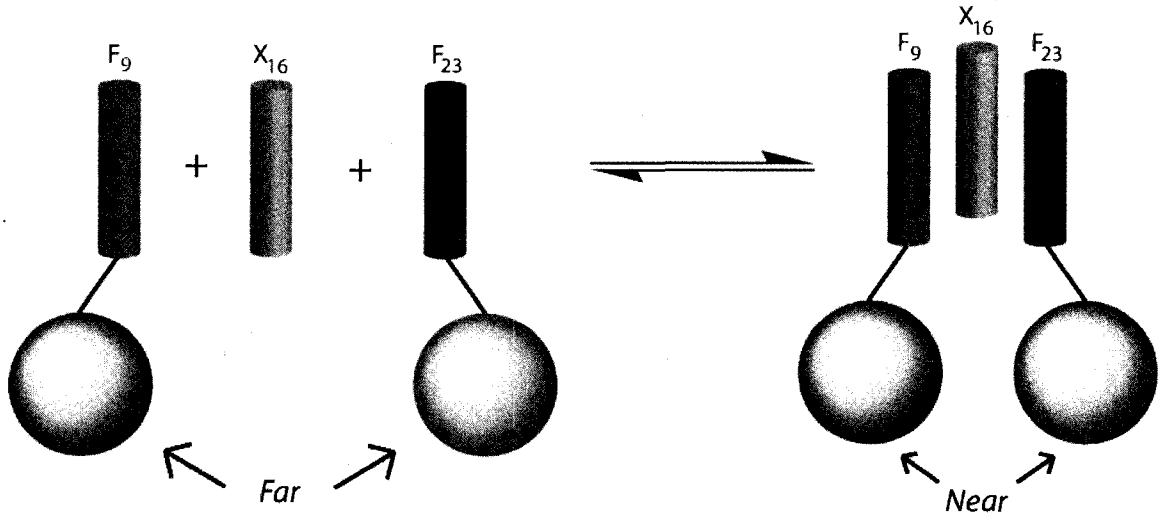

Figure 9. F_9:X_{16}:F_{23} complex as linchpin for protein-protein interactions. Without the X_{16} peptide, the two proteins (red and purple spheres) will be separated in solution. Upon addition of the X_{16} peptide and trimer formation the two proteins should approach each other in solution.

The F_9 sequence can be derivatized to a particular protein sequence and the F_{23} sequence can be appended to a different protein. Upon the addition of the X_{16} peptide to a mixture of the two expressed proteins, one would expect trimer formation, thereby bringing the two proteins in close proximity to each other at relatively low protein concentration.

2-4: Experimental Section

Peptide Synthesis. Amino acids (including cyclohexylalanine) were obtained from NovaBiochem (San Diego). Peptides were synthesized according to the *in situ* neutralization protocol developed by Kent.[4] Each peptide was purified by reverse-phase HPLC (C-18 column, solvent A: 1% CH_3CN in H_2O, 0.1% (v/v) CF_3CO_2H; solvent B: 10% H_2O in CH_3CN, 0.07% (v/v) CF_3CO_2H), and the identity of purified peptides was confirmed by electrospray mass spectrometry (Finnegan LCQ-Duo). All peptides are C-

terminally amidated and N-terminally acetylated; each contains an acetamidobenzoate group on the sidechain nitrogen of a solvent-exposed lysine as a spectroscopic label.

Circular Dichroism Spectroscopy. All experiments were performed on an Aviv model 202 circular dichroism spectrometer. Equipped with a Microlab 500 series automated titration assembly. Sample concentrations were measured by UV absorbance of the acetamidobenzoate label at 270 nm. Wavelength data are the average of three scans from 250 to 200 nm in 1 nm steps. Thermal denaturation experiments monitored at 222 nm were run from 0° to 90°C in two-degree steps, at a two-degrees/minute rate of increase with one-minute equilibration and data averaging at each temperature. T_m values were obtained from minima of the first derivative of θ vs. 1/T plots.[5] Guanidinium titrations were performed using the automated titration assembly. The signal at 222 nm was recorded for solutions of constant peptide concentration with guanidine hydrochloride concentrations varied from 0 to 3 M. Data were collected for one minute at each step, with ten-minute equilibrium times (solutions were stirred during equilibration but not data collection).

Analytical Ultracentrifugation. Sedimentation equilibrium experiments were performed using a Beckman XL-I analytical ultracentrifuge equipped with an An60-Ti rotor. Data were collected using 12 mm path length six-sector centerpieces at 270 nm. Samples were dialyzed against the reference buffer at 4 °C overnight. Data were collected at 38,000 and 48,000 r.p.m. at concentrations spanning 17-55 μM. Samples were equilibrated at 38,000 r.p.m. for 16 hours, followed by the collection of two scans

four hours apart. The speed was then increased to 48,000 r.p.m., followed by a 16 hour equilibration, and collection of two scans four hours apart, as before. Each scan consisted of 10 replicates at 0.002 cm radial steps. Solvent densities and partial molar volumes were calculated in the manner prescribed by Laue.[6] Data were analyzed using Origin and fit to ideal single-species models.

Guanidine Denaturation Fit. Guanidine denaturation profiles were obtained on an Aviv model 202 circular dichroism spectrometer equipped with a Microlab 500 series titrator. A 10 μM solution of peptide in PBS buffer (10 mM Phosphate, 150 mM NaCl, pH=7.4) was titrated with a second solution identical to the first but containing 6 M guanidine hydrochloride (GdnHCl). The raw data were converted to mean residue elipticity (MRE) and fit using the model outlined below.

Observed MRE values (θ_{obs}) were fitted assuming that folded and unfolded baselines are linear functions of denaturant concentration:

$$\theta_{obs} = f_u(\theta_u + a[GdnHCl]) + (1 - f_u)(\theta_f + b[GdnHCl]) \qquad (1)$$

Where f_u = fraction unfolded, θ_u) and θ_f) are MREs of unfolded and folded peptides, and a and b are parameters describing the guanidine dependence of the observed unfolded and folded baselines. The fraction unfolded is calculated according to equation (2), assuming a monomer-trimer equilibrium with equilibrium constant K_{unf}.

$$f_u = \sqrt[3]{k\left(\frac{1}{2}+\frac{\sqrt{3}\sqrt{4k+27}}{18}\right)} - \frac{1}{3}\frac{k}{\sqrt[3]{\frac{1}{2}+\frac{\sqrt{3}\sqrt{4k+27}}{18}}} \qquad (2)$$

where:

$$k = \frac{K_{unf}}{27C_{tot}^2} \qquad (3)$$

and C_{tot} = [trimer] = 1/3 [total peptide].[7] The equilibrium constant, in turn, is calculated from the observed unfolding energy, assuming a linear extrapolation model in which the true folding energy (ΔG_{H2O}) is assumed to be a linear function of the observed value and the denaturant concentration (equation 4).[8]

$$K_{unf} = e^{\frac{-\Delta G_{H_2O}}{RT}} \qquad \Delta G_{H_2O} = \Delta G_{obs} + m[GdnHCl] \qquad (4)$$

The observed data were fit using this model and a non-linear least squares fit, with ΔG_{H2O}, θ_u, θ_f, a, b, and m as the parameters, employing a Microsoft Excel macro.[9] Error estimates were calculated according to another macro by de Levie.[10]

Ni-NTA Affinity Tag Experiments (Figure 10). A 0.5 mL sample of a 50% slurry of Ni-NTA agarose (Qiagen) in an Eppendorf tube was centrifuged for 30 s, followed by removal of the supernantant. Peptide solution was added, and the tube was repeatedly

inverted for 5 min. The sample was centrifuged (30 s), and the supernatant (flow-through fraction) was removed. The procedure was then repeated with 1 mL of buffer (wash fraction) and 1 mL of buffer containing 250 mM imidazole (elution fraction), except that the wash fraction was not agitated for 5 min. Solutions were analyzed by reverse-phase HPLC. All solutions were 10 μM in total peptide concentration.

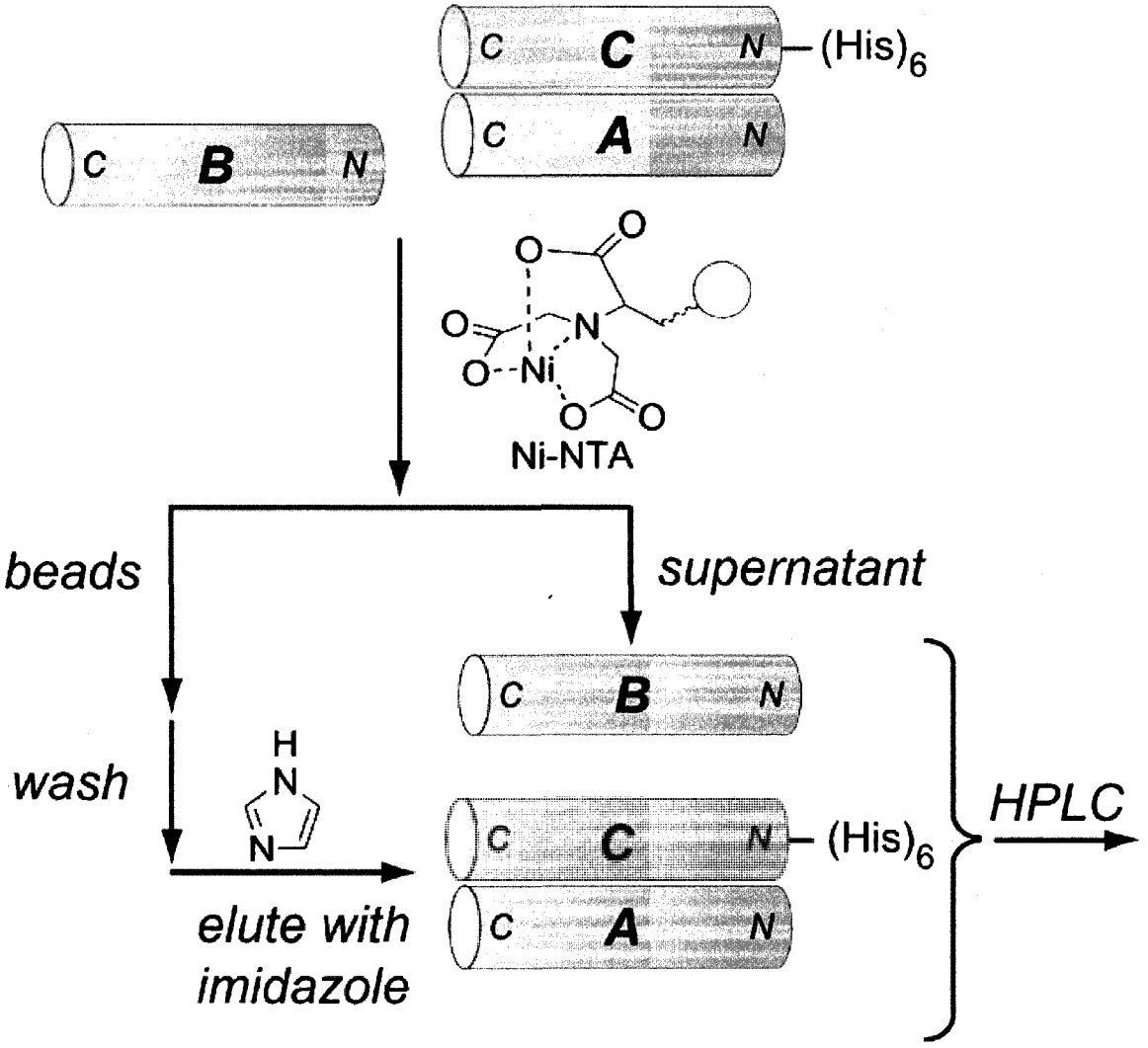

Figure 10. Ni-NTA affinity tag analysis scheme. Initially, peptide **A** is specifically bound to peptide **C**, which bears an N-terminal Gly-Gly-$(His)_6$ affinity tag. Upon exposure to Ni-NTA agarose beads, peptide **C** is bound to the agarose beads through the His tag, and peptide **A** is bound through it's interaction with peptide **C**. Only peptide B, which does not interact with the beads or the his tagged peptide, remains unbound. After supernatant removal and washing with blank buffer, bound material is eluted by treatment with imidazole buffer solution. HPLC analysis reveals the identity of unbound (supernatant fraction) and bound (elution fraction) material. Peptides A and B are intended to represent all binding and non-binding peptides, respectively. Thus any higher order aggregates are analyzed in the same manner.

2-5: References Cited

(1) (a) Kwok, S.C.; Hodges, R.S. *J. Biol. Chem.* **2004,** *279*, 21576-21588. (b) Ibarra-Molero, B.; Zitzewitz, J.A.; Matthews, C.R. *j. Mol. Biol.* **2004**, *336*, 989-996. (c) Walshaw, J.; Wollfson, D.N. *Struct. Biol.* **2003**, *144*, 349-361. (d) Kohn, W.D.; Kay, C.M.; Hodges, R.S. *J. Mol. Biol.* **1998**, *283,* 993-1012. (e) Harbury, P.B.; Zhang, T.; Kim, P.S.; Alber, T. *Science* **1993**, *262*, 1401-1407. (f) O'Shea, E.K.; Klemm, J.D.; Kim, P.S.; Alber, T. *Science* **1991**, *254*, 539-544.

(2) Travisano, P.; Kennan, A.J. *Org. Lett.* **2004**, *6,* 4219-4222.

(3) (a) Schnarr, N.A.; Kennan, A.J., *J. Am. Chem. So..*, **2001**, *123*, 11081-11082. (b) Schnarr, N.A.; Kennan, A.J., *J. Am. Chem. Soc.*, **2002**, *124*, 9779-9783. (c) Schnarr, N.A.; Kennan, A.J., *J. Am. Chem. Soc.*, **2003**, *125*, 667-671. (d) Schnarr, N.A.; Kennan, A.J., *J. Am. Chem. Soc.*, **2003**, *125*, 6364-6365. (e) Schnarr, N.A.; Kennan, A.J., *J. Am. Chem. Soc.*, **2003**, *125*, 13046-13051.

(4) Schnoelzer, M.; Alewood, P.; Jones, A.; Alewood, D.; Kent, S.B.H. *Int. J. Pept. Protein Res.* **1992**, *40,* 180-193.

(5) Cantor, C.R.; Schimmel, P.R. *Biophysical Chemistry of Macromolecules, Pt. 3: The Behavior of Biological Macromolecules*; W.H. Freeman: New York, NY, 1980, p.1132.

(6) Laue, T.M.; Shah, B.D.; Ridgeway, T.M.; Pelletier, S.L. in *Analytical Ultracentrifugation in Biochemistry and Polymer Science*; Harding, S.E., Rowe, A.J., Horton, J.C., Eds.; The Royal Society of Chemistry: Cambridge, 1992; pp 90-125.

(7) Jelesarov, I; Lu, M. *J. Mol. Biol.*, **2001**, *307*, 637-656.

(8) (a) Santoro, M.M.; Bolen, D.W. *Biochemistry* **1988,** *27*, 8063-8068. (b) Becktel, W.J.; Schellman, J.A. *Biopolymers* **1987**, *26*, 1859-1877.

(9) Harris, D.C. *J. Chem. Educ.* **1998**, *75*, 119-121.

(10) De Levie, R. *J. Chem. Educ.* **1999**, *76*, 1594-1598.

Chapter 3

Design of a Visna Fusion Protein Mimic

HIV, SIV, and visna depend on coiled-coil surface recognition for viral infectivity. The fusion mechanism for lentiviruses highlights the important role that peptides play in viral entry (Figure 1).[1] Because the trimer-of-hairpins structure is required for membrane fusion, it has become an attractive drug target.[2] Our goal was to develop an efficient binding interface mimic. The first virus undertaken was HIV.[3] Using that successful model as a foundation we designed an interface mimic for the visna virus.

3-1: Designed Visna Fusion Protein Mimic

According to X-ray crystal structure studies performed by Kim and co-workers, the visna virus undergoes a similar viral infection pathway to that of HIV (Figure 1).[4]

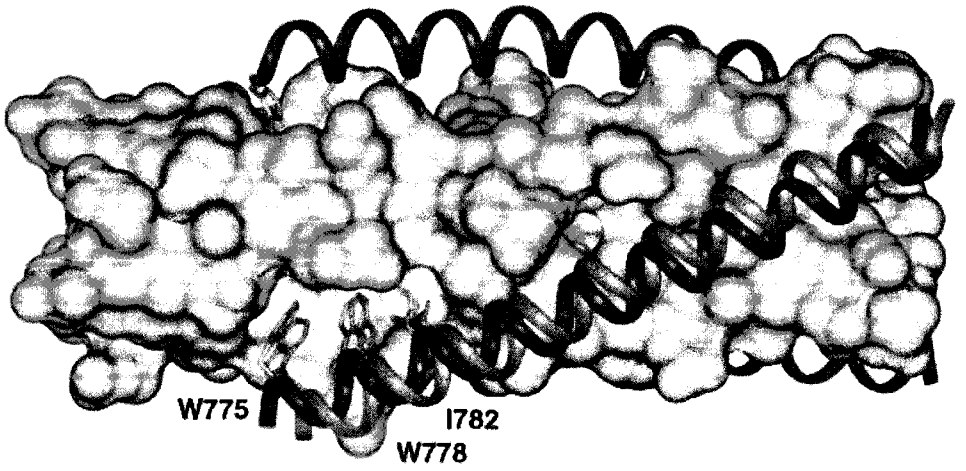

Figure 1. Crystal structure for visna trimer-of-hairpins. The coiled-coil was represented as a molecular surface with the hydrophobic binding pocket shaded yellow. With the N-terminal coiled-coils superimposed, two different C-terminal peptides are shown. The visna peptides are light blue and the HIV C-terminal peptides are shown in light green. This illustrates the similarities between the two viral infection pathways.

Hence it utilizes a trimer-of-hairpins motif in order to facilitate membrane fusion during viral entry. Utilizing the tic-tac-toe system to garner self-assembly we grafted the natural visna binding pocket onto the interface between the T_{16} peptide and the T_{23} peptide of the Tic-Tac-Toe self-assembly system. The helical wheel diagram illustrates the binding

pocket on the trimer (Figure 2). All important residues identified by Kim and co-workers are highlighted in red. The green residues surround the critical amino acids, and the important Trp, Trp, Ile sequence is highlighted in blue on the ligand peptide.

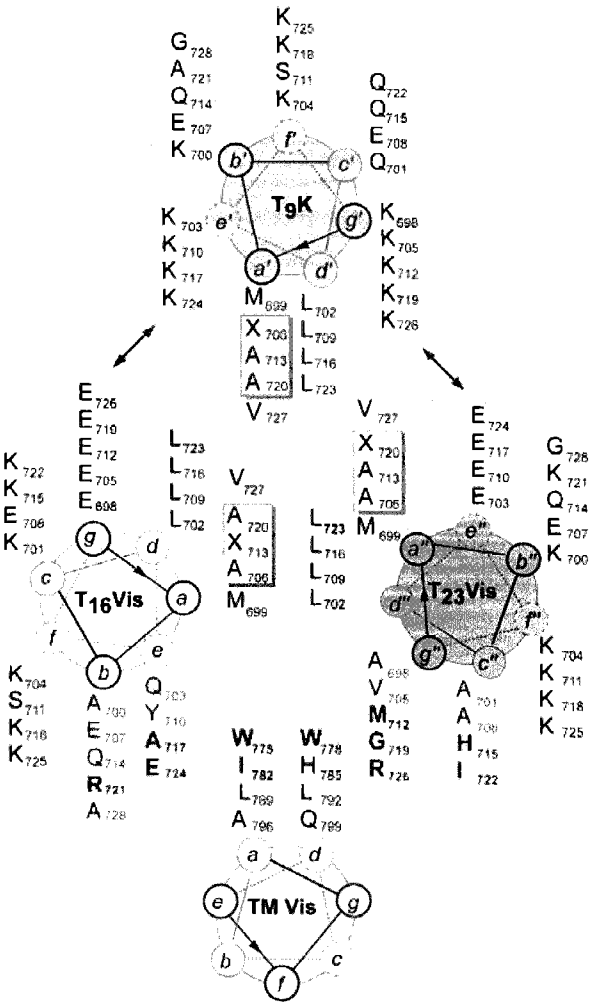

Figure 2. Visna helical wheel diagram with primary sequences. Critical amino acids needed for binding in red. Amino acids that flank the critical ones are green. And the key Trp, Trp, Ile highlighted in blue on the ligand.

For the new visna system the trimer peptides were labeled T_9K, $T_{16}Vis$, $T_{23}Vis$ and the ligand peptide was TM Vis. The other two interfaces, one between T_9K and $T_{16}Vis$, and the other between T_9K and $T_{23}Vis$, were electrostatically matched with lysine and glutamic acid amino acids. These two interfaces assisted in solubilizing the trimer and discouraging aggregation.

The incorporation of the natural sequences from the visna virus brought a new set of challenges for understanding the extinction coefficients of the peptides. Previously all designed tic-tac-toe peptides contained an acetamidobenzoate group (Aba) as a spectroscopic tag. The extinction coefficient of a peptide with this tag was known to be 18069 at 270 nm, but this value was true only if there are no other amino acids in the peptide that absorb light at that wavelength. The TM Vis peptide contained two tryptophans which are known to absorb light around 270 nm. Upon calculating the extinction coefficient by ProtParam,[5] it was found that the untagged peptide would have an extinction coefficient of 11160 at 280 nm. This calculated extinction coefficient value was added to the known 18069 value for the Aba tag, and the final extinction coefficient became 29229 at 270 nm.

This extinction coefficient was indirectly confirmed through NMR experiments with 2,2-dimethyl-2-silapentane-5-sulfonic acid (DSS) as an internal standard (Appendix 1).[6] DSS was a popular internal standard for use with peptides and proteins because of its high water solubility. Because of the low electronegativity of the silicon, the three identical methyl groups were extremely shielded, and they yielded a characteristic singlet with a chemical shift of 0.0.

In this experiment an unknown concentration of peptide was added to a known concentration of DSS. A one-dimensional proton NMR study was conducted on the peptide/DSS sample, and the integration of the aromatic protons from the peptide could be directly related to the integration of the singlet for the three methyl groups on DSS. By knowing the concentration of DSS in solution one can calculate the concentration of peptide in the solution. Using Beer's law one can back-calculate from the absorbance of the solution the extinction coefficient of the peptide.

Although there were numerous literature precedents for using DSS as an NMR internal standard, this experiment was repeated using T_9K in order to test the validity of the procedure. T_9K was well characterized and understood to have an extinction coefficient of 18069 at 270 nm. The internal standard NMR experiment was validated by confirming the extinction coefficient for T_9K as 18069 at 270 nm.

3-2: Proof of Principle: Visna Ligand Binding

Once the extinction coefficients had been elucidated, CD experiments commenced on the visna mimic. T_9K, $T_{16}Vis$, and $T_{23}Vis$ were mixed in equimolar amounts and studied with CD to determine if a helical structure was forming. The equimolar mixture of the three peptides showed a classical α-helical trace with minima at 208 nm and 222 nm (Figure 3).

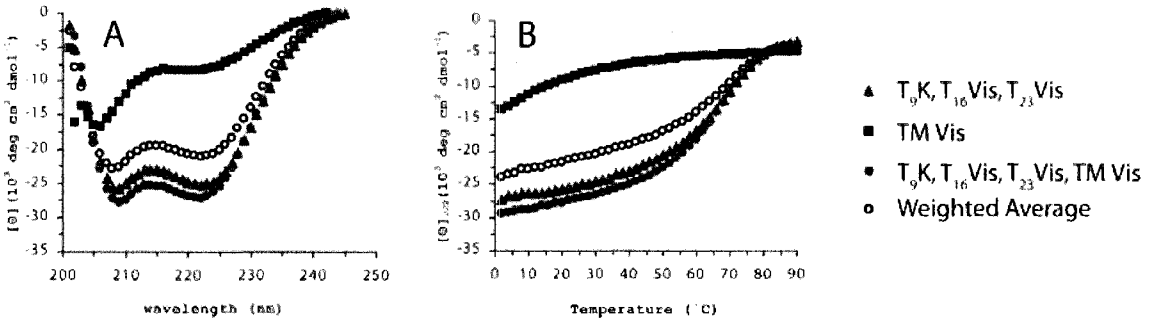

Figure 3. CD analysis for visna mimic. Wavelength (**A**) and thermal unfolding (**B**) data for visna trimer (green triangles), ligand (blue squares), trimer plus ligand complex (red circles), and weighted average of trimer signal and ligand signal (open black circles).

A solution of only the TM Vis peptide gave a random coil signature. The truly exciting experiment was that involving the equimolar mixture between the visna trimer and the ligand. If the two constituents were not interacting during the CD experiment one would expect to see a signal around the weighted average of the two individual CD signals. Fortunately that was not the result; the CD signal for the trimer plus the ligand was much greater that that of the weighted average. In fact, the signal for the trimer plus ligand was more helical than the signal for the trimer only, and this implies that the ligand becomes helical upon binding.

Although the CD experiments illustrated that the ligand was interacting with the trimer in a favorable manner and the complex was helical, they yielded little definitive information about the stoichiometry of the complex. Ni-NTA affinity experiments were conducted on both the trimer and the trimer plus the ligand. In both sets of experiments the T_9K was labeled with a six histidine tag, T_9K_{his}. For the trimer alone, all three peptides were mixed in an equimolar ratio and after the affinity experiment the elution fraction contained all three in an equimolar ratio (Figure 4).

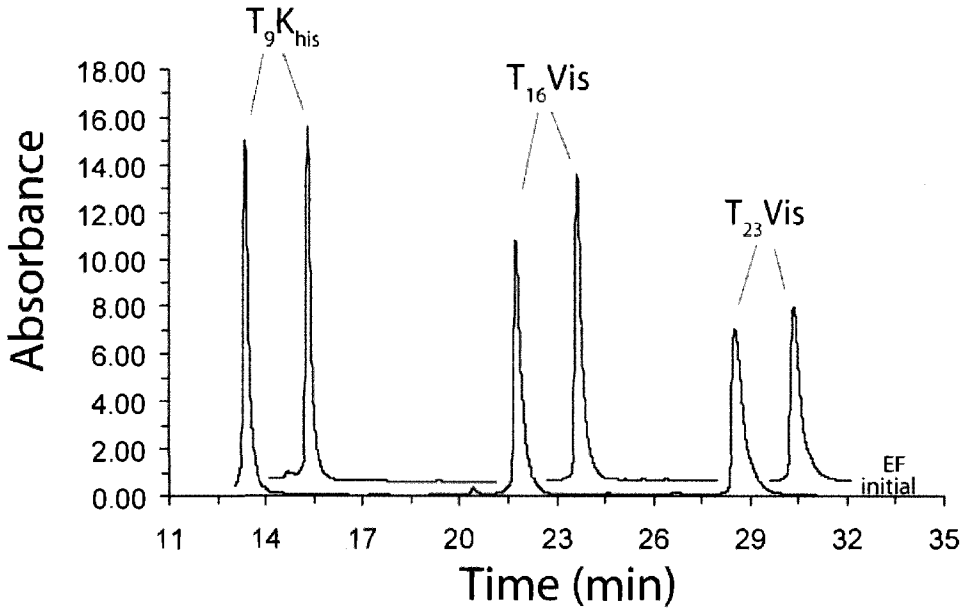

Figure 4. Ni-NTA affinity tag experiment for the visna trimer. T_9K_{his} with its two trimer binding partners T_{16}Vis and T_{23}Vis retained in the elution fraction.

This result supports the fact that the trimer was self-assembling in solution. The affinity experiment with the trimer plus ligand revealed that the ligand binds to the trimer in an equimolar ratio (Figure 5). The three trimer peptides had the same extinction coefficient; hence, the HPLC chromatographs show that the integration for each of their peaks was equal. The ligand had a greater extinction coefficient so its HPLC peak integration was much larger than those of the trimer peptides. Once the integrations were corrected for the varying extinction coefficients it was determined that the elution fraction molar ratios were equal.

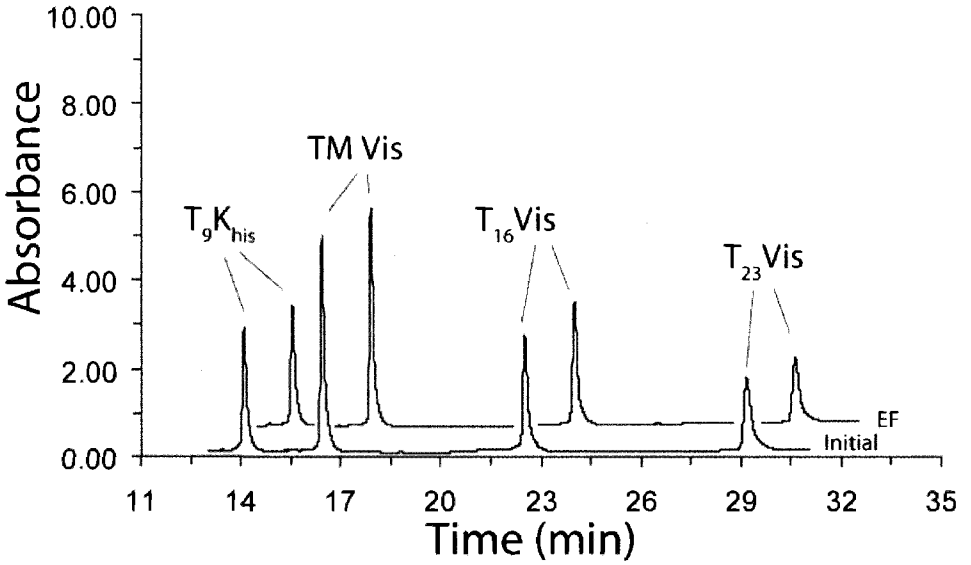

Figure 5. Ni-NTA affinity tag experiment for the visna trimer plus ligand. T_9K_{his} retained three binding partners T_{16}Vis, T_{23}Vis, and TM Vis in the elution fraction. Because of the greater extinction coefficient of TM Vis the ligand peak was larger than the three trimer peaks. When corrected for the difference in extinction coefficient the ratios between the four peptides were equal.

Another experiment used to test the stoichiometry between the trimer and ligand was a continuous variation plot on the CD.[7] In this experiment seven solutions of varying trimer-to-ligand ratios were analyzed by CD wavelength scans. The solutions varied from all trimer (1.0) to all ligand (0.0). The solutions were labeled by the mole fraction of trimer. The 222 nm helicity was plotted against the mole fraction of trimer in solution. Since the helicity of the system increased with the binding of the ligand one would expect the most helical signal from the correct stoichiometry. If the stoichiometry between the trimer and the ligand were correct, one would expect the most helical data point to be located at 0.5. If the stoichiometry between the trimer and ligand was incorrect, one would expect the minimum to occur at different solution.

The continuous variation plot for the visna trimer and the ligand supported the hypothesis that the stoichiometry between the two components was correct (Figure 6). The data points between 1.0 and 0.5 fell near each other so it was very difficult to

conclude too much from the data, other than that the ligand in solution appeared to be bound. After the 0.5 data point the helicity took a sharp decline. Because the ligand was a random coil in solution alone, this sharp decline indicated that there was an excess of unbound ligand. Overall this supported the idea that the stoichiometry between the trimer and ligand was correct.

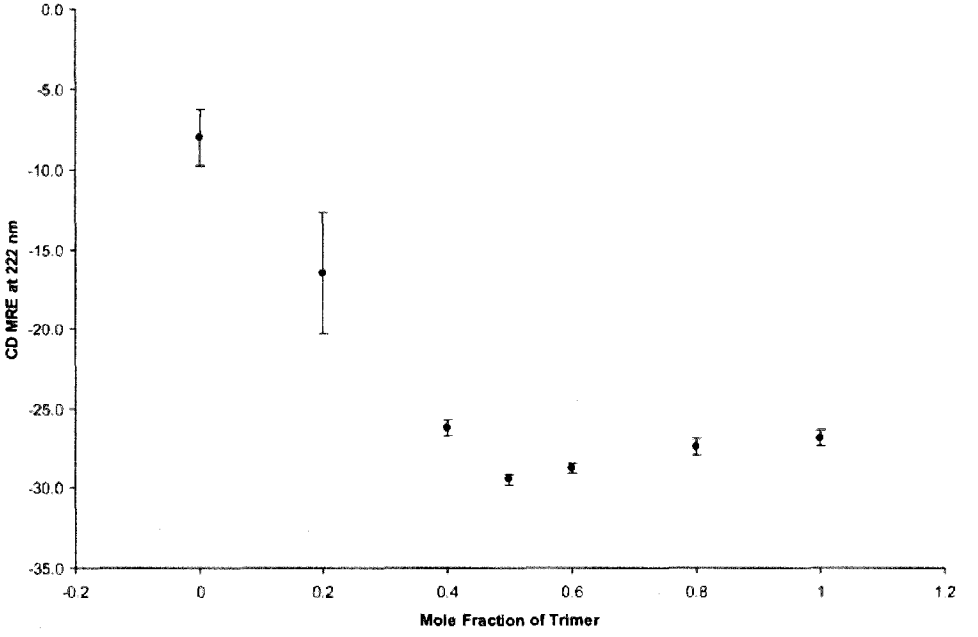

Figure 6. Continuous variation plot for visna trimer and ligand. Increasing the amount of ligand in the solution increased the standard deviation of the data. The 0.2 data point proved to be extremely difficult to analyze because of abnormally low trimer concentration.

With a well-behaved trimer that bound the ligand, analytical ultracentrifugation (AUC) was used to confirm the molecular weights of the complexes in solution. Analysis of the AUC data for the trimer gave an apparent molecular weight of 11700 daltons, which was only 2.3 % from the expected value of 11433 daltons. The trimer plus ligand AUC experiment yielded an apparent molecular weight of 15100 daltons, which was 0.8 % from the expected value of 15223 daltons. These results confirm that

the designed trimer was self-assembling and was binding the ligand effectively in solution.

3-3: Importance of Binding Pocket Explored

The visna fusion protein mimic trimer incorporated the appropriate residues at the T_{16} and T_{23} trimer interface to bind the ligand peptide, but all of the previous experiments did not test the possibility that the ligand was binding in a non-specific manner. Although this seemed like a highly unlikely scenario considering the above experiments, more empirical data was collected using a control trimer. In this control trimer half of the binding pocket was eliminated. A new peptide, T_{23}E/K, was substituted for the standard T_{23}Vis. When incorporated into the trimer, the new peptide displayed lysine side chains into the main portion of the binding pocket (Figure 7). CD and Ni-NTA affinity experiments were conducted with the control trimer.

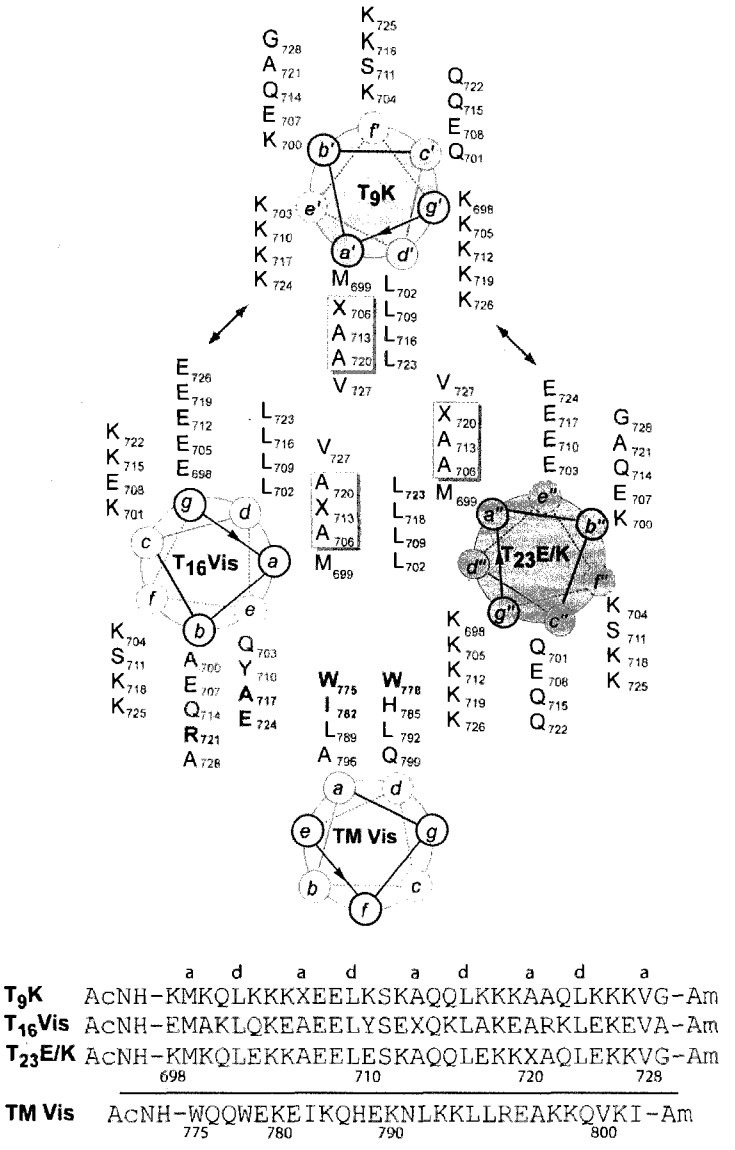

Figure 7. Helical wheel diagram for the control trimer with the ligand. Half of the binding pocket was removed by substituting T_{23}E/K for T_{23}Vis.

The control trimer differed greatly from the original visna trimer in that the control trimer plus ligand signal overlaid with the weighted average (Figure 8). That implied that the ligand was not interacting with the control trimer. The helicity of the control trimer was slightly greater than that of the original visna trimer. However this observation made sense considering that lysine, a helix promoting amino acid, was substituted for the original amino acids.

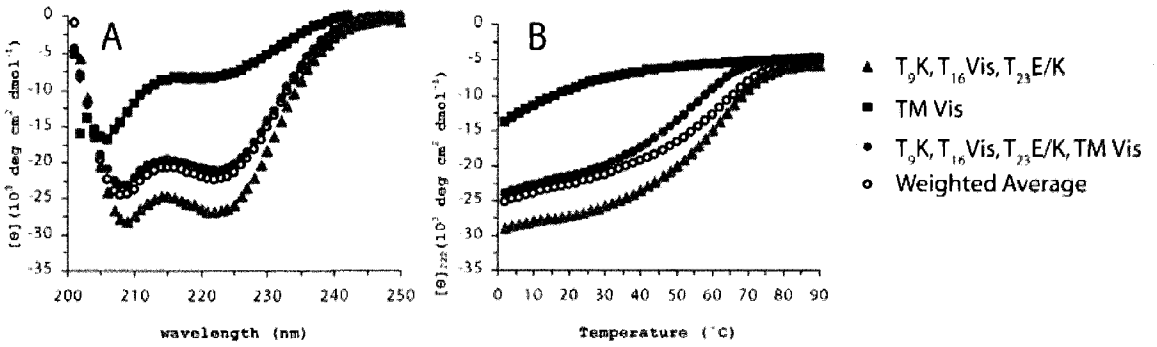

Figure 8. CD analysis for control trimer. Wavelength (**A**) and thermal unfolding (**B**) data for control trimer (green triangles), ligand (blue squares), control trimer plus ligand complex (red circles), and weighted average of control trimer signal and ligand signal (open black circles).

The Ni-NTA affinity assay with the control trimer supported the results found with the CD experiments. With T_9K_{his} substituted in the trimer, only a minimal amount of ligand was retained in the elution fraction (Figure 9). However, the trimer peptides were retained in a 1:1:1 fashion, indicating trimer formation. Overall, there was some interaction between the control trimer and the ligand, but when compared to the original visna trimer, the interaction was quite minimal.

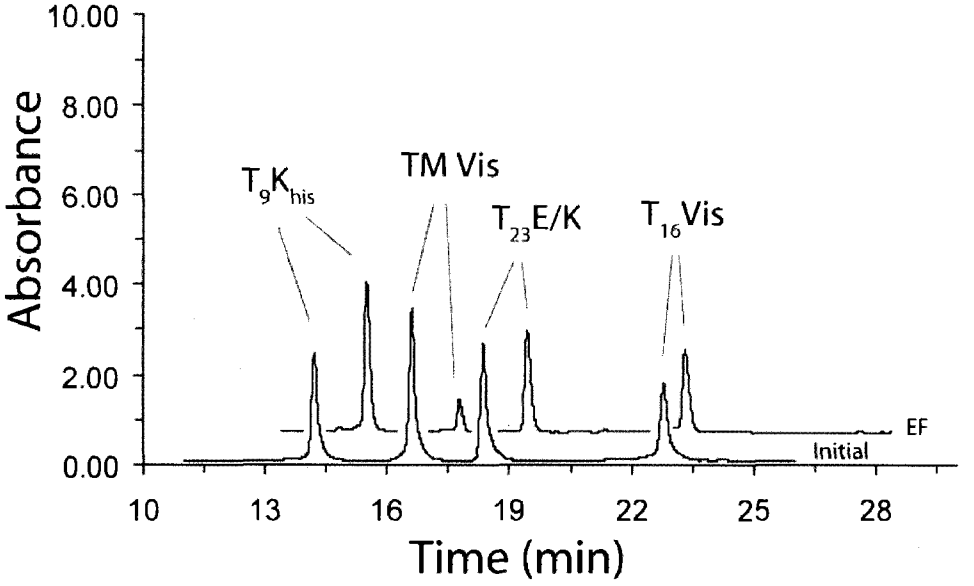

Figure 9. Ni-NTA affinity experiment with the control trimer. The control trimer had a reduced ability to bind the ligand compared with the full visna trimer mimic.

The control trimer demonstrated the importance of the full binding pocket. Upon removal of half of the binding pocket, binding of the ligand to the trimer was greatly reduced. This supported the validity of the visna trimer as a suitable fusion protein mimic, but the interaction between the trimer and the ligand was not well understood. Further studies were required to provide greater insight into which amino acids played an important role in ligand binding.

3-4: Experimental Section

Circular Dichroism Experiments: as described in Section 2-4.

Ni-NTA Affinity Experiments: as described in Section 2-4.

Analytical Ultracentrifugation Experiments: as described in Section 2-4 except that Ultrascan was used instead of Origin to analyze the data. The single-component ideal model was used to fit the data.

Extinction Coefficient Determination by NMR: UV absorbance at 270 nm recorded for monomeric peptide solution. Known amount of 2,2-dimethyl-2-silapentane-5-sulfonate (DSS) added to peptide solution. A ^{1}H NMR was taken on the 500 MHz Varian instrument. In order to calculate the concentration of peptide, the integration for the aromatic protons and the DSS protons must be normalized according to their respective number of protons (Equation 1 and 2).

$$y = \frac{\text{Integration of aromatic protons}}{\text{Number of aromatic protons}} \tag{1}$$

$$z = \frac{\text{Integration of DSS protons}}{\text{Number of DSS protons}} \tag{2}$$

The ratio between the normalized aromatic proton value and DSS proton value can be used to calculate the concentration of peptide in solution (Equation 3)

$$\frac{y}{z} = \frac{c}{[DSS]} \quad \text{where } c = \text{peptide concentration} \tag{3}$$

With the observed UV absorbance one can calculate the extinction coefficient from Beer's law (Equation 4)

$$\varepsilon = \frac{A}{bc} \quad \text{where } b = \text{pathlength}, A = \text{absorbance} \tag{4}$$

Continuous Variation Plot: Seven individual solutions were mixed with varying visna trimer and ligand ratios in PBS buffer (Table 1). These solutions were all labeled according to their mole fraction of trimer. Peptide ratios were checked by HPLC on a C18 reverse phase analytical column. It was important to note that the concentration of trimer was used during the experiment to calculate the mole fraction, not the total peptide concentration.

	Solution	1	0.8	0.6	0.5	0.4	0.2	0
Set A (μM)	T_9K	3.33	3.08	2.73	2.50	2.22	1.43	0.00
	TM vis	0.00	0.77	1.82	2.50	3.33	5.71	10.00
	$T_{16}Vis$	3.33	3.08	2.73	2.50	2.22	1.43	0.00
	$T_{23}Vis$	3.33	3.08	2.73	2.50	2.22	1.43	0.00
Set B (%)	T_9K	33.33	29.37	24.52	21.66	18.43	10.56	0.00
	TM vis	0.00	11.88	26.44	35.03	44.72	68.32	100.00
	$T_{16}Vis$	33.33	29.37	24.52	21.66	18.43	10.56	0.00
	$T_{23}Vis$	33.33	29.37	24.52	21.66	18.43	10.56	0.00

Table 1. Individual continuous variation solutions. **Set A** showed the individual component desired concentrations. **Set B** was the expected HPLC integration percentage for each peptide peak when corrected for their extinction coefficient.

Each solution was initially mixed so the total peptide concentration was 10 μM. But all solution concentrations were checked by UV/vis absorbance at 270 nm, and the calculated concentration was used for the MRE calculation (Equation 5).

$$MRE = \frac{\text{mdeg}}{\#residues \times conc. \times l \times 10} \quad (5)$$

After each solution contained the correct ratios of peptides, the solution was monitored by CD. The averaging time for the CD was raised from 1 second to 5 seconds; all other parameters for the standard wavelength experiment remained the same as in Section 2-4. The data point at for each solution at 222 nm was plotted against the mole fraction of the solution to produce the continuous variation plot. Error analysis was calculated from the standard deviation of all the data collected at 222 nm from each solution.

3-5: References Cited

(1) (a) Markosyan R.M.; Ma, X.; Lu, M.; Cohen, F.S.; Melikyan, G.B. *Virology*, **2002**, *302*, 174-184. (b) Eckert, D.M.; Kim, P.S. *Ann. Rev. Biochem.* **2001**, *70*, 777-810.

(2) (a) Chan, D.C.; Chutkowski, C.T.; Kim, P.S. *PNAS*, **1998,** *95*, 15613-15617. (b) Root, M.J.; Kay, M.S.; Kim, P.S. *Science*, **2001**, *291*, 884-888. (c) Bewley, C.A.; Louis, J.M.; Ghirlando, R.; Clore, G.M. *J. Biol. Chem.,* **2002,** *277*, 14238-14245. (d) Cianci, C.; Langley, D.R.; Dischino, D.D.; Sun, Y.; Yu, K.L.; Stanley, A.; Roach, R.; Li, Z.; Dalterio, R.; colono, R.; Meanwell, N.A.; Krystal, M. *PNAS*, **2004,** *101*, 15046-15051.

(3) Schnarr, N.A.; Kennan, A.J. *JACS*, **2004**, *126*, 10260-10261.

(4) Malashkevich, V.N.; Singh, M.; Kim, P.S. *PNAS*, **2001**, *98*, 8502-8506.

(5) ProtoParam was a free web based program available at http://www.expasy.ch/tools/protparam-doc.html which calculated the extinction coefficient based upon the primary sequence of the peptide.

(6) (a) Larive, C.K.; Jayawickrama, D.; Orfi, L. *Applied Spectroscopy*, **1997**, *51*, 1531-1536. (b) Friedrich, C.L.; Rozek, A.; Patrzykat, A.; Hancock, R.E.W. *J. Biol. Chem.*, **2001,** *26*, 24015-24022. (c) Lindhout, D.A.; Thiessen, A.; Schieve, D.; Sykes, B.D. *Protein Science*, **2003**, *12*, 1786-1791. (d) Wishart, D.S.; Bigam, C.G., Holm, A.; Hodges, R.S.; Sykes, B.D. *Journal of Biomolecular NMR*, **1995**, *5*, 67-81. (e) Larive, C.K.; Lunte, S.M.; Zhong, M.; Perkins, M.D.; Wilson, G.S.; Gokulrangan, G.; Williams, T.; Afroz, F.; Schoneich, C.; Derrick, T.S.; Middaugh, C.R.; Bogdanowich-Knipp, S. *Analytical Chemistry*, **1999**, *71,* 389R-423R.

(7) (a) Huang, C.Y. *Methods in Enzymology*, **1982,** *87*, 509-525. (b) Davydox, D.R.; Fernando, H.; Halpert, J.R. *Biophysical Chemistry*, **2006**, *123*, 95-101. (c) Loukas, Y.L. *Analyst*, **1997**, *122*, 377-381.

Chapter 4

Fluorescence Studies with the Visna Mimic

With a well-behaved visna mimic in hand we sought to investigate more specific interactions between the trimer and the ligand as well as to get a better understanding of the equilibria among the various peptides in solution. Fluorescence spectroscopy was chosen as a suitable technique to further our understanding of this system.[1] We wanted to answer the question: do the tryptophan residues on the ligand peptide play an important role in ligand binding to the mimic? It was already shown by Kim and co-workers using X-ray crystallography that the two tryptophan sidechains packed into the hydrophobic pocket.[2] One would hope that our mimic was performing in a similar manner to the natural N-terminal coiled-coil. Also we hoped to determine the K_d between the visna trimer and the ligand. Other fluorescence studies between various coiled-coil systems served as guides while we developed these new experiments.[3]

4-1: Understanding Tryptophan Fluorescence

There are three amino acids that contribute to the natural fluorescence of proteins, tryptophan, tyrosine, and phenylalanine. These amino acids are called intrinsic fluorophores. Although all three amino acids can contribute to protein fluorescence, the tryptophan sidechains, indole groups, are the main source of intrinsic fluorescence from proteins.[4] They are also responsible for the vast majority of UV absorbance. What makes the tryptophan fluorescence so interesting is the sensitivity it displays for its local environment. Ligand binding, protein-protein interactions, and protein unfolding can all be studied by monitoring the spectral shift in the tryptophan amino acids involved with the interaction.[5]

Tryptophan has an excitation wavelength of 280 nm and an emission wavelength that varies within the range of 310 nm to 350 nm. This emission wavelength is

dependent on the polarity of the environment. Tryptophans exposed to a polar environment, like water, or that are hydrogen bonded, will emit a longer emission wavelength, around 350 nm. On the other hand, tryptophans that are in an apolar environment will emit a shorter wavelength, about 310 nm. Proteins with well understood conformational structures have been used to illustrate this concept (Figure 1).

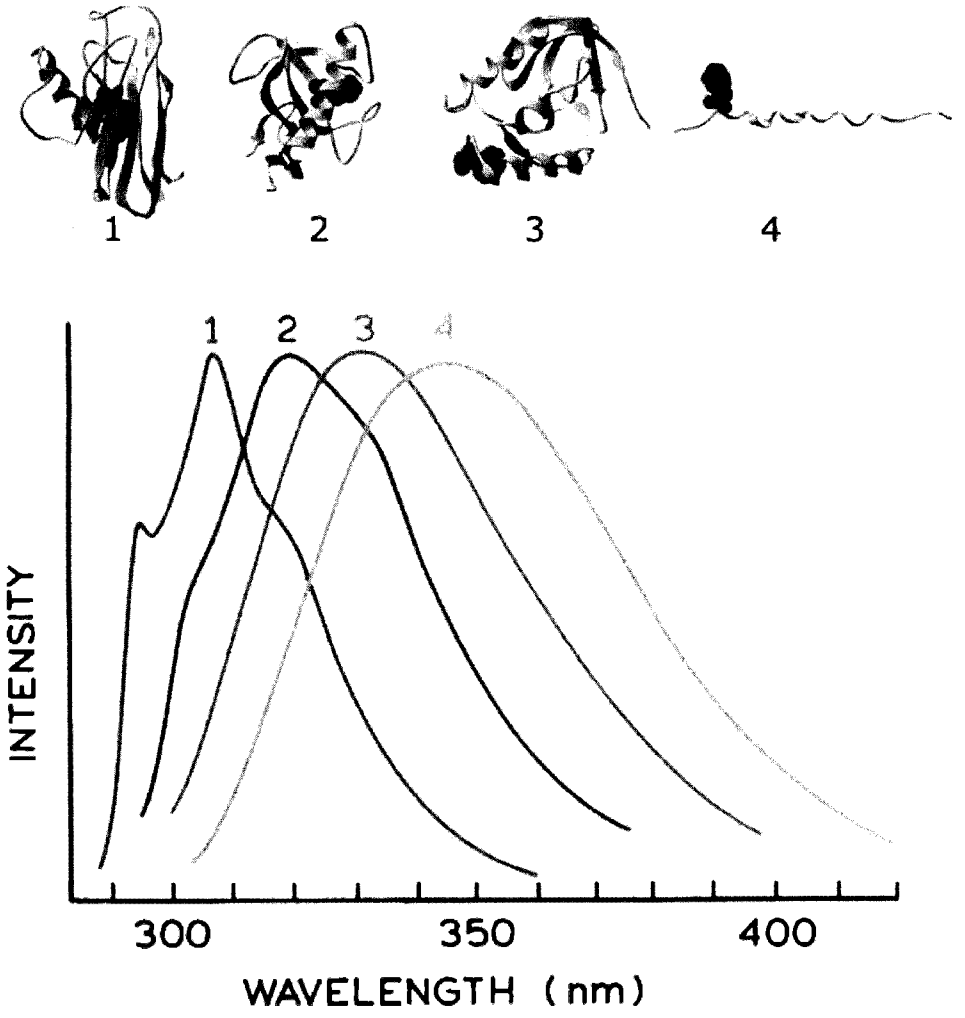

Figure 1. Varying tryptophan emission spectra for different local environments. Emission spectra for apoazurin Pfl, ribonuclease T_1, staphylococcal nuclease, and glucagon, for 1 to 4, respectively. Revised from Lakowitz.[4]

The first protein, apoazurin Pfl, has the tryptophan sidechain well folded into the middle of the protein; hence, the emission wavelength is shifted to a shorter wavelength. The last protein illustrated, glucagon, has its tryptophan sidechain exposed to the solvent. Therefore its emission wavelength is the longest. This same principle was used on the visna mimic to test ligand binding.

4-2: Tryptophan Fluorescence of the Visna Mimic

Since the visna ligand peptide contained two tryptophans, initial experiments were conducted on the ligand alone to get a baseline emission signal. Those were quickly followed with analysis of the visna trimer plus the ligand (Figure 2).

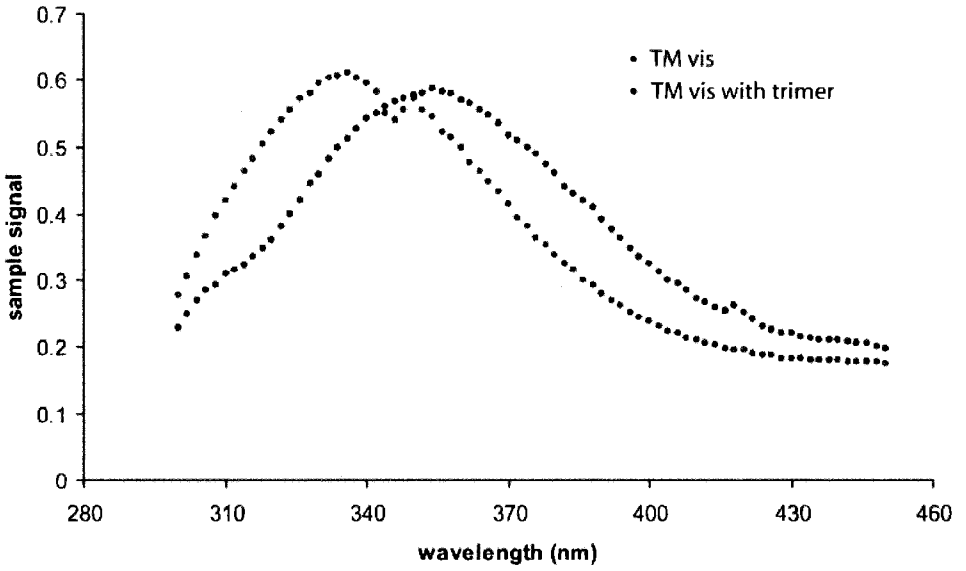

Figure 2. Emission spectra for two separate solutions, one containing only the ligand, TM vis, and the other containing the ligand plus the trimer. The emission maximum for the ligand only solution was 354 nm, and the emission maximum for the ligand plus the trimer was shifted to 336 nm. The shorter hump in the ligand with the trimer signal may be a result of unbound ligand or an impurity in the solution.

It is important to note that the visna trimer did not contain any intrinsic fluorophores, so any change in spectra was from the two tryptophans on the ligand. The solution of the ligand gave a maximum signal of 354 nm. This result was consistent with a solvent-

exposed tryptophan sidechain, and correlated with the CD spectrum which demonstrated that the ligand alone in solution adopted a random coil. The signal for the ligand with the trimer shifted to 336 nm. This was consistent with a change from a polar local environment to a nonpolar environment. The minor hump in the trimer-plus-ligand signal could be a result of unbound ligand or an impurity in the solution, but considering the location, it corresponded well with extra ligand.

This result was further studied by titrating the trimer against a solution of ligand. In this new experiment, the concentration of the ligand was held reasonably constant while a solution of trimer was titrated into the cuvette. After each titration an emission wavelength scan was taken (Figure 3). Over the course of a 20-step titration, the maximum emission wavelength shifted from 354 nm to 342 nm. This demonstrated that the tryptophans were playing a role in ligand binding.

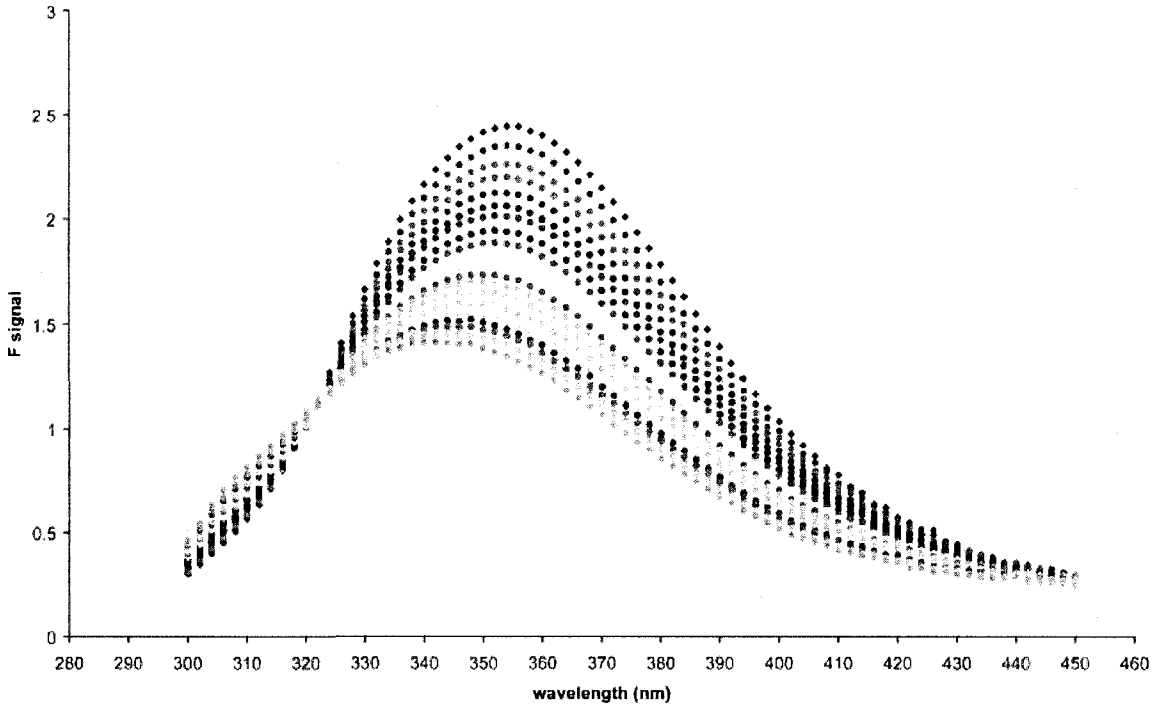

Figure 3. Emission spectra from tryptophans on visna ligand. As the trimer was titrated into the solution the overall signal dropped but more importantly the maximum emission wavelength shifted to 340 nm.

In order to conclude that this shift in signal was a result of the tryptophans binding into the hydrophobic pocket, these experiments were repeated with the visna control trimer which had half of the binding pocket mutated. Over a similar range of trimer concentrations, the control trimer exhibited a different effect on the tryptophan spectra. Instead of shifting to a shorter wavelength, the maximum emission signal remained fairly constant. Although there was some drop in the overall fluorescence signal, the maximum stayed around 354 nm (Figure 4).

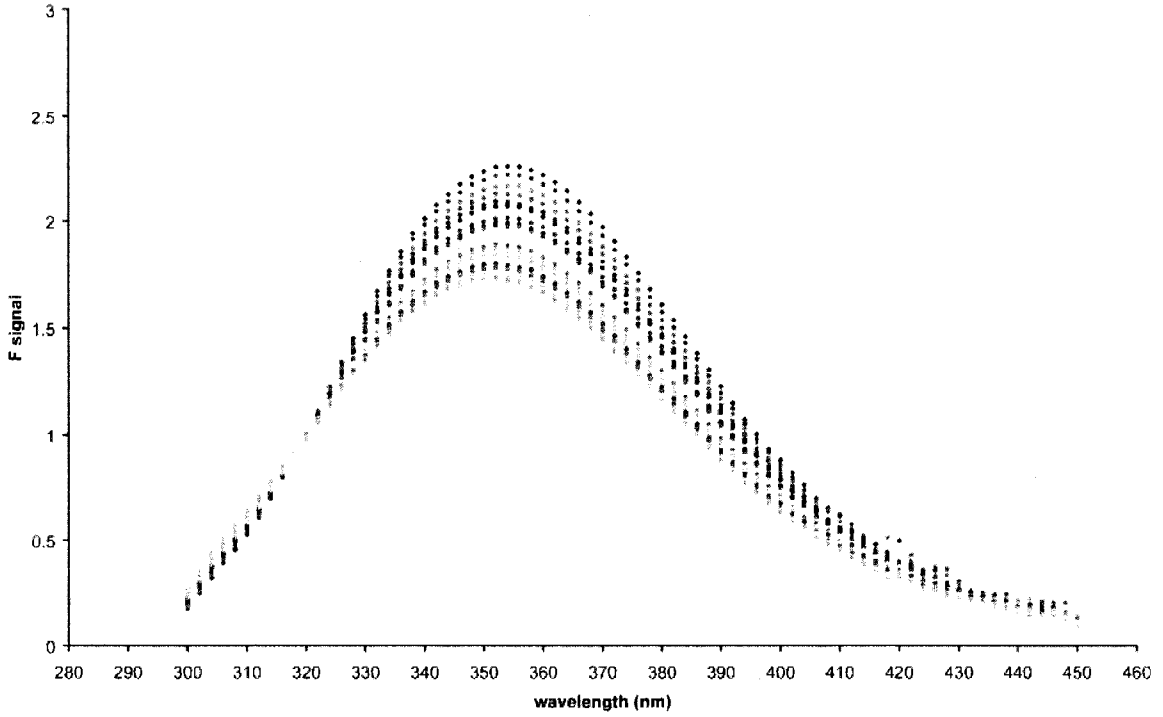

Figure 4. Emission spectra for visna ligand with control trimer. The maximum signal stayed constant over the course of the titrations.

These two experiments supported the initial hypothesis that the two tryptophans played a central role in peptide binding. They also supported the necessity for the presence of the whole hydrophobic pocket in order to successfully bind the ligand. Moreover, the tryptophan fluorescence experiments illustrated that the visna mimic was binding the ligand in a fashion similar to that bound in early X-ray crystal structures completed by Kim and co-workers.

4-3: Fluorescein, an Extrinsic Fluorophore

Numerous investigations had studied the attachment of fluorophores to coiled-coils.[6] In one study, Gellman and co-workers concluded that many fluorophores induced higher-order aggregation amongst well-characterized coiled-coils.[3a] For their studies, they fluorescently tagged the leucine zipper region of the oncoprotein Jun with four

different fluorophores, pyrenebutyric acid, fluorescein, 7-diethylcoumarin-3-carboxylic acid, and 7-hydroxycoumarin-3-carboxylic acid (Figure 5).

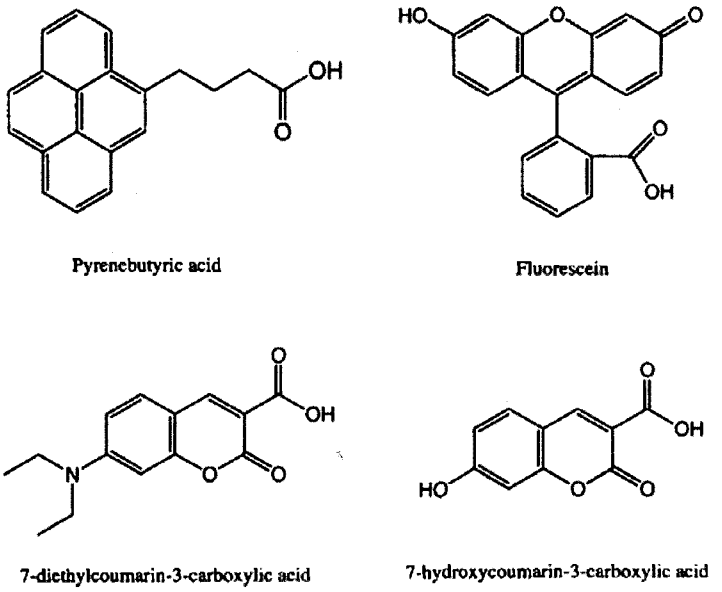

Figure 5. Fluorophores used by Gellman and co-workers to determine the effect they exerted on the dimerization of Jun.

Jun was known to form a homodimer in solution. Fluorescence quenching was monitored and used as an indication of dimerization, and the aggregation was determined by AUC. Of the fluorophores that were tested, fluorescein was the fluorescent tag that exerted a weaker aggregation promoting effect, although the weakest effect was exhibited by the 7-hydroxycoumarin.

In addition to minimizing aggregation, fluorescein had a number of advantages over tryptophan, of which the most important for the following experiments would be a higher quantum yield. The quantum yield is the number of emitted photons relative to the number of absorbed photons. The higher quantum yield leads to better emission intensity, and better emission intensity allows one to study interactions at a much lower

concentration. Fluorescein was a good fluorophore to use when studying dissociation constants, K_d, in the nanomolar concentration range.

New peptides had to be synthesized to incorporate the fluorescein tag. A cysteine was appended to the primary sequence of both T_9K (T_9K_{fluor}) and TM vis (TM vis_{fluor}). Fluorescein maleimide, a thiol-reactive reagent, was used to fluorescently label the two new peptides. With the fluorescently-labeled peptides in hand we commenced with fluorescence polarization experiments.

4-4: Elucidation of Dissociation Constants

Fluorescence polarization experiments are dependent on molecular movements over the course of the fluorophore's relaxation time (Figure 6). The fluorescently-labeled peptide in solution alone is a relatively small molecule that has a high rotational diffusion. All fluorescently tagged peptides aligned with the excitation axis will be excited. During the excited lifetime of the fluorescein, the peptide will rotate. Because of the high rotational diffusion, the fluorescein will emit in a different direction than the excitation axis. This yields a low degree of polarization. If the fluorescently-labeled peptide is bound by the two trimer binding partners, this complex will have a slower rotational diffusion. Once the fluorescein is excited, the peptide bound in the trimer will not rotate as much as the free peptide, and it will emit in the same direction as the excitation axis. This corresponds to a high degree of polarization. Plotting the polarization versus the binding partner concentration and fitting it to a binding equation (eq 1) yielded the dissociation constant, K_d, between the trimer peptides and the fluorescently labeled peptide.

$$y = m\left(\frac{x^H}{x^H + K_d{}^H}\right) + b \qquad (1)$$

(In this equation y equals the polarization, x equals the total peptide concentration, m is a scaling factor, b is the baseline correction factor, and H is the Hill coefficient and this equation assumes that the K_d is greater than the concentration of fluorescently-labeled peptide in solution.)

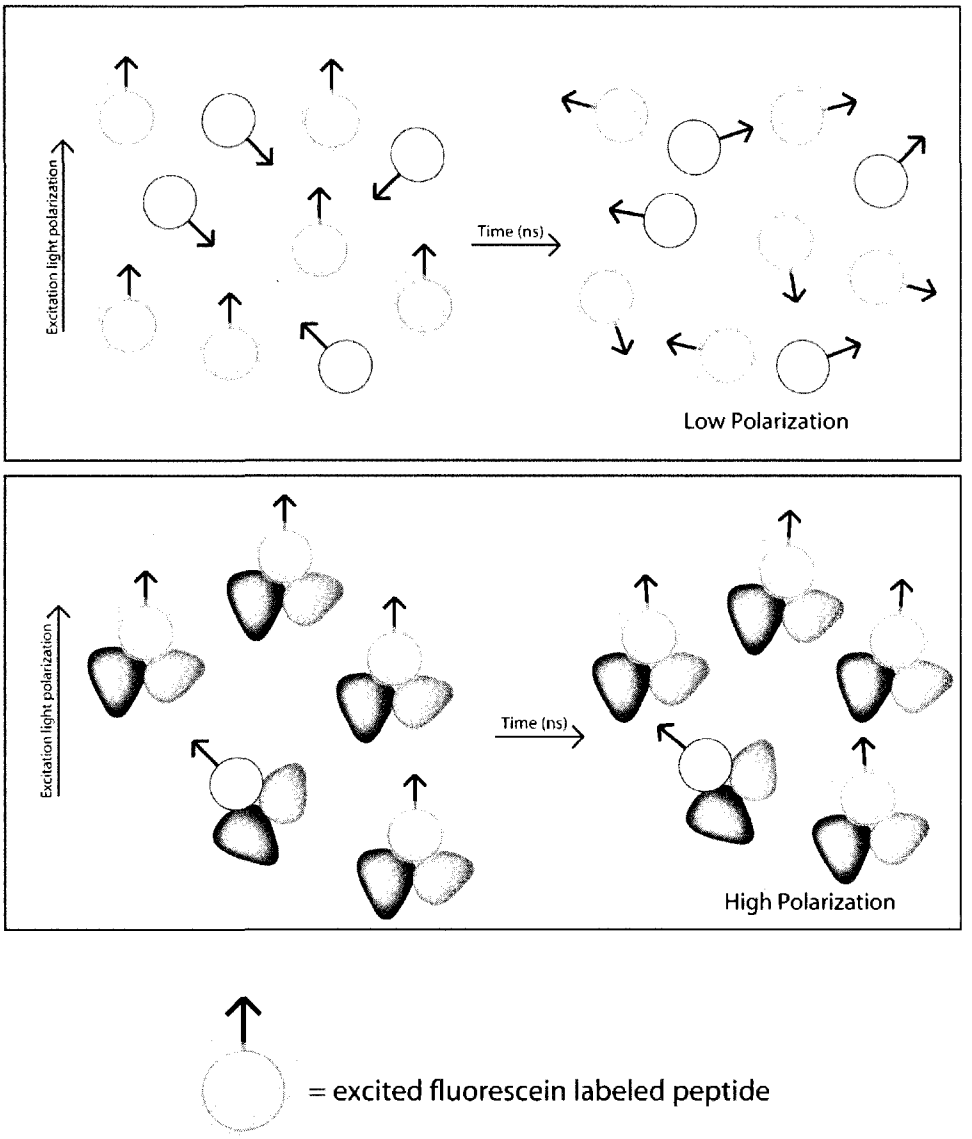

Figure 6. Diagram of polarization assay. The small peptide has a high degree of rotational freedom which yields a low polarization while the small peptide bound in the trimer has a much slower rotational diffusion and yields a higher polarization.

As in the previous example, the T_9K peptide was fluorescently tagged and polarization experiments were conducted between T_9K_{fluor} and the T_{16}Vis and T_{23}Vis peptides. The experiments were done on two different instruments. An Aviv ATF-105 spectrofluorometer was used for the first experiment. In this experiment 24 different solutions were individually analyzed in a cuvette. The excitation was locked at 491 nm and the emission was monitored at 518 nm. The intensity (I) of fluorescence emission was recorded for each polarizer position, I_{vv}, I_{vh}, I_{hh}, I_{hv}. From those parameters the anisotropy of the solution was calculated. The solution anisotropies were plotted against the solution concentrations and the binding equation was applied to calculate the K_d (Figure 7). In this experiment the K_d for the T_9K_{fluor} interacting with the T_{16}Vis and T_{23}Vis peptides was found to be about 330 nM.

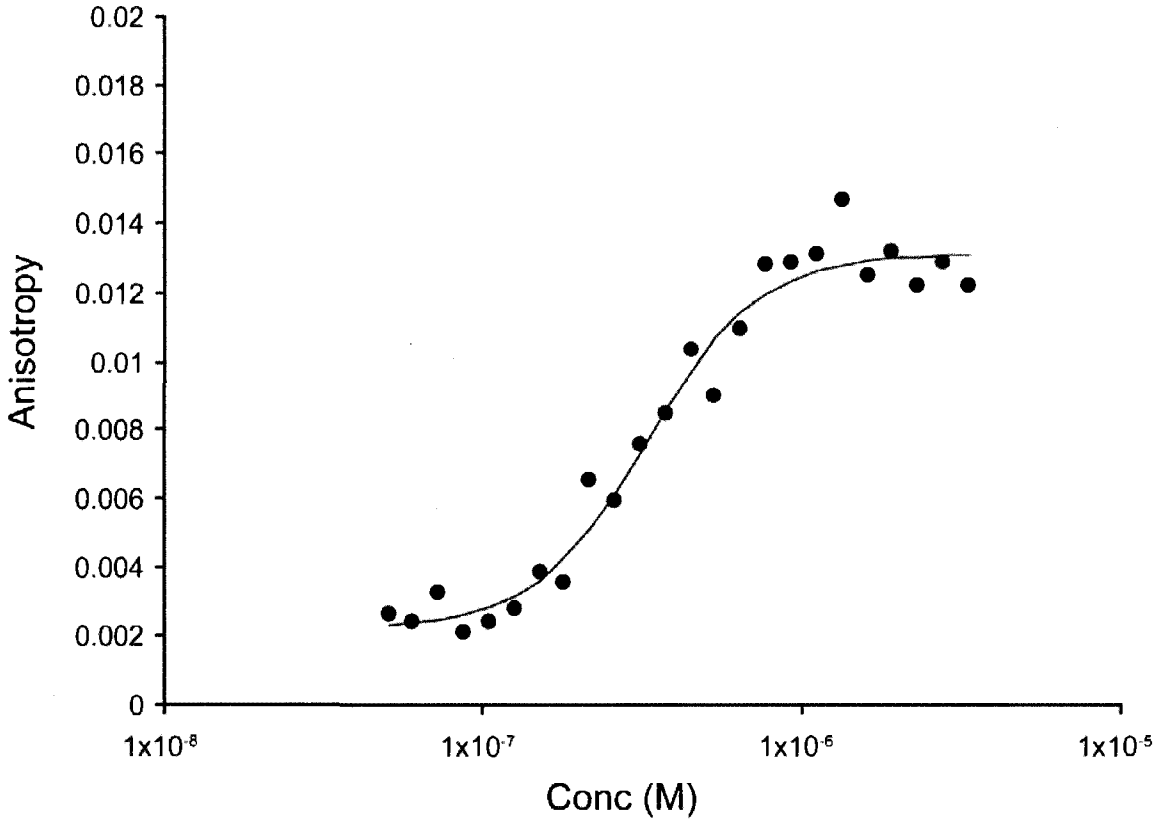

Figure 7. Plot of anisotropy versus solution concentration for the T_9K_{fluor} binding with T_{16}Vis and T_{23}Vis. Data collected with the Aviv Spectrofluorometer.

This experiment was repeated on a Perkin Elmer multilabel plate reader. For this experiment the same solutions from the above experiment were transferred to a 384 well plate. Again the samples were excited and the emission intensities monitored. The polarization for each sample was calculated and plotted against its sample concentration. The data was fit to a binding equation and the K_d was calculated to be about 330 nM (Figure 8).

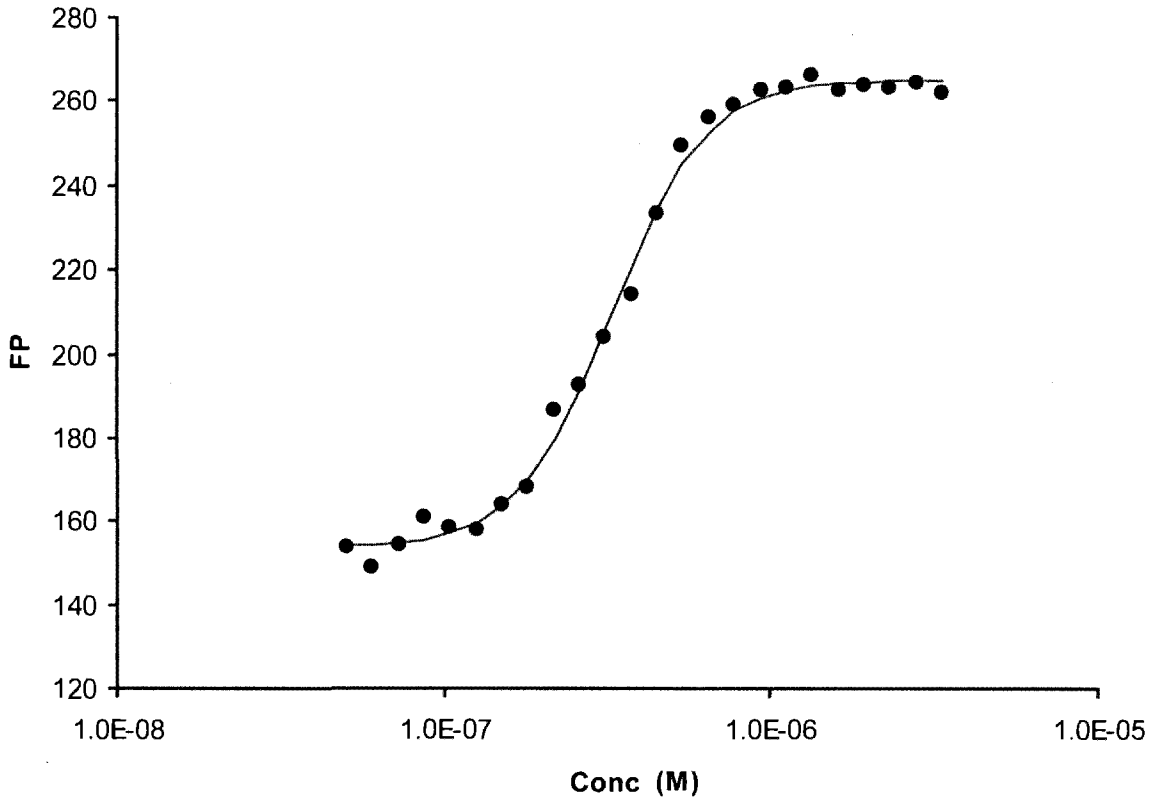

Figure 8. Plot of polarization versus solution concentration for the labeled T_9K binding with T_{16}Vis and T_{23}Vis. Data collected with the Perkin Elmer plate reader.

Since the K_d from both fluorescence instruments was nearly the same, both would work equally well for future experiments. However other factors played into the decision to use the Perkin Elmer instrument. First, the experiment time was much shorter for the Perkin Elmer instrument. The average analysis time was about 30 minutes on the automated Perkin Elmer instrument but half a day for the manual Aviv instrument. Also the amount of material necessary to conduct the experiment was much greater for the Aviv. Thus, the Perkin Elmer instrument was better suited for greater productivity.

The TM vis peptide was then synthesized with a cysteine appended to the end of the sequence. It was then coupled to fluorescein maleimide and purified for fluorescence experiments. On the Perkin Elmer instrument, 24 solutions of the labeled ligand were

monitored against varying concentrations of the visna trimer. Again the data was plotted and fit with the binding equation (Figure 9). The K_d was calculated to be about 170 nM.

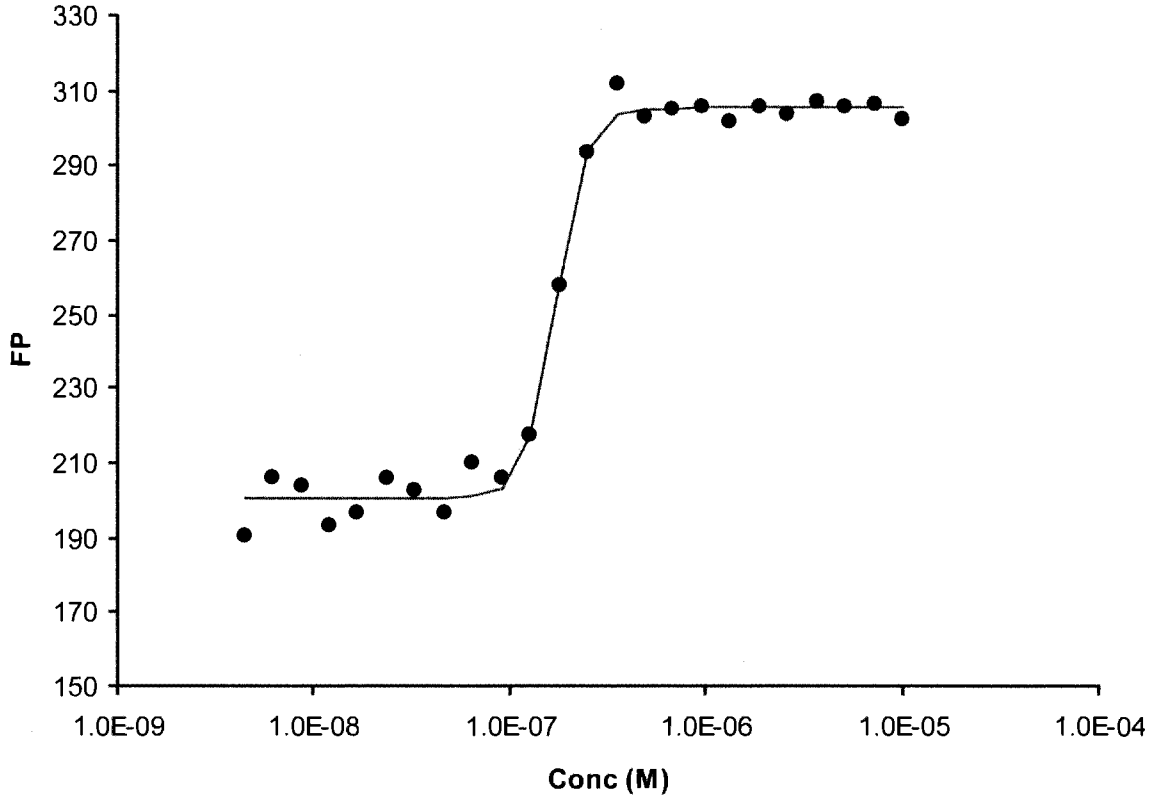

Figure 9. Plot of polarization versus solution concentration for the labeled TM Vis peptide binding with the visna mimic. Data collected with the Perkin Elmer plate reader.

These fluorescence studies provided new insight into the behavior of the peptides. We were able to conclude that the trpytophans were playing a critical role in peptide binding. Also the whole hydrophobic binding pocket was deemed necessary for ligand peptide binding. Finally we were able to determine a K_d for the T_9K peptide binding with its trimer binding partners and a K_d for the ligand binding to the trimer. In looking to the future these studies can be extended to numerous viral mimics as well as their associated control trimers.

4-5: Experimental Section

Tryptophan Fluorescence Assay. All experiments were performed on an Aviv ATF-105 Spectrofluorometer with the polarizers removed. Sample concentrations were measured by UV absorbance of the acetamidobenzoate label at 270 nm. Emission scans are the average of three individual scans from 300 nm to 450 nm with a 2 nm step. All signals were background corrected. The excitation wavelength was 280 nm for all solutions. The trimer solutions were titrated into the TM vis solution manually and allowed to equilibrate for one minute while stirring the solution. The concentration of the solution after the final titration was analyzed by UV absorbance to check the overall titration accuracy.

Fluorescein Maleimide Coupling.

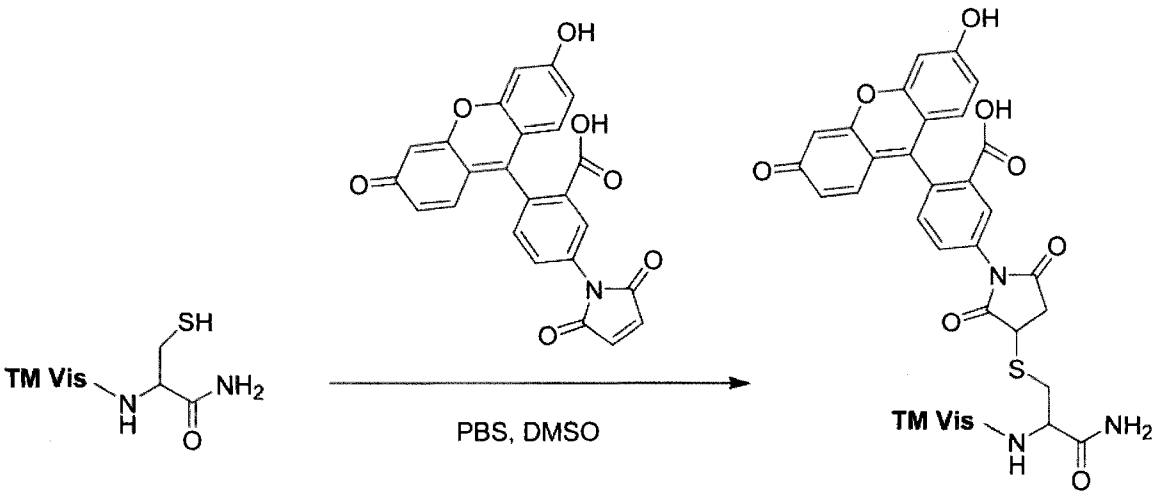

To a round bottom flask equipped with a stir bar a solution of TM vis (395.2 mL, 132.5 nmol) was added fluorescein maleimide (0.53 mg, 9 equiv). Dimethyl sulfoxide was added until the fluorescein maleimide dissolved. Solution was stirred in the dark at room temperature for 2 hours. Purification commenced as described in section 2-4. Same reaction conditions were used for the T_9K coupling to fluorescein maleimide.

Fluorescence Polarization Assay. Solution preparation for both instruments was similar. The only parameter that changed with the overall volume of the samples. For the Perkin Elmer the volume needed was 75 μL, while the Aviv instrument required 150 μL. The labeled peptide was held at a constant concentration while the binding partners underwent a serial dilution. Data collection was done manually with the Aviv instrument, in that the intensity for each of the polarizer configurations was recorded and then the anisotropy was calculated from those values. The Perkin Elmer only reported a polarization value for each solution. The results were plotted and fit according to the following binding equation. Also solution concentrations were checked after analysis to determine the correct dilution.

Binding Equation Calculations. The K_d calculations were completed with an Excel macro. Fits were optimized using the solver function to minimize the chi^2 value. The Excel macro was validated through comparing fit results with fits from Kaleidagraph using the same above equation.

4-6: References Cited

(1) (a) Prystay, L.; Gosselin, M.; Banks, P. *Journal of Biomolecular Screening*, **2001**, *6*, 141-151. (b) Knight, S.M.G.; Umezawa, N.; Lee, H.S.; Gellman, S.H.; Kay, B.K. *Analytical Biochemistry*, **2002**, *300*, 230-236. (c) Lukas, T.J.; Burgess, W.H.; Prendergast, F.G.; Lau, W.; Watterson, D.M. *Biochemistry*, **1986**, *25*, 1458-1464. (d) Weber, G.; Shinitzky, M. *PNAS*, **1970**, *65*, 823-830.

(2) Malashkevich, V.N.; Singh, M.; Kim, P.S. *PNAS*, **2001**, *98*, 8502-8506.

(3) (a) Daugherty, D.L.; Gellman, S.H. *JACS*, **1999**, *121*, 4325-4333. (b) Gochin, M.; Savage, R.; Hinckley, S.; Cai, L. *Biol. Chem.*, **2006**, *387*, 477-483. (c) Talaga, D.S.;

Lau, W.L.; Roder, H.; Tang, J.; Jia, Y.; Degrado, W.F.; Hochstrasser, R.M. *PNAS*, **2000,** *97*, 13021-13026.

(4) Lakowitz, J.R. *Principles of Fluorescence Spectroscopy*, Springer Science+Business Media, LLC: New York, NY, 2006, p.63.

(5) (a) Meagher, J.L.; Beechem, J.M.; Olson, S.T.; Gettins, P.G.W. *J Bio Chem*, **1998**, *273*, 23283-23289. (b) Kintrup, M.; Schubert, P.; Kunz, M.; Chabbert, M.; Alberti, P.; Bombarda, E.; Schneider, S.; Hillen, W. *Eur J Biochem*, **2000**, *267*, 821-829. (c) Gasymov, O.K.; Abduragimov, A.R.; Yusifov, T.N.; Glasgow, B.J. *Biochem Biophys Res Comm*, **1997**, *239*, 191-196. (d) Wong, C.Y.; Eftink, M.R.; *Biochemistry*, **1998**, *40*, 14754-14762.

(6) Morii, H.; Ichimura, K.; Uedaira, H. *PROTEINS: Structure, Function, and Genetics*, **1991**, *11*, 133-141.

Chapter 5

Validating the HIV Mimic

Preliminary work on the HIV fusion protein mimic was done by Nate Schnarr, who designed the trimeric coiled-coil and found that the native ligand sequence bound to it. Further work was done with the system by Brent Mann, who tested known HIV inhibitors against the designed mimic. Upon the departure of the latter member, our laboratory continued testing other known inhibitors against the designed mimic.

5-1: Background of Known HIV Inhibitors

Peter Kim and co-workers developed short peptide inhibitors that were designed to bind into the hydrophobic binding pocket on the N-terminal coiled-coil. The first one studied in our laboratory by Brent Mann was the D-peptide. This D-peptide was shown by Kim and co-workers to bind the hydrophobic pocket.[1] This was illustrated by an X-ray crystal structure of the D-peptide bound in the hydrophobic binding pocket on the N-terminal coiled-coil (Figure 1).

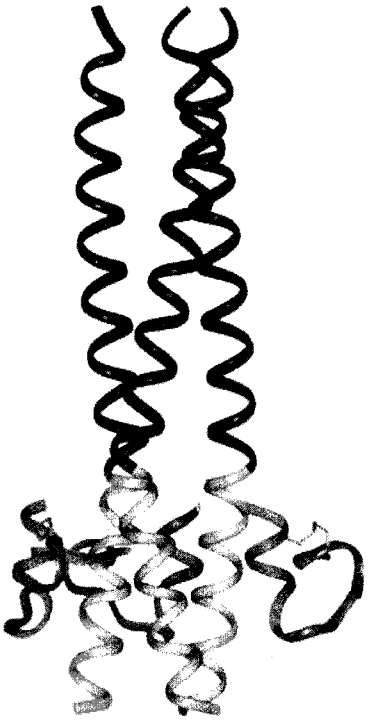

Figure 1. Crystal structure of D-peptide bound to N-terminal coiled-coil hydrophobic pocket. The segment with the hydrophobic binding pocket is shown in grey with the inhibitor shown in green and purple.

Brent Mann synthesized the D-peptide and demonstrated that our HIV mimic bound this peptide as well. This was done with Ni-NTA affinity experiments. CD experiments were conducted on the complex; because of the relatively unstructured nature of the D-peptide upon binding, the CD signal of the trimer plus the D-peptide overlaid with the expected weighted average. However, AUC confirmed that the D-peptide was truly binding to the HIV mimic.

With that inhibitor binding nicely to the trimer, other inhibitors were tested. Kim and co-workers developed another series of small, peptide inhibitors designed to be helical in solution before binding to the hydrophobic pocket.[2] Standard peptide-based inhibitors would become coiled upon binding to the binding pocket. With the helicity

pre-organized, these inhibitors would not undergo the energetic penalty associated with the loss of conformational entropy upon binding.

The first inhibitor from this series studied by Brent Mann was the C14Aib peptide. Although this was not the best inhibitor from the group it was the simplest to synthesize. The two α-aminoisobutyric (Aib) acid amino acids promoted helix formation (Figure 2).

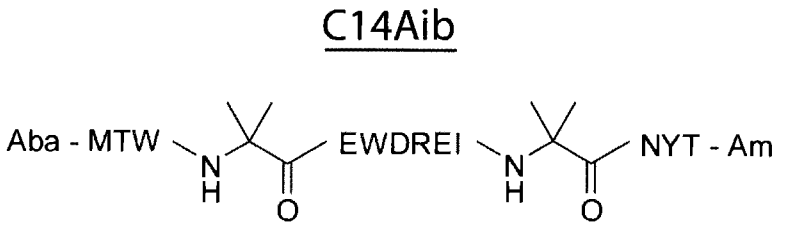

Figure 2. Sequence of C14Aib peptide. Highlighted in red are the key Trp, Trp, Ile residues. Drawn out are the two Aib amino acids. The peptide was capped at the N-terminus with Aba.

Brent Mann synthesized the peptide and conducted Ni-NTA affinity experiments on it against the HIV mimic. Unfortunately the C14Aib peptide was not recognized by the HIV mimic. Very little of the peptide was retained in the elution fraction during the Ni-NTA experiments (Figure 3). The vast majority of the C14Aib peptide remained in the supernatant. CD and AUC experiments also supported the idea that the C14Aib peptide was not binding to the HIV mimic.

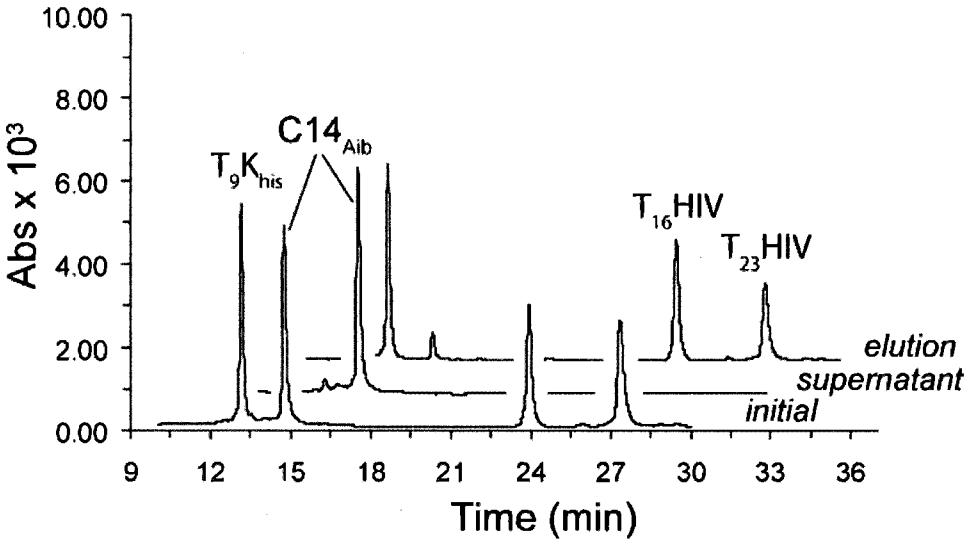

Figure 3. Ni-NTA results for C14Aib peptide with HIV mimic. With the T_9K_{his} peptide the HIV trimer is retained but very little of the C14Aib peptide remains in the elution fraction. The vast majority of the peptide washed through in the supernatant.

5-2: Synthesis of C14linkmid

According to previous work by Kim and co-workers the C14Aib peptide was not the best inhibitor of the series. The best inhibitor was the C14linkmid peptide (Figure 4).

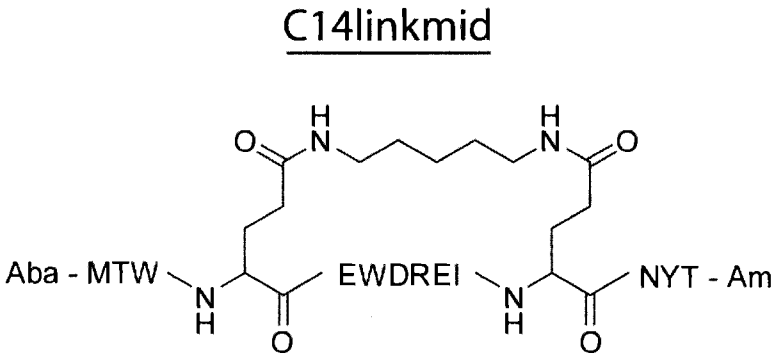

Figure 4. Sequence of C14linkmid. The key Trp, Trp, Ile residues are highlighted in red. Two glutamic acid sidechains are shown linked together by cadaverine. The N-terminus was capped with Aba.

The helical conformation for the C14linkmid was determined through chemical crosslinking instead of incorporation of helix-promoting amino acids. Following the Kim

procedure, before the synthesis of the peptide, an unnatural amino acid had to be synthesized. It involved a peptide-coupling reaction between an unprotected glutamic acid sidechain and a mono-Boc protected cadaverine (pentane-1,5-diamine) molecule. This unnatural amino acid was incorporated into the peptide during standard Fmoc peptide synthesis. After completion of the primary sequence the synthesis was then carried on by selective deprotection of an allyl-protected glutamic acid residue, followed by the removal of the Boc group. Finally, coupling between the free amine and the other carboxylic acid with cleavage from the resin yielded C14linkmid.[3]

Unfortunately one could no longer purchase mono-protected cadaverine and the synthesis of it was quite lengthy so I set out to develop a new, simplified synthesis of C14linkmid. Our synthesis began with Boc solid phase peptide synthesis of the peptide, **1**. Included were two orthogonally protected glutamic acid sidechains (Scheme 1), one protected with a fluorenylmethyl group, the other with an allyl group. The synthesis commenced with selective deprotection of the fluorenylmethyl to afford a carboxylic acid, **2**. Then cadaverine was coupled to the carboxylic acid, to give **3**. This was followed by Boc protection of the free amine, to give **4**. Selective deprotection of the allyl protected glutamic acid sidechain, produced **5**. Finally, TFA removal of the Boc group and standard peptide coupling formed the final linked peptide, **7**. After cleavage from the resin and HPLC purification the peptide was ready to be used in further studies with the HIV mimic.

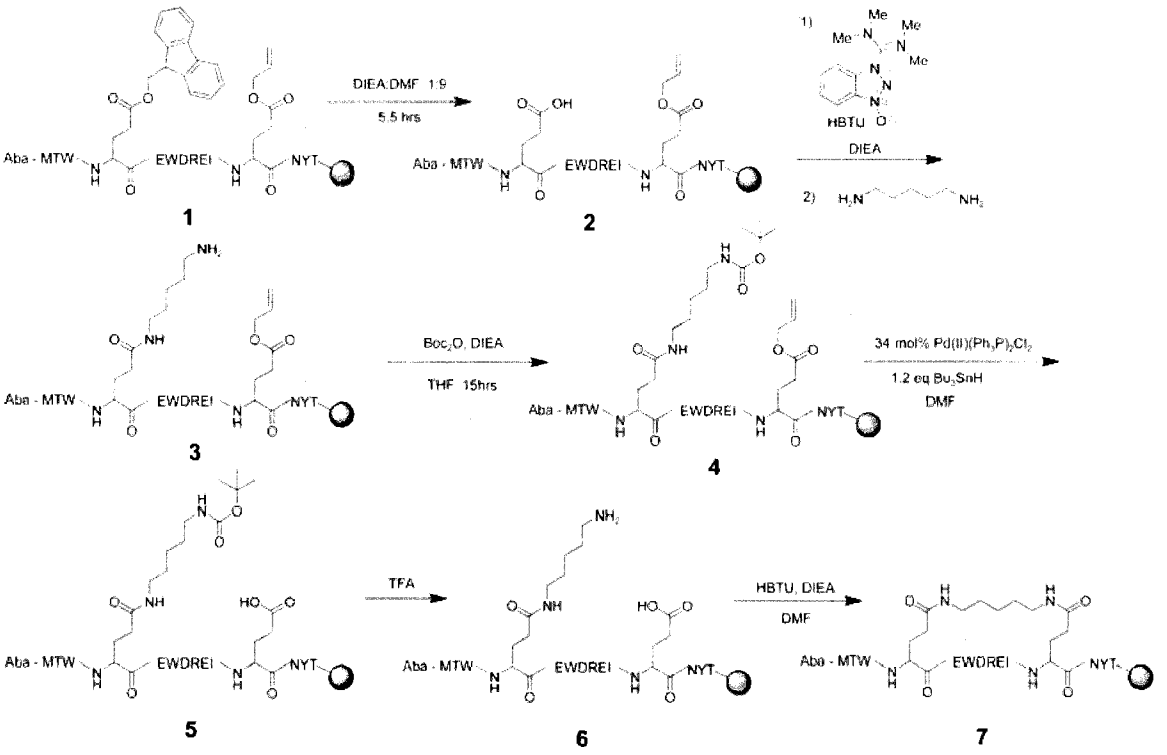

Scheme 1. Synthesis of C14linkmid.

The C14linkmid peptide performed very similarly to the C14Aib peptide. The Ni-NTA experiments were the most informative. With an equimolar mixture of all peptides, a 1:1 ratio between the HIV mimic and the C14linkmid peptide, the HIV mimic retained very little C14linkmid in the elution fraction. The Ni-NTA experiment was repeated only this time with a three fold excess of C14linkmid peptide. This experiment yielded a similar result with the vast majority of C14linkmid contained in the supernatant fraction and very little of it in the elution fraction (Figure 5).

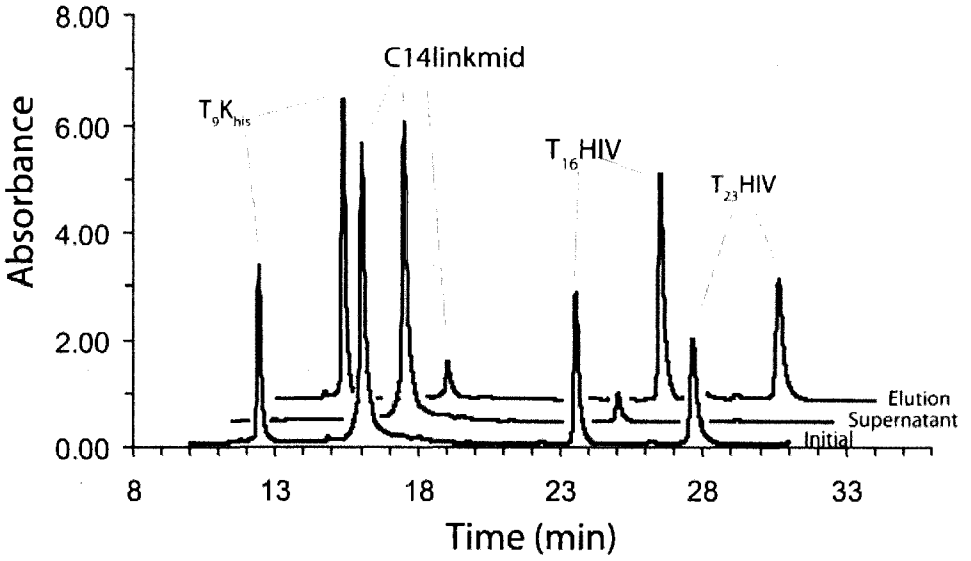

Figure 5. Ni-NTA affinity assay with excess C14linkmid peptide. With the T_9K_{his} peptide the HIV trimer is retained but very little of the C14linkmid peptide remains in the elution fraction. As with the C14Aib the vast majority of the peptide washed through in the supernatant.

5-3: Validity of HIV Mimic

Although the HIV mimic did a poor job of binding the C14Aib peptide and C14linkmid peptide, it is a validate mimic in that it can bind the natural gp41 ligand. These two inhibitors were designed from a similar construct. It could be that the conformational restrictions placed on the peptide through both helix-inducing amino acids and chemical linkers truly inhibit their ability to bind our model. Also these two peptides place an emphasis on the Trp, Trp, Ile motif. This raises the question, considering our mimic can bind the gp41 ligand peptide which has the same Trp, Trp, Ile motif, what difference was there between the gp41 ligand and these inhibitor peptides? There may be other important interactions that are being overlooked with these inhibitors.

Also the D-peptide did bind well to the HIV mimic and that peptide does not even contain the Trp, Trp, Ile motif. Since this has been an attractive drug target, there are

numerous new potential inhibitors to test.[4] Further work needs to be conducted on this mimic with new inhibitors in order to get a better feel for the validity of our HIV mimic.

5-4: Experimental Section

Circular Dichroism Experiments: as described in Section 2-4.

Ni-NTA Affinity Experiments: as described in Section 2-4.

Peptide Synthesis of C14linkmid: as described in Section 2-4.

On resin modification of C14linkmid:

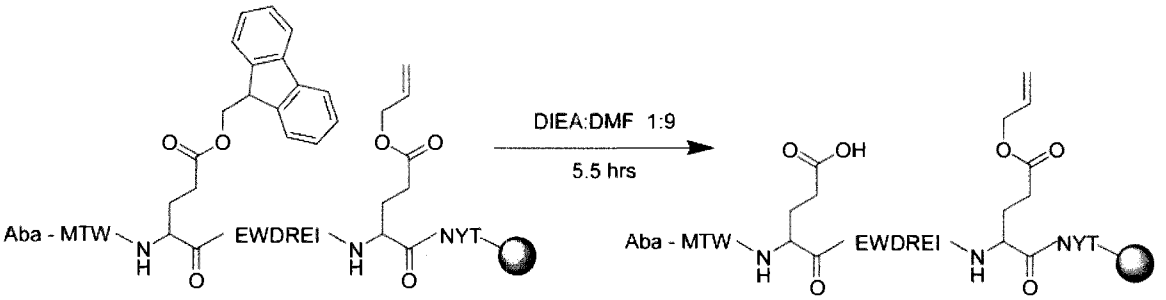

1 2

A round bottom flask was equipped with a stir bar. The flask was charged with the synthesized peptide on resin (0.562 g, 0.332 mmol peptide) and a 1:9 N,N diisopropylethylamine (DIEA) : dimethylformamide (DMF) solution (5.6 mL, 3.2 mmol). This was allowed to stir at room temperature for 5.5 hours. Resin was then transferred to the fritted shaker vessel and rinsed with dichloromethane (DCM) and DMF.

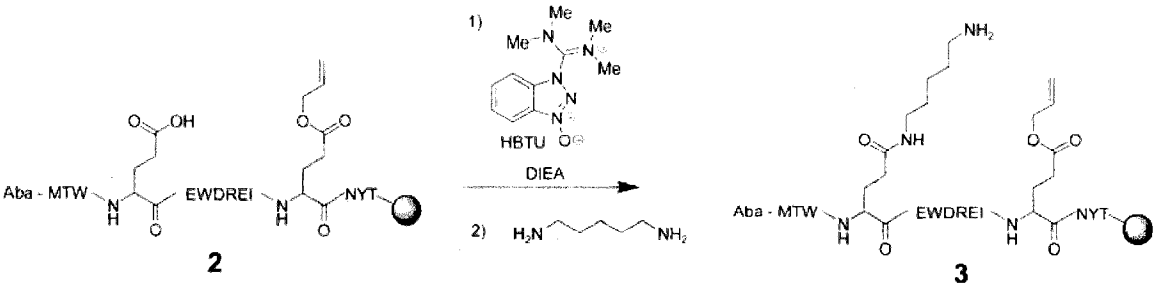

A standard fritted peptide shaker vessel was charged with **2** (0.2115 g, 0.1248 mmol), *N,N,N',N'*-Tetramethyl-*O*-(1*H*-benzotriazol-1-yl)uronium hexafluorophosphate (HBTU, 0.0493 g, 1 equivalent), and DIEA (0.034 mL, 1.5 equiv.). Reaction vessel was allowed to shake for 2 minutes at room temperature. At which point, cadaverine (0.1 mL, 8 equiv.) was added. Vessel was allowed to shake for 20 minutes. Resin was rinsed with DMF and DCM. Performed Kaiser Test to confirm presence of free amine.

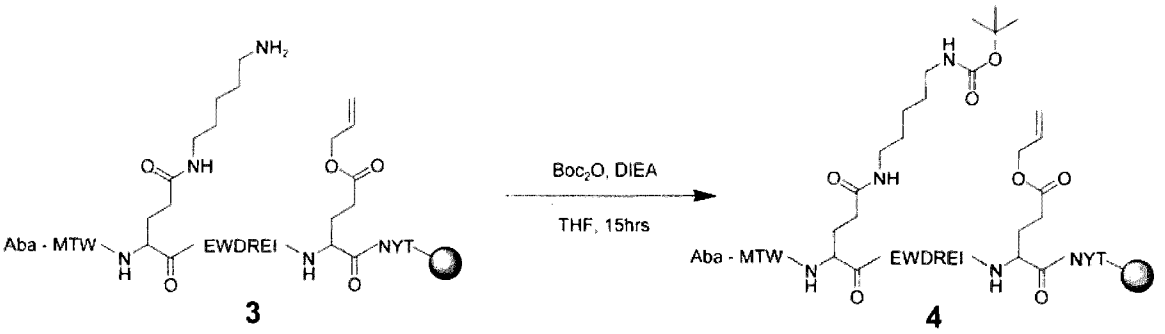

A round bottom flask equipped with a stir bar and chilled to 0 °C was charged with **3** (0.2115 g, 0.1248 mmol), di-*tert*-butyl dicarbonate (0.0136 g, 0.5 equiv.), tetrahydrofuran (0.3 mL), dichloromethane (3mL), and DIEA (0.14 mL, 6.5 equiv.). The reaction was allowed stirred for 15 hours and allowed to warm to room temperature. The resin was then transferred to a shaker vessel and washed with DMF, and DCM. A Kaiser Test was performed on the resin to check for free amines. Washed with ether and solvent removed *in vacuo*.

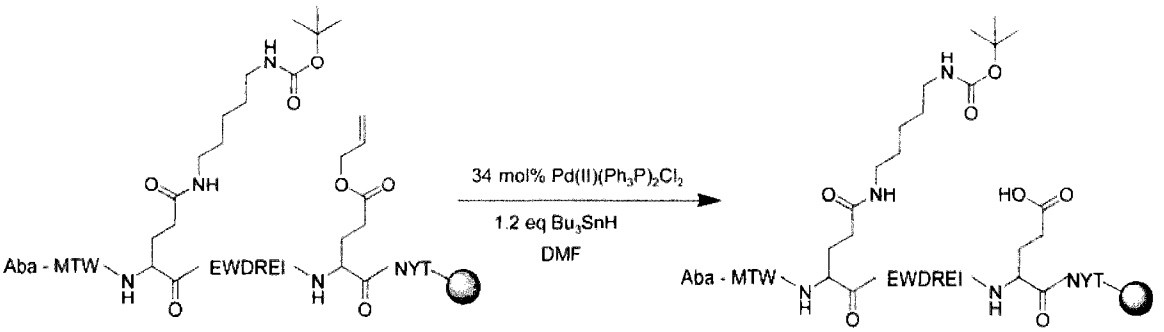

4 **5**

A round bottom flask equipped with a stir bar was charged with **4** (0.2115 g, 0.1248 mmol), DMF (2 mL), Bis(triphenylphosphine)palladium(II) dichloride (15 mg, 34 mol%), and tributyltin hydride (0.04 mL, 1.2 equiv.) added dropwise. The reaction was allowed to stir for 90 minutes at room temperature. Resin was then transferred to shaker vessel and washed with DMF, ethyl acetate, DCM, and DMF again. Water and dilute HCl added to vessel and allowed to shake for 10 minutes. Rinsed resin with DMF.

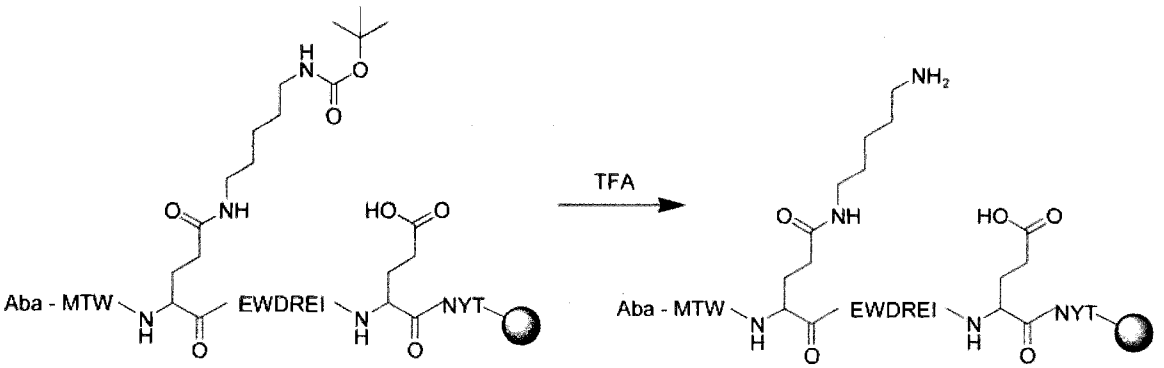

5 **6**

A shaker vessel was charged with **5** (0.2115 g, 0.1245 mmol) and neat trifluoroacetic acid (5mL) and allowed to shake for 1 minute. The trifluoroacetic acid was removed and another aliquot of trifluoroacetic acid was added to the shaker vessel. Again it was allowed to shake for 1 minute. A Kaiser Test was performed to confirm the presence of a free amine.

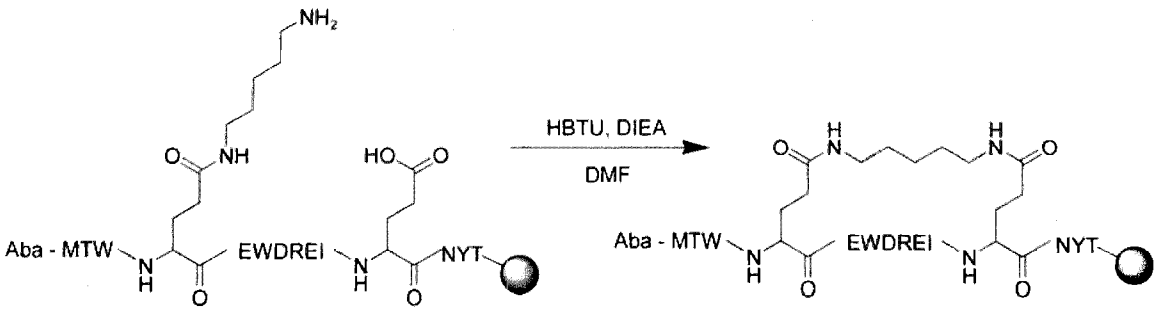

6 **7**

A standard fritted peptide shaker vessel was charged with **6** (0.2115 g, 0.1248 mmol), *N,N,N',N'*-Tetramethyl-*O*-(1*H*-benzotriazol-1-yl)uronium hexafluorophosphate (HBTU, 0.0470 g, 1 equivalent), and DIEA (0.032 mL, 1.5 equiv.). Reaction vessel was allowed to shake for 20 minutes at room temperature. Resin was rinsed with DMF and DCM. Performed Kaiser Test to confirm absence of free amine. Resin was rinsed with ether and solvent was removed *in vacuo*.

5-5: References Cited

(1) Eckert, D.M.; Malashkevich, V.N.; Hong, L.H.; Carr.P.A.; Kim, P.S. *Cell*, **1999**, *99*, 103-115.

(2) Sia, S.K.; Carr, P.A.; Cochran, A.G.; Malashkevich, V.N.; Kim, P.S. *PNAS*, **2002**, *99*, 14664-14669.

(3) Skelton, N.J.; Chen, Y.M.; Dubree, N.; Quan, C.; Jackson, D.Y.; Cochran, A.; Zobel, K.; Deshayes, K.; Baca, M.; Pisabarro, M.T.; Lowman, H.B. *Biochemistry*, **2001**, *40*, 8487-8498.

(4) (a) Wang, D.; Lu, M.; Arora, P.S. *Angewandte Chemie-International Edition*, **2008**, *10*, 1879-1882. (b) Welch, B.D.; VanDemark, A.P.; Heroux, A.; Hill, C.P.; Kay, M.S. *PNAS*, **2007**, *104*, 16828-16833. (c) Deng, Y.Q.; Zheng, Q.; Ketas, T.J. Moore, J.P.; Lu, M. *Biochemistry*, **2007**, *46*, 4360-4369. (d) Liu, S.W.; Wu, S.G.; Jiang, S.B.

Current Pharmaceutical Design, **2007**, *13*, 143-162. (e) Stephens, O.M.; Kim, S.; Welch, B.D.; Hodsdon, M.E.; Kay, M.S.; Schepartz, A. *JACS*, **2005**, *127*, 13126-13127. (f) Jiang, S.; Lu, H.; Liu, S.; Zhao, Q.; He, Y.; Debnath, A.K. *Antimicrobial Agents and Chemotherapy*, **2004**, *11*, 4349-4359.

Chapter 6

Conclusions

The well defined secondary structures of coiled-coils render them particularly well suited for studies in the design of tunable self-assembling systems.

6-1: Design of a Self-Assembling Trimeric Coiled-Coil with a Phenylalanine Core

Coiled-coils are formed by the superhelical twisting of two or more individual peptides whose primary sequence exhibits a heptad repeat (*abcdefg*). Interstrand recognition involves two interfaces: a hydrophobic pocket made up of *a*/*d* side chains, and a hydrophilic interface involving *e*/*g* contacts. Prior to work conducted in our laboratory, means to control trimer stoichiometry (i.e. to ensure an ABC complex from an equimolar mixture of peptides A, B, and C) were limited to electrostatic matching of the *e*/*g* interface. This method required numerous substitutions that might otherwise be available for studying addition interactions. We sought to control heterotrimer formation using only core residues. It was believed that the packing of one large and two small side chains together would lead to a favorable complex. Since parallel coiled-coils contain alternating core layers of *a* and *d* resides, substitutions introduced at the same *a* position of the primary sequence are juxtaposed in the complex. One of the first systems designed in our laboratory incorporated cyclohexylalanine (X) packed against two alanines in three consecutive *a* layers of the hydrophobic pocket.[1]

I have extended this model by replacing the cyclohexylalanine with phenylalanine (F). Besides conferring the potential advantages of purely natural sequences (e.g., *in vivo* expression), such an alternative allows for the design of trimers with varying stability through mixed-core systems.[2]

All four mixed-core trimers exhibited similar helicity by circular dichroism, but their thermal stabilities varied inversely with the number of phenylalanine residues. Further characterization was conducted by chemical denaturation, and each complex displayed a single cooperative unfolding transition. Unfolding free energies differed by over 3 kcal/mol between the most and least stable assemblies, and the correlation with phenylalanine content held (i.e. the more phenylalanine residues the less stable the trimer). Finally, analytical ultracentrifugation confirmed the oligomerization state as trimeric.

Overall, these data confirmed that phenylalanine side chains could assume the role of large hydrophobic groups in a 2:1 small:large matching scheme. Although complex stability was gradually diminished by increasing phenylalanine content, even the F_9:F_{16}:F_{23} assembly remained a perfectly viable trimeric coiled-coil. In addition to providing an alternative to cyclohexylalanine for controlling trimer assembly, introduction of phenylalanine side chains established a mechanism for smooth variation in complex stability without sacrificing specificity. The mixed-core system comprised of F_9:X_{16}:F_{23} is particularly well suited for future experiments involving the expression of two proteins with the F_9 and F_{23} sequences appended to them, and the use of the X_{16} peptide as a linchpin to bring the two proteins together.

6-2: Design of Fusion Protein Surface Mimics

A broad range of enveloped viruses depend on coiled-coil surface recognition for infectivity. We have been interested in members of the lentiviral family: Human Immunodeficiency Virus (HIV), Simian Immunodeficiency Virus (SIV), and Visna virus, the sheep analog of HIV.

Specifically in the case of HIV, entry of the viral contents into the target cell is mediated by the envelope protein gp41, which facilitates fusion of the viral and cellular membranes.[3] The process involves a "trimer-of-hairpins" structure in which the C-terminal region of gp41 binds to a hydrophobic pocket on the outside of the N-terminal trimeric coiled-coil. With the protein anchored into each membrane, this interaction brings the two membranes into proximity, leading to eventual fusion and hence infection.

Because the trimer-of-hairpins structure is required for membrane fusion, it has become an attractive drug target. Studies on the native N-terminal coiled-coil have been limited due to the hydrophobic C-peptide binding sites on each of its threefold symmetric surfaces. These hydrophobic binding pockets tend to lead to aggregation of the protein in aqueous solution. My goal was to develop an efficient, water soluble, binding interface mimic utilizing the self-assembling trimeric coiled-coil. The first viral protein investigated in our laboratory by Nate Schnarr was HIV gp41.[4] In the HIV model, the C-peptide binding pocket was grafted onto one of the three interfaces of our designed heterotrimer. Using that successful HIV model as a foundation, I have developed an interface mimic for the visna virus. The peptides T_9K, $T_{16}Vis$, and $T_{23}Vis$ comprise the N-terminal coiled-coil mimic and TM Vis is the C-peptide.

A control trimer was also synthesized in which the *g* position of $T_{23}Vis$ was persubstituted with lysine; this substitution effectively eliminated half of the binding pocket for the ligand peptide. The validity of the designed visna mimic and control trimer was tested via three main experiments: circular dichroism, Ni-nitrilotriacetic acid (NTA) affinity tagging, and analytical ultracentrifugation.

The circular dichroism experiments demonstrated that the visna mimic formed an α-helix and that it favorably interacted with the ligand peptide. Because the signal for the trimer-plus-ligand was more helical than the trimer signal alone, the ligand peptide gained helicity upon interaction with the trimer. The opposite was true for the control trimer that contained only half the binding pocket. During those experiments, the control trimer plus the ligand signal overlaid with the weighted average of the control trimer and the monomeric ligand signal; therefore, the ligand did not interact with the control trimer.

The T_9K peptide was derivatized with a Gly-Gly-$(His)_6$ tag, producing a new sequence (T_9K_{his}) that binds to nickel nitrilotriacetic acid agarose beads. NTA-affinity tagging experiments were conducted to determine the binding partners for T_9K_{his}. The visna trimer bound with the ligand in an equimolar fashion. On the other hand, the control trimer showed minimal bound ligand.

Analytical ultracentrifugation was implemented to obtain a solution phase molecular weight for the entire complex of the visna trimer with the ligand bound. The expected weight for the visna trimer plus the ligand was 15223 daltons. The calculated value from the fit of the experiment came to 15100 daltons. This final set of data confirmed that the designed visna trimer was an appropriate mimic for the fusion protein.

With an appropriate visna mimic in hand, new fluorescence experiments were designed to probe the binding properties of the ligand with the trimer. First, T_9K was coupled with fluorescein maleimide. Polarization experiments were conducted with varying amounts of the trimeric binding partners to elucidate a K_d for T_9K binding to the other two trimer peptides. The polarization experiments were repeated with the ligand fluorescently labeled and the unlabeled trimer titrated against it. Fluorescence studies

were conducted to probe the role of the two tryptophans in the binding pocket. It was shown that the tryptophans played an important role in ligand binding to the viral mimic.

In summary, the self-assembling trimeric coiled-coil system provided a unique scaffold to develop a viral fusion protein mimic. From that work, a visna fusion protein mimic has been designed, synthesized, and validated as a good mimic through multiple experimental methods.

6-3: References Cited

(1) (a) Schnarr, N.A.; Kennan, A.J. *JACS*, **2001**, *123*, 11081-11082. (b) Schnarr, N.A.; Kennan, A.J. *JACS*, **2002**, *124*, 9779-9783. (c) Schnarr, N.A.; Kennan, A.J. *JACS*, **2003**, *125*, 667-671.

(2) Travisano, P.; Kennan, A.*J, Org. Lett.*, **2004**, *6*, 4219-4222.

(3) (a) Markosyan R.M.; Ma, X.; Lu, M.; Cohen, F.S.; Melikyan, G.B. *Virology*, **2002**, *302*, 174-184. (b) Eckert, D.M.; Kim, P.S. *Ann. Rev. Biochem.* **2001**, *70*, 777-810.

(4) Schnarr, N.A.; Kennan, A.J. *JACS*, **2004**, *126*, 10260-10261.

Appendix 1

NMR Spectra

T_9K

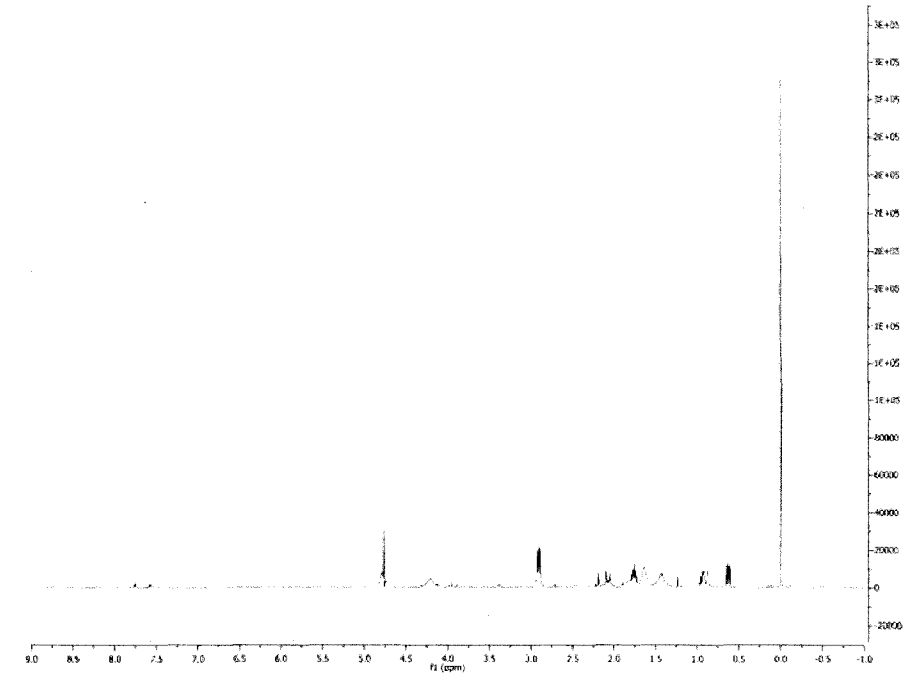

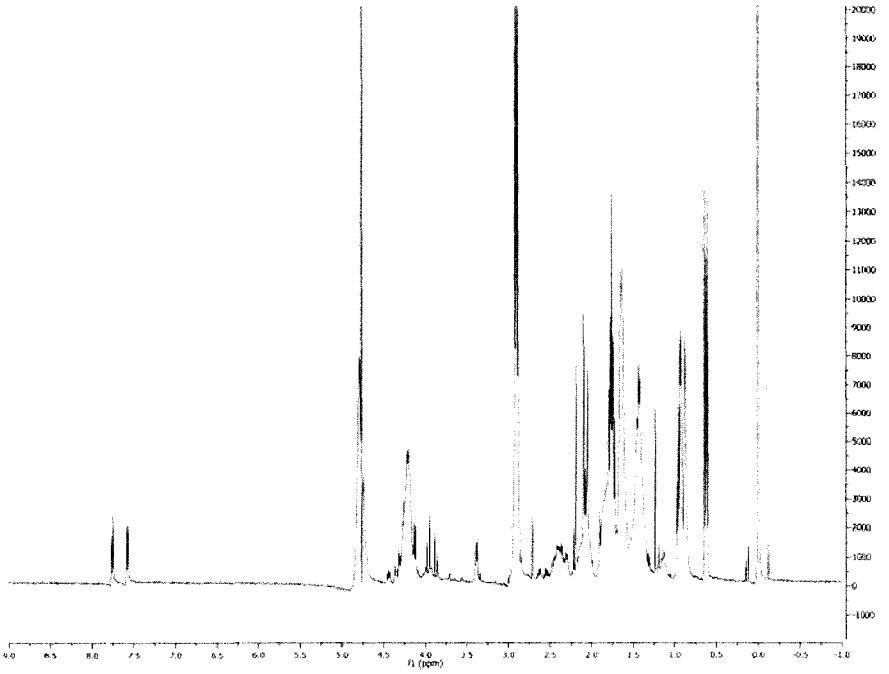

TM Vis

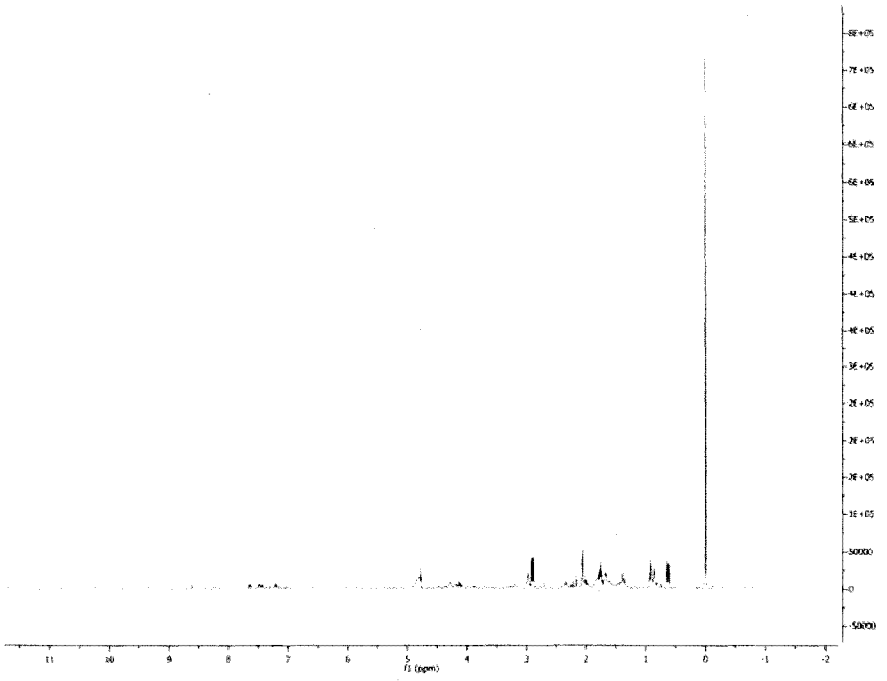

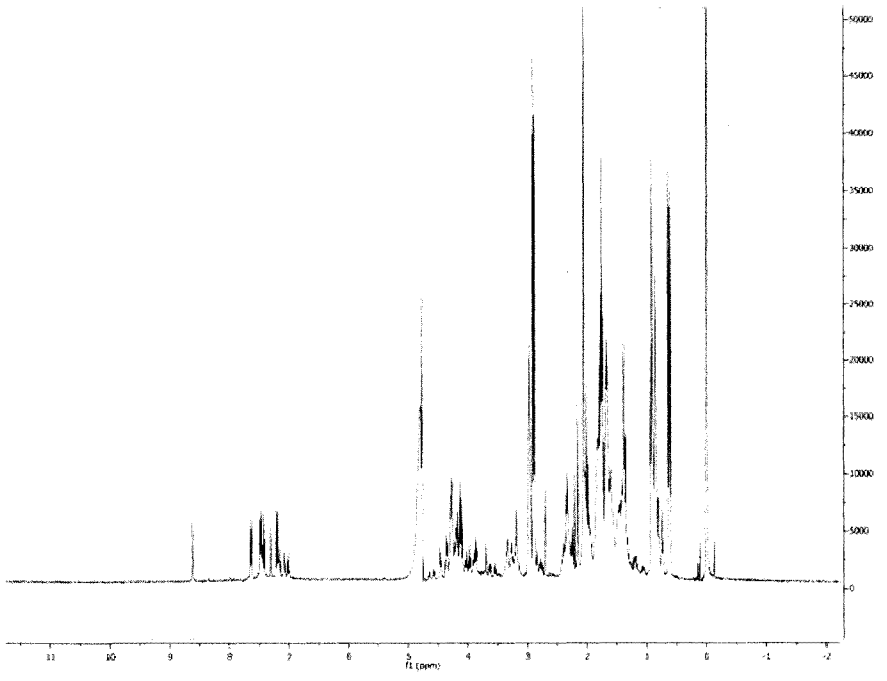

Appendix 2

Peptide Characterization

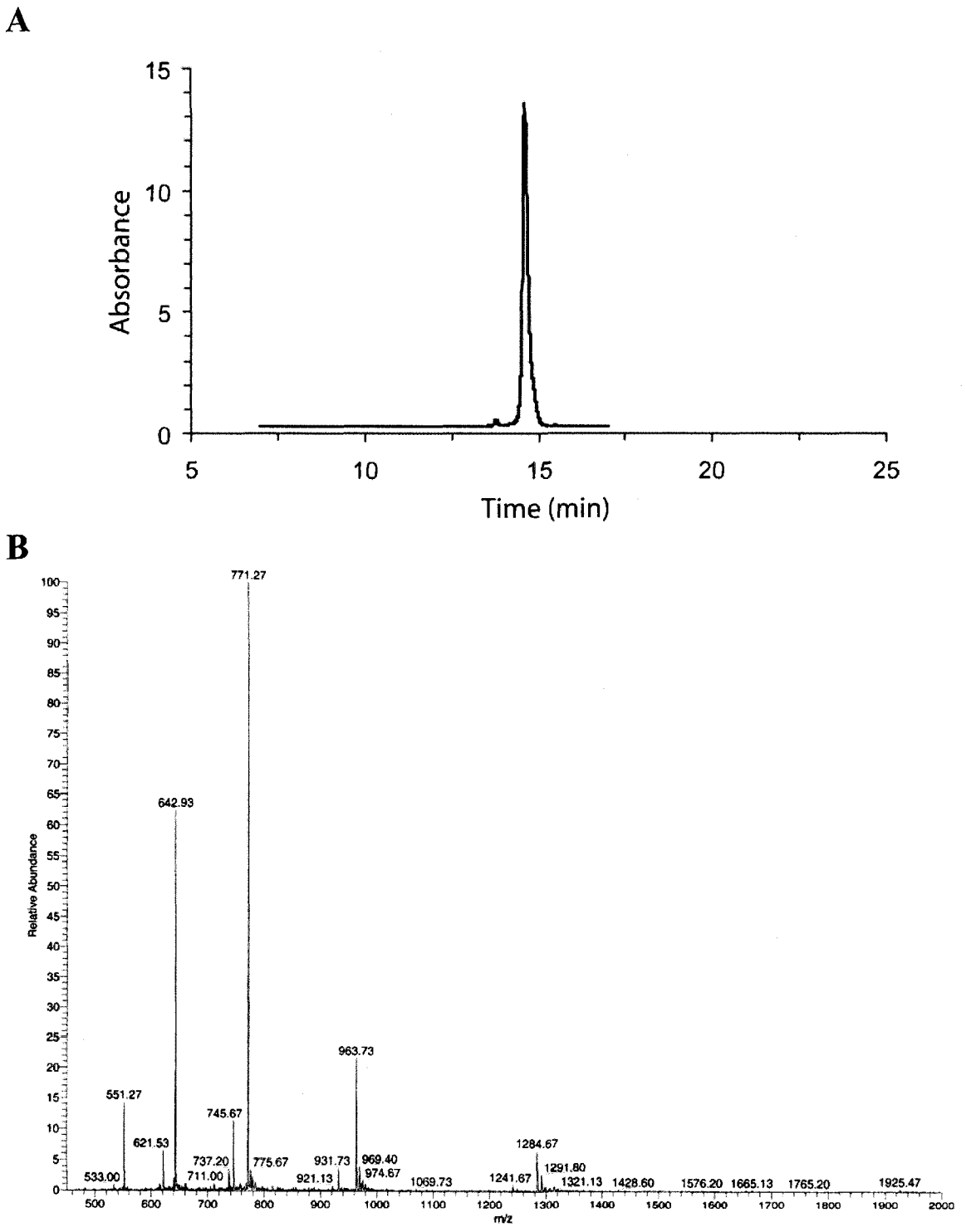

Figure 1. Characterization of T_9K. (A) HPLC of purified material, (B) Electrospray mass spec raw data for purified material (MW_{calc} = 3850).

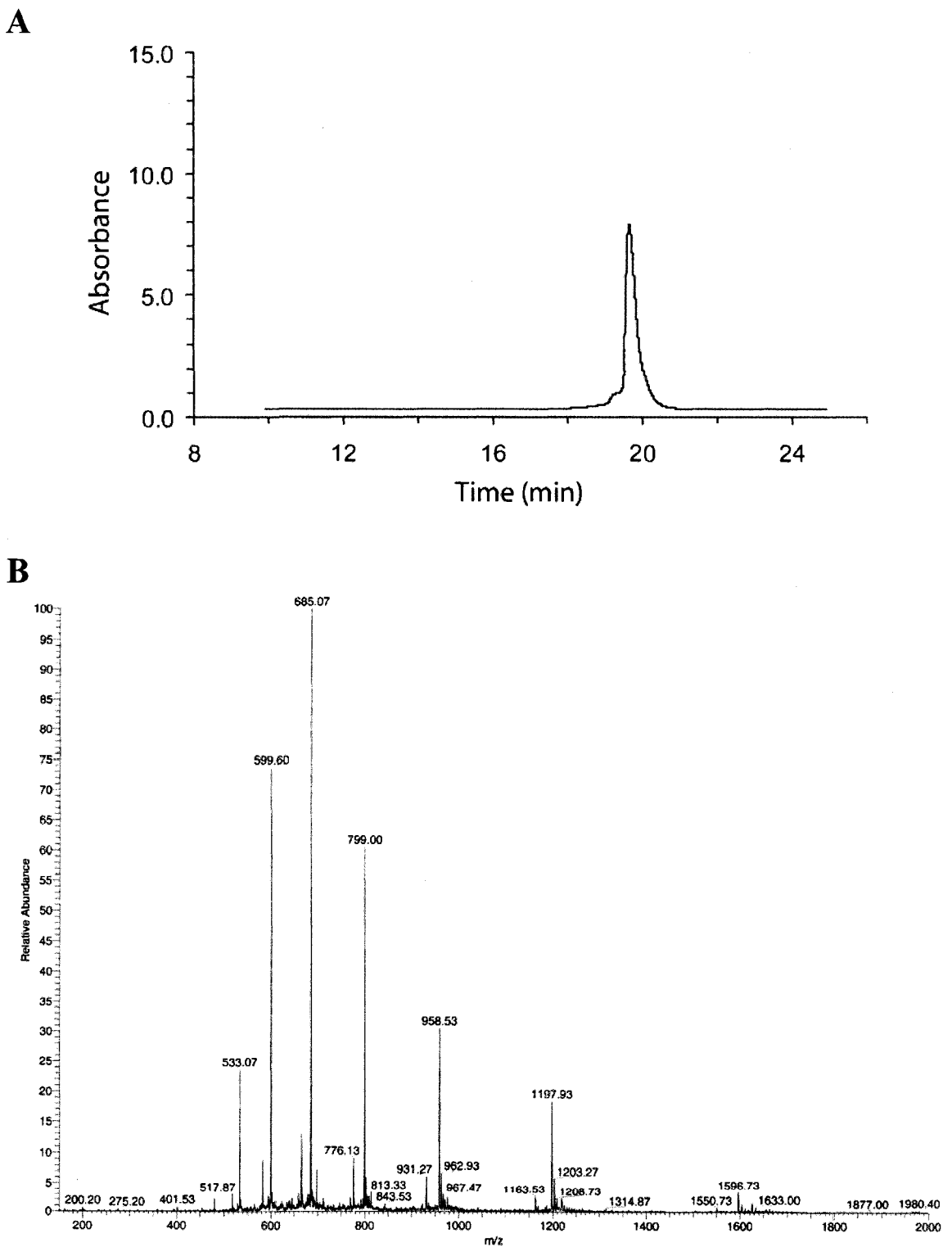

Figure 4. Characterization of T_9K_{his}. (A) HPLC of purified material, (B) Electrospray mass spec raw data for purified material ($MW_{calc} = 4787$).

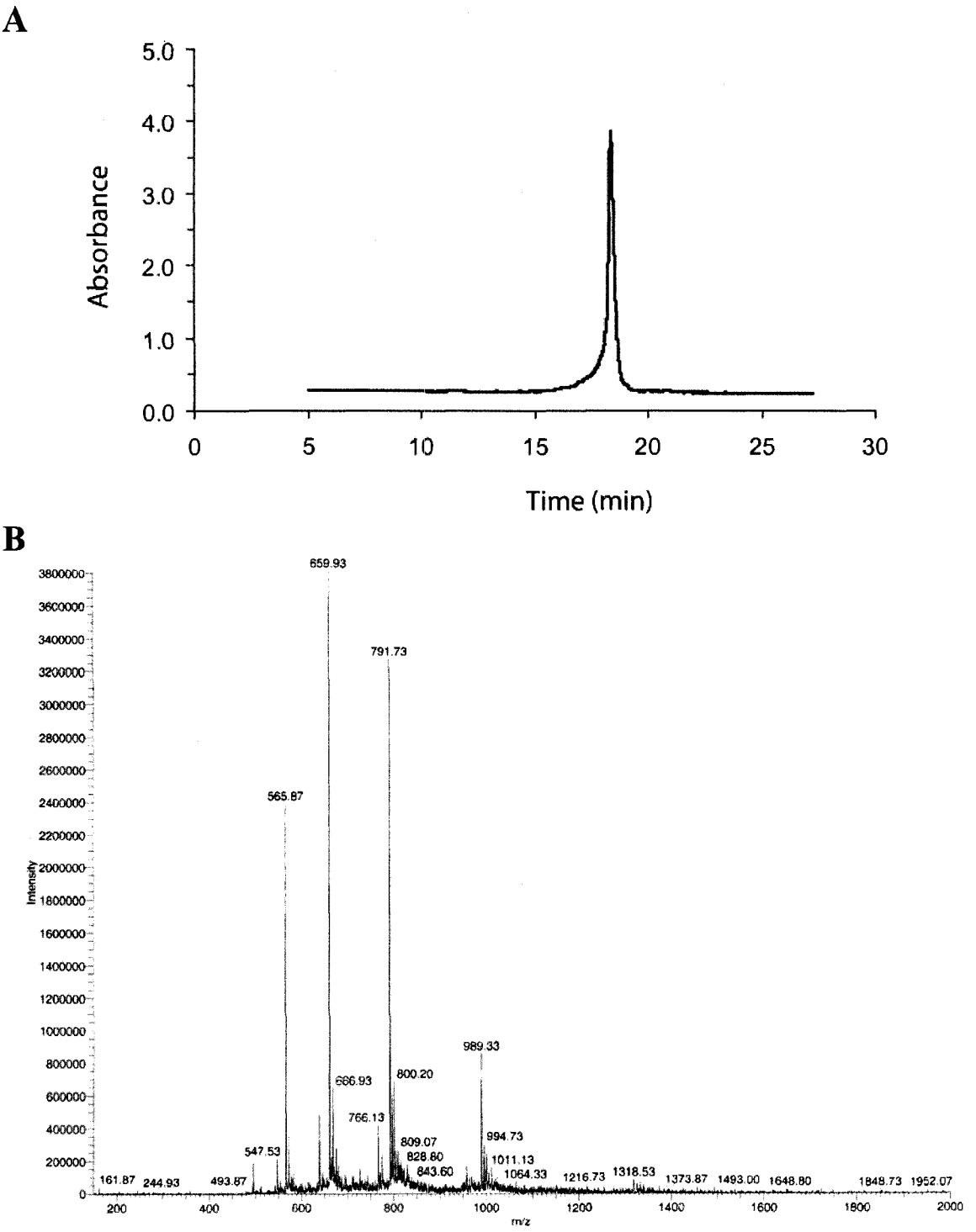

Figure 2. Characterization of T_9K+C. (A) HPLC of purified material, (B) Electrospray mass spec raw data for purified material ($MW_{calc} = 3953$).

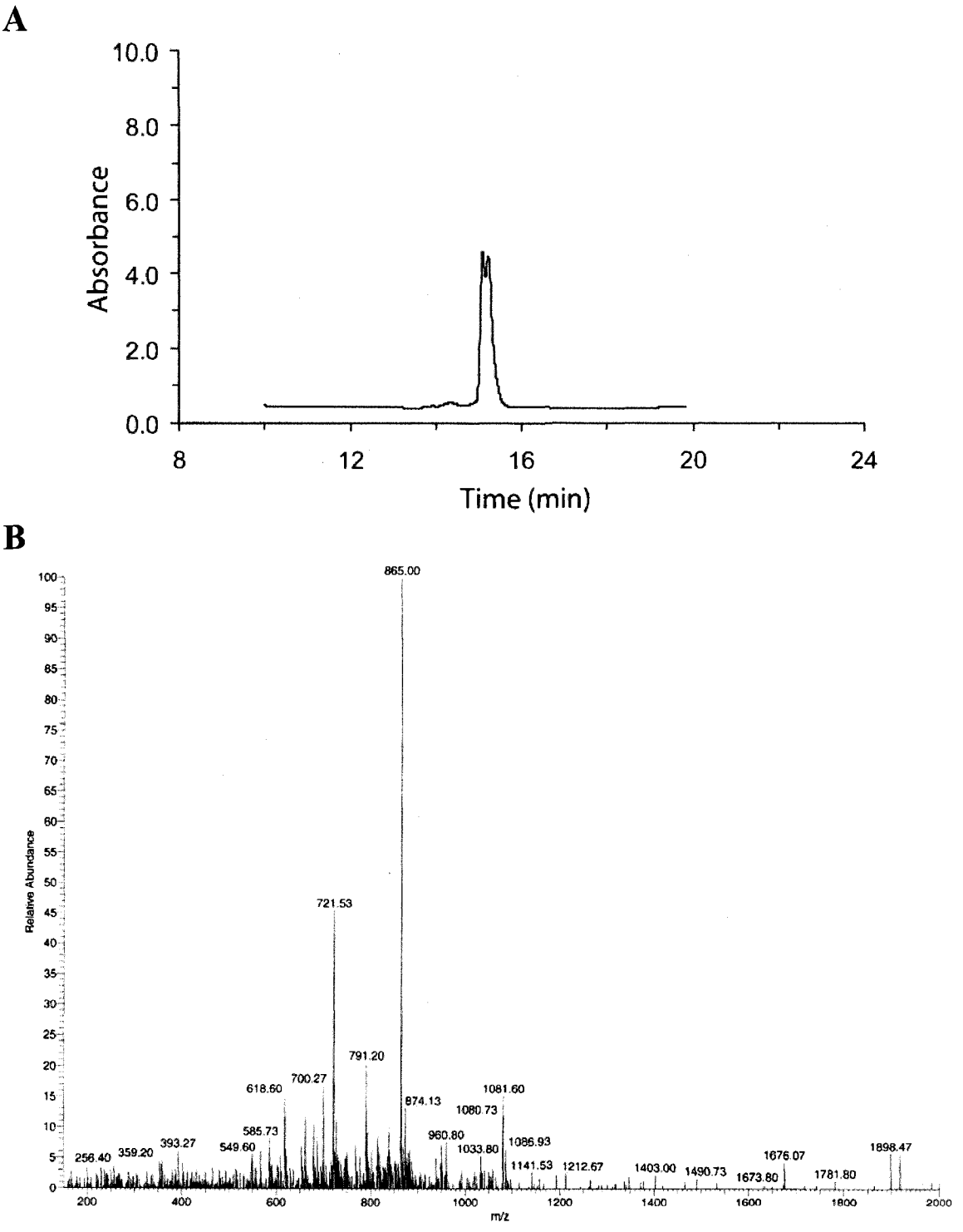

Figure 3. Characterization of T_9K_{fluor}. (A) HPLC of purified material, (B) Electrospray mass spec raw data for purified material (MW_{calc} = 4382).

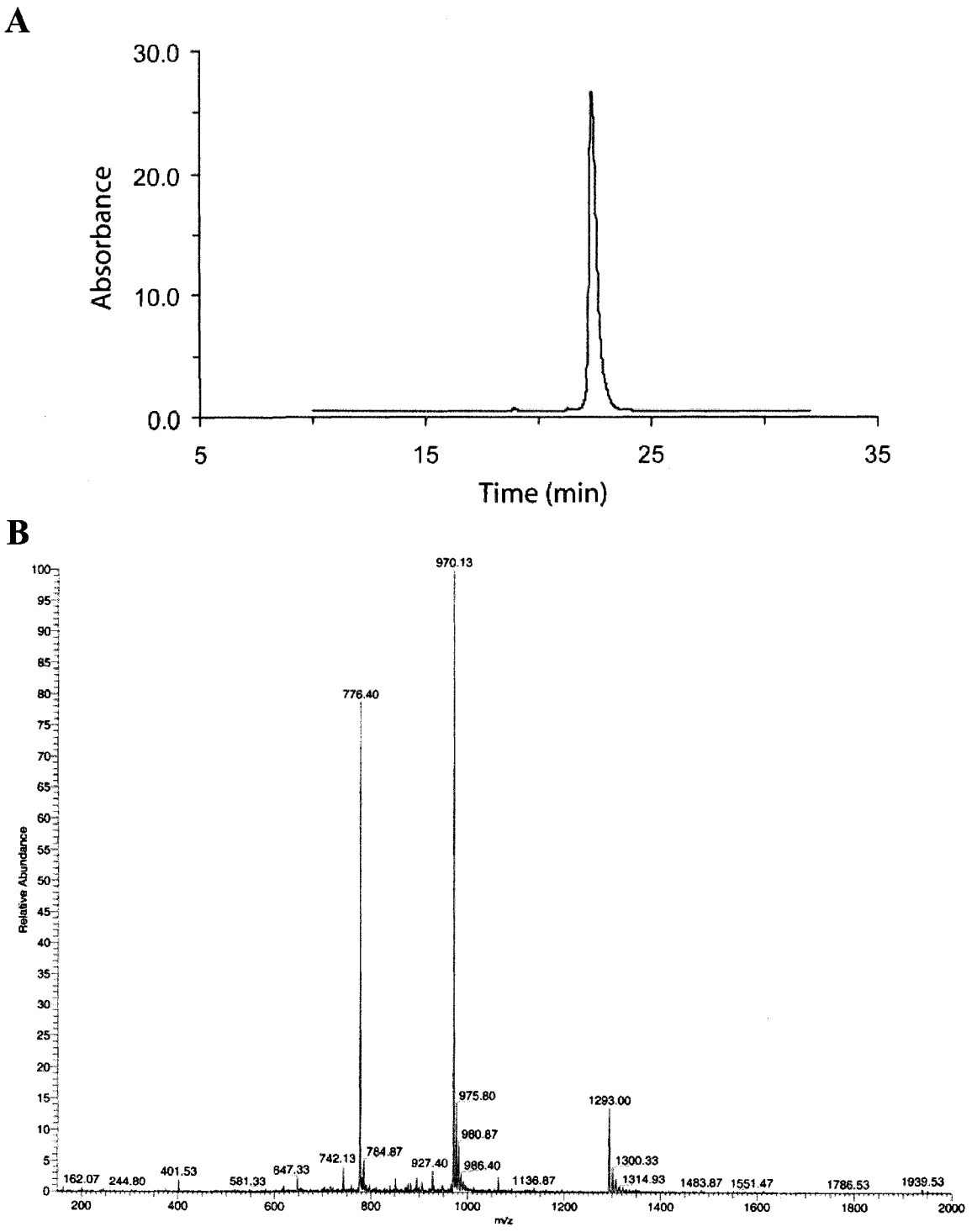

Figure 5. Characterization of T_{16}Vis. (A) HPLC of purified material, (B) Electrospray mass spec raw data for purified material (MW_{calc} = 3876).

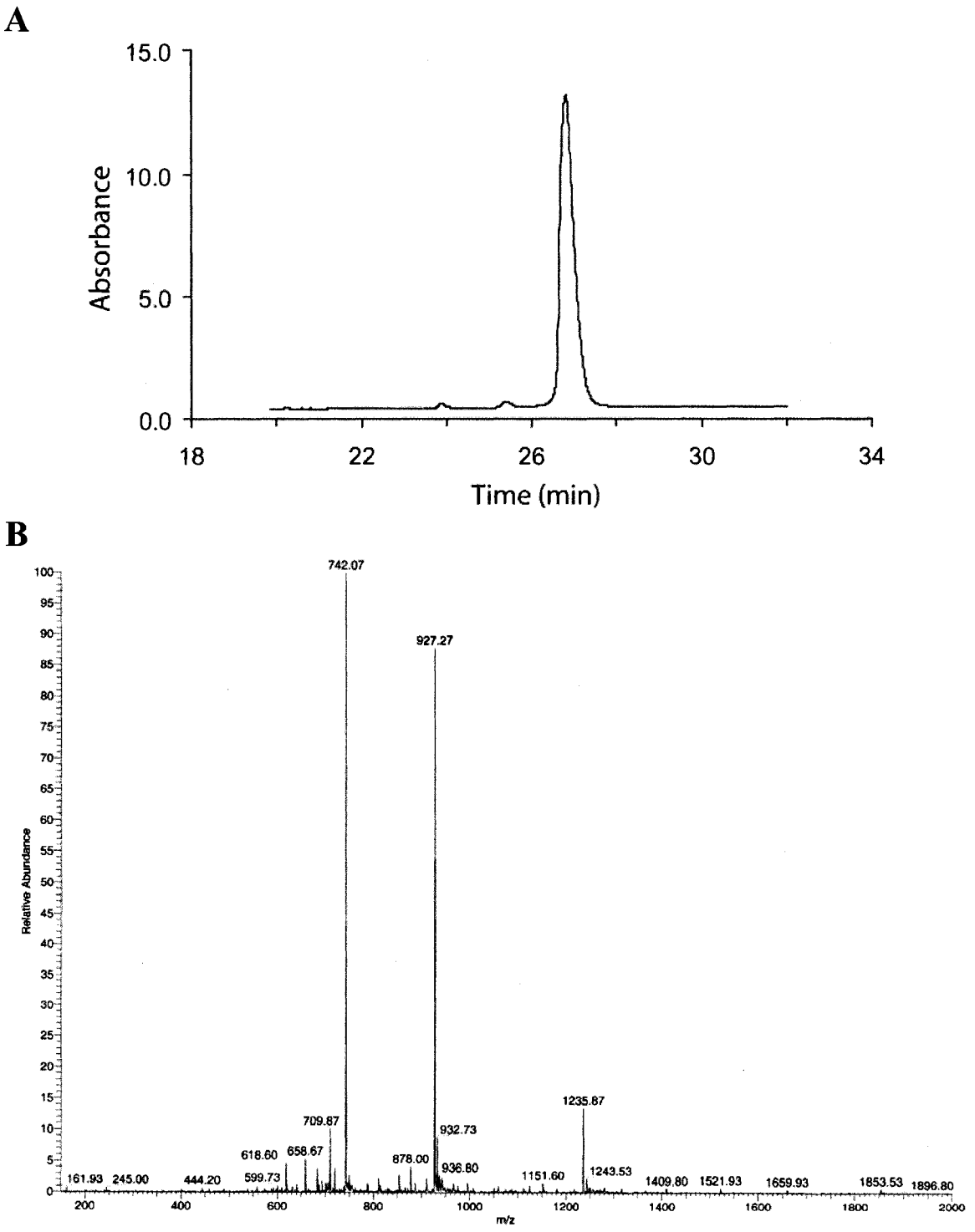

Figure 6. Characterization of T_{23}Vis. (A) HPLC of purified material, (B) Electrospray mass spec raw data for purified material (MW_{calc} = 3705).

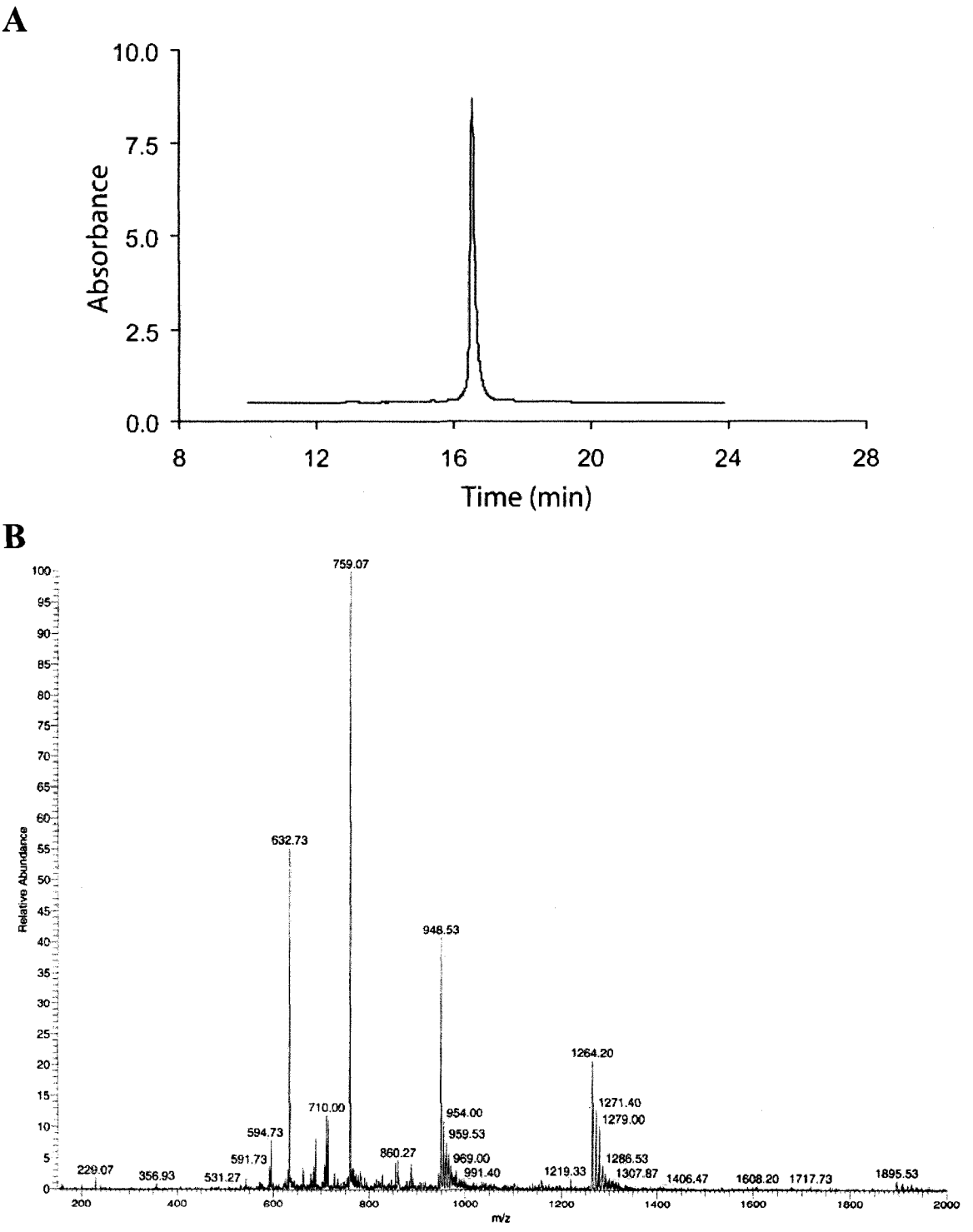

Figure 7. Characterization of TM Vis. (A) HPLC of purified material, (B) Electrospray mass spec raw data for purified material ($MW_{calc} = 3790$).

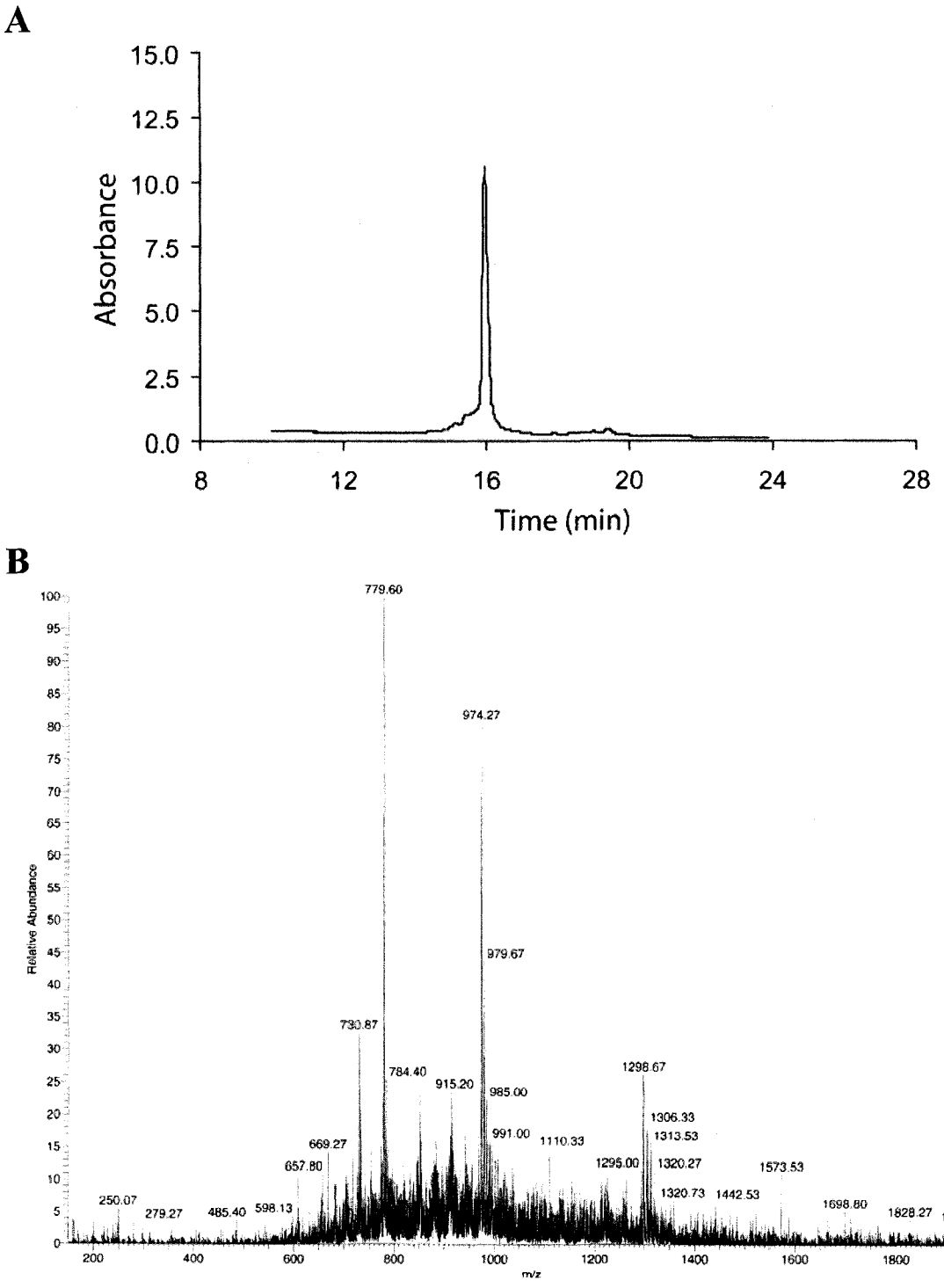

Figure 8. Characterization of TM Vis + C. (A) HPLC of purified material, (B) Electrospray mass spec raw data for purified material (MW_{calc} = 3893).

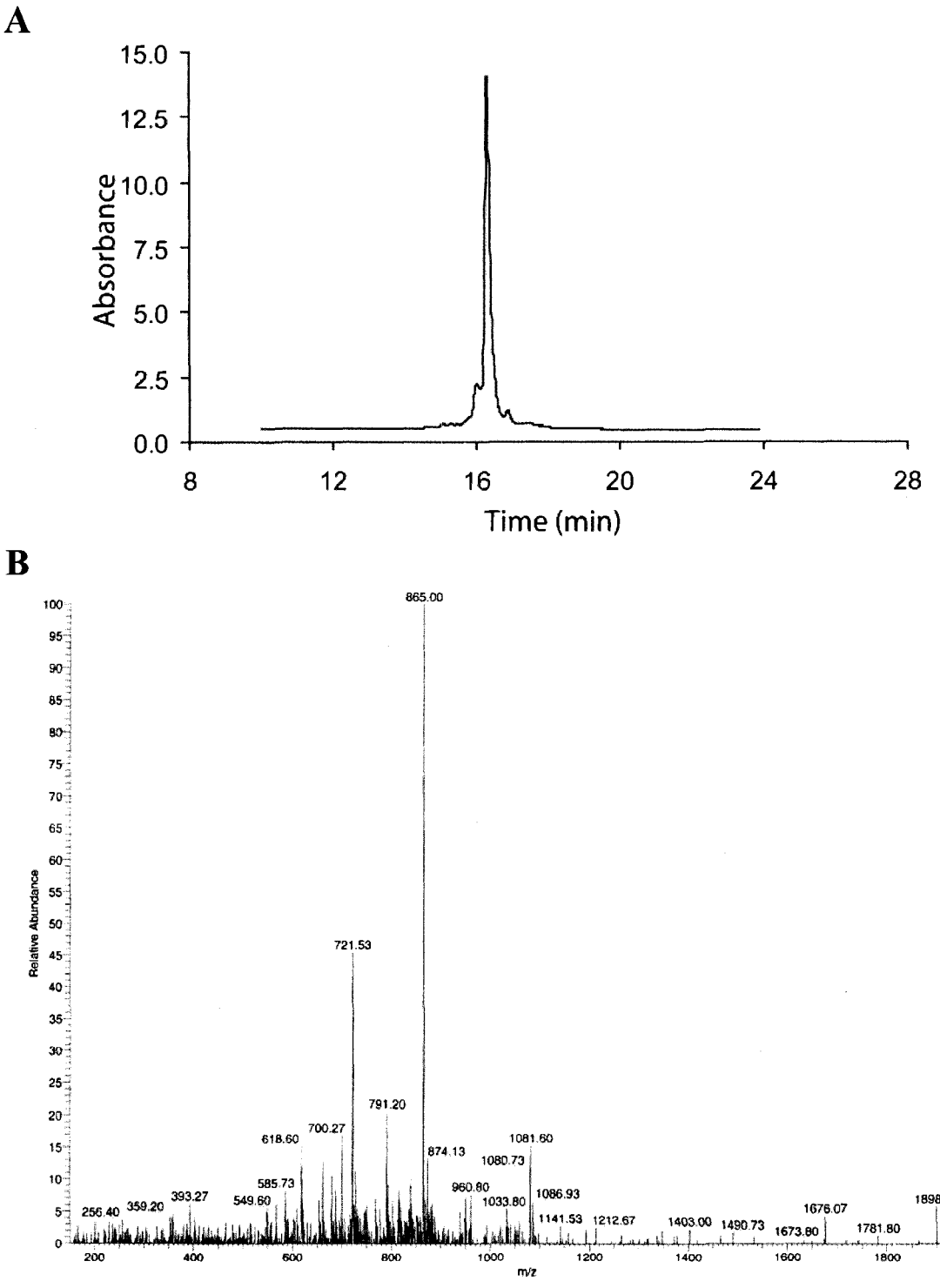

Figure 9. Characterization of TM Vis_{fluor}. (A) HPLC of purified material, (B) Electrospray mass spec raw data for purified material ($MW_{calc} = 4321$).

A

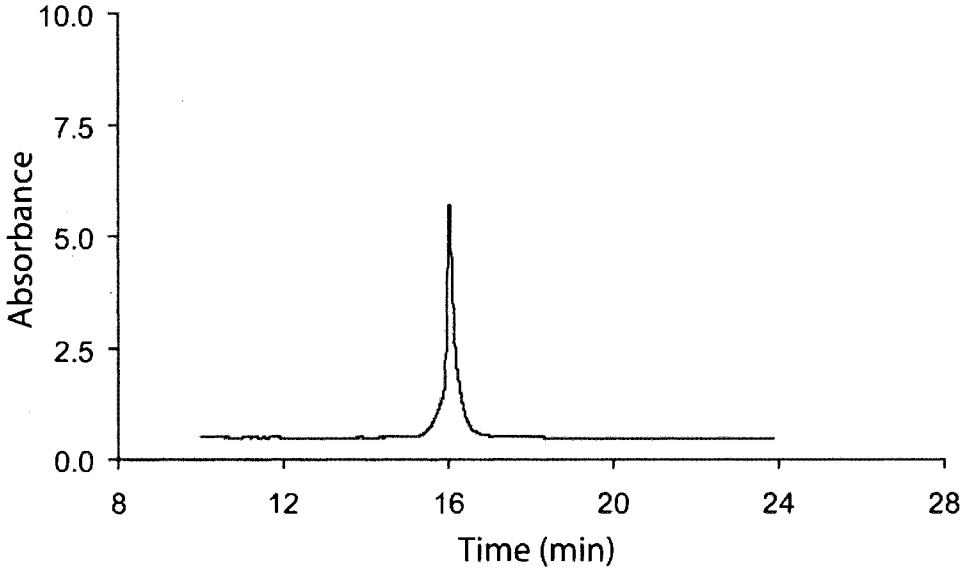
10.0
7.5
5.0
2.5
0.0
Absorbance
8
12
16
20
24
28
Time (min)

B

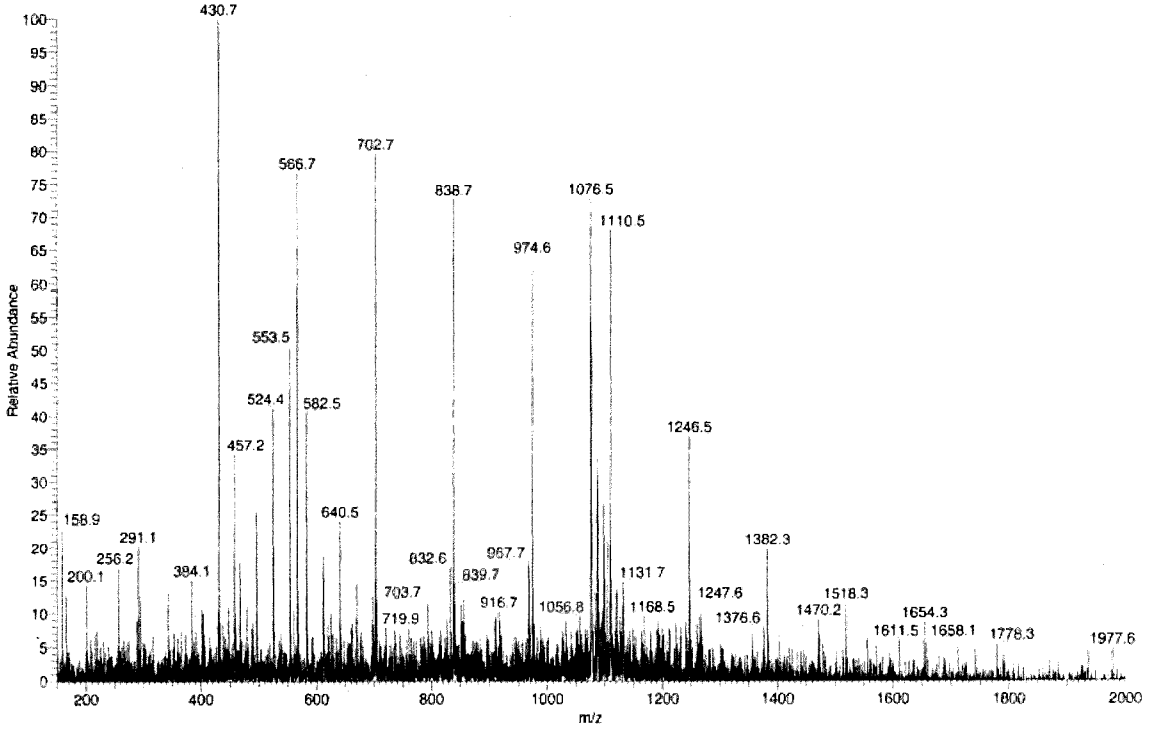
Relative Abundance
m/z
430.7
702.7
566.7
838.7
1076.5
1110.5
974.6
553.5
524.4
582.5
457.2
1246.5
640.5
158.9
291.1
256.2
200.1
384.1
632.6
967.7
839.7
703.7
719.9
916.7
1056.8
1131.7
1168.5
1247.6
1376.6
1382.3
1470.2
1518.3
1611.5
1654.3
1658.1
1778.3
1977.6

C

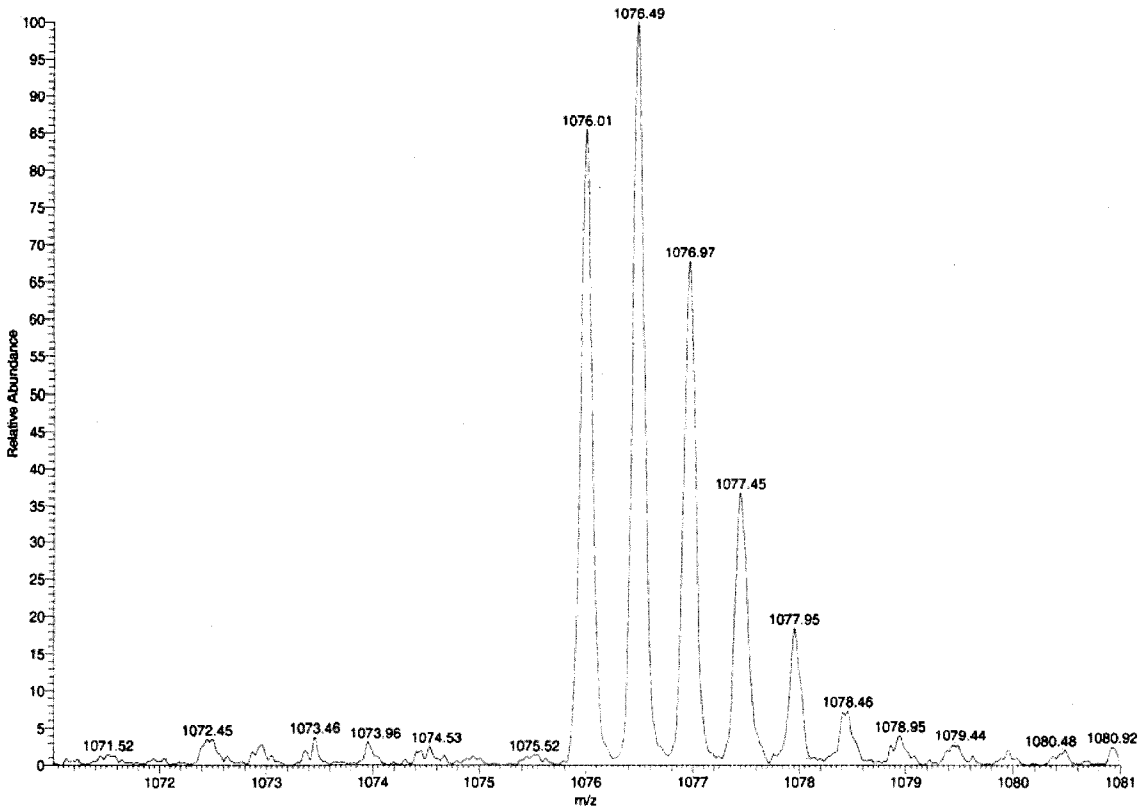

Figure 10. Characterization of C14linkmid. (A) HPLC of purified material, (B) Electrospray mass spec raw data for purified material, (C) detailed view of correct peak ($MW_{calc} = 2128$).